# Targeting Dedifferentiated Melanoma: Exploring the Role of MECOM in Melanoma Phenotype Switching

*A thesis submitted to fulfil the requirements of the degree of Master of Philosophy*

Laura Emily Nicholls

Centenary Institute

Faculty of Medicine and Health

The University of Sydney

May 2026

# STATEMENT OF ORIGINALITY

This is to certify that the content of this thesis is my own work. This thesis has not been submitted for any other degree or purpose.

I certify that the intellectual content of this thesis is the product of my own work, and that all assistance received in preparing this thesis and all sources have been acknowledged.

Laura Emily Nicholls

# ACKNOWLEDGEMENTS

We rarely get formal opportunities to express deep gratitude to people who have made meaningful contributions to the way we experience and move through life.

Dr Jessamy Tiffen – thank you for the endless support, belief, and care you have shown for me, this project, and my time with the lab. I am so grateful for the leadership and insight you showed in noticing, acknowledging, and providing, at every stage, what I needed to succeed. Your guidance navigating what was, at times, a frustrating project was incredibly valuable to me.

Dr Cindy Tseng – thank you for teaching me absolutely everything that is required to function in the lab. Thank you for your eternal patience and support when I would inevitably forget how to function again. I am so appreciative of the way you engaged with my project intellectually, with genuine interest, and genuine care for the outcome. Your expertise made this project possible. I am especially grateful that you helped me so many times with the Ultracentrifuge, which I continue to fear to this day.

Dr Sara Alavi – thank you for your generosity and support throughout my project, your genuine interest and the sharing of your knowledge. Thank you for being so genuinely helpful and kind at every opportunity.

To the other lab members – Leeca, Gabe, Harrison and Ariana – I am genuinely grateful for the time we spent together. I enjoyed every chat, every coffee, and every meal shared.

Dr Justin Wong – thank you for your generosity in offering to be my co-supervisor, for engaging with my project and your guidance whenever needed.

Drs Chirag Parsania and Gavin Sutton – I am grateful for the bioinformtics expertise you both provided in support of this work.

Josh – in so many ways, this could not have happened without you. Thank you for your deep and unwavering support over many, many years.

My family – for trusting me that 10 years at university is the right amount.

My friends – Nicole, Michelle, Ibrahim, Ben, Josh, and many more. Rants, bants or whatever I needed, you were always there.

The Arena – a place of catharsis, sublimation, and joy. Thank you to all the staff and regulars for making it so.

I am also grateful to the Cancer and Gene Regulation Laboratory, Centenary Institute – Mehdi for his help designing my cloning experiments, Cynthia for all her practical help and tips and tricks (I could not have done it without you!), and Dr Bailey for the generous gift of the FUW plasmid.

There are so many other people who have been central to the success of my project, whether they might recognise that contribution directly or not. My colleagues at Notre Dame – your friendship and mentorship kept me grounded as a clinician, which allowed me the space and confidence to grow as a researcher. More than that, the day each week I spent each week in your company, benefitting from your wisdom, skills, knowledge and friendship was affirming in a way I hadn't anticipated. I truly loved working with you all. Likewise, to my students – it was a privilege to get to know you all and (hopefully) make a positive impact in your lives. That experience will always remain meaningful to me. The other researchers and students at Centenary – Dilini, JB, Hannah, the whole VB lab, Seaky, and everyone who contributes to the general culture – thank you. This has been a wonderful place to work.

I would also like to express my gratitude to Professor Rotraud Wieser, from the Medical University of Vienna, for her unhesitating offer to share her MECOM and EVI1 plasmids with us. While I didn't end up using them, I am deeply appreciative of her generosity and commitment to the spirit of scientific collaboration.

I would also like to acknowledge the Sydney Cytometry Core Research Facility, a joint initiative of Centenary Institute and the University of Sydney, for assistance with FACS.

The results published here are in part based upon data generated by the TCGA Research Network: https://www.cancer.gov/tcga.

# GENERATIVE AI ATTRIBUTION STATEMENT

During the preparation of the thesis the author used Microsoft Copilot for the purposes of text enhancement. The use of this generative AI tool includes paraphrasing and sentence structure. The author confirms that where text was modified by generative AI, the content was reviewed for possible errors, inaccuracies, and bias. The author takes full responsibility for the submitted thesis and ensures the work is their own and has used generative AI within the parameters of use.

# AUSTRALIAN GOVERNMENT SUPPORT STATEMENT

This research was supported by an Australian Government Research Training Program (RTP) Scholarship.

# ABSTRACT

Despite major advances in immunotherapy and targeted treatments, resistance and disease progression remain significant challenges in advanced melanoma. Phenotype switching from a melanocytic to a dedifferentiated, stem-like state underlies therapy resistance, yet the transcriptional regulators driving this plasticity are incompletely understood. MECOM, a zinc-finger transcription factor and proto-oncogene, is highly mutated in melanoma and implicated in lineage specification and oncogenic signalling in other cancers. This study investigated MECOM's functional role in melanoma phenotype regulation and its clinical relevance in the context of immune checkpoint therapy.

Using lentiviral models, we modulated MECOM expression in melanoma cell lines representing distinct differentiation states. MECOM overexpression in melanocytic cells enhanced proliferation, migration, and clonogenic survival, and modestly increased sensitivity to ferroptosis-inducing drugs, whereas knockdown in dedifferentiated cells produced inconsistent effects on growth and ferroptosis vulnerability. These findings suggest MECOM acts as a permissive factor for aggressive traits rather than a dominant driver of phenotype switching. Analysis of clinically annotated datasets revealed that higher MECOM expression and *MECOM* missense mutations were associated with improved survival in anti–PD-1-treated patients, particularly in ipilimumab-experienced subgroups, and correlated with an inflamed but myeloid-suppressed tumour microenvironment enriched for interferon signalling. Conversely, low MECOM tumours were more frequently associated with brain metastases, aligning with NGFR-driven invasive states described in recent transcriptomic studies. Pathway analysis indicated that MECOM expression correlates with PI3K–AKT–mTOR and KRAS signalling signatures, consistent with its proposed role in oncogenic programs.

Collectively, these findings position MECOM as a context-dependent regulator in melanoma, influencing proliferative and immune phenotypes rather than acting as a sole determinant of dedifferentiation. MECOM may serve as a biomarker of immune responsiveness and a potential therapeutic target, warranting further mechanistic studies integrating genome-wide binding analyses, multi-omics profiling, and validation in larger immunotherapy cohorts.

# TABLE OF CONTENTS

# LIST OF FIGURES

# LIST OF TABLES

# LIST OF ABBREVIATIONS

AML – Acute Myeloid Leukemia

BET - Bromodomain and Extra-Terminal motif proteins

ChIP-seq – Chromatin Immunoprecipitation sequencing

CRISPR – Clustered Regularly Interspaced Short Palindromic Repeats

CtBP – C terminal binding protein

EMT – Epithelial-to-Mesenchymal Transition

GPX4 – Glutathione Peroxidase 4

HDAC – Histone deacetylase

ICI – Immune Checkpoint Inhibitor

IFN – Interferon

MAPK – Mitogen-Activated Protein Kinase

MHC – Major Histocompatibility Complex

MDS – Myelodysplastic Syndrome

MECOM – MDS1 and EVI1 Complex Locus

MITF – Microphthalmia-associated Transcription Factor

NGFR – Nerve Growth Factor Receptor

PD-1 – Programmed Cell Death Protein 1

PI3K – Phosphoinositide 3-Kinase

ROS – Reactive Oxygen Species

RNA-seq – RNA sequencing

shRNA – Short Hairpin RNA

siRNA – Small Interfering RNA

ssGSEA – Single Sample Gene Set Enrichment Analysis

TCGA – The Cancer Genome Atlas

TGF-β – Transforming Growth Factor β

TIL – Tumour-Infiltrating Lymphocyte

TMB – Tumour Mutational Burden

TME – Tumour Microenvironment

TYRO3 – Tyrosine-Protein Kinase Receptor TYRO3

UVB – Ultraviolet B radiation

# CHAPTER 1: INTRODUCTION

## 1.1 MELANOMA

Skin cancer is the most commonly diagnosed cancer in Australia, with approximately two in three Australians diagnosed with a skin cancer by the age of 70. While the majority of these are non-melanoma skin cancers, melanoma is notable for causing more deaths than any other form of skin cancer (1). Australia and New Zealand have the highest incidence of melanoma in the world at more than 15 times the estimated global rate, with approximately 69 cases diagnosed each year per 100,000 people (2, 3). Historically, advanced melanoma carried a poor prognosis, with median survival under one year (2). However, the treatment landscape has changed dramatically over the past decade. Immune checkpoint inhibitors and targeted therapies have dramatically improved outcomes for advanced melanoma. In the CheckMate 067 trial, combination immunotherapy with nivolumab and ipilimumab achieved a 10-year overall survival rate of approximately 52%, compared to less than one year median survival prior to 2011 (4). For resectable stage III disease, neoadjuvant immunotherapy has recently emerged as a new standard, with the NADINA trial reporting 12-month event-free survival of 83.7% versus 57.2% with adjuvant therapy (5). However, even among initial responders, adaptive resistance frequently develops, leading to disease progression and limiting long-term benefit (6). Moreover, immune checkpoint inhibitors are associated with immune-related adverse events, which can affect multiple organ systems and may be severe or life-threatening (7). Melanoma therefore continues to impose a significant clinical burden, and also a substantial economic burden, with treatment costs exceeding AU$200 million annually (8). Understanding the biological mechanisms driving melanoma progression and therapy resistance remains critical to improving outcomes.

### 1.1.1 AETIOLOGY

Cutaneous melanoma is a malignant neoplasm arising from melanocytes, pigment-producing cells located in the basal layer of the epidermis. Melanocytes synthesize melanin, which determines skin colour and provides photoprotection. The major environmental risk factor for melanoma is ultraviolet (UV) radiation from sunlight, which induces an exceptionally high mutational burden in these tumours (9), typically through the introduction of single or tandem C → T nucleotide transitions (10). Activating mutations in the BRAF and NRAS oncogenes are common drivers of melanoma development (11, 12), yet these mutations seem to occur early in the disease process as they have also been found in benign and dysplastic naevi (13). Additional genetic events, such as loss of tumour suppressor genes or acquisition of further oncogenic changes, are required for malignant transformation. Melanoma is also highly immunogenic, largely due to its high mutational burden, which generates neoantigens – mutated protein fragments presented by major histocompatibility complex (MHC) molecules to T cells, initiating an antitumour immune response (14). This is thought to be a major contributing factor to the success of immunotherapies in melanoma compared to other types of cancers.

### 1.1.2 Treatments and Treatment Resistance

Drawing on these known pathogenic mechanisms, novel treatments for melanoma have been developed. The current first-line therapies for advanced melanomas leverage the immunogenic nature of the tumours, countering its characteristic evasion of the immune system and thus bolstering the antineoplastic immune response. These include nivolumab (a programmed death 1 [PD-1] checkpoint inhibitor) and ipilimumab (a cytotoxic T-lymphocyte–associated antigen 4 [CTLA-4] checkpoint inhibitor) (15). However, as previously mentioned, the development of resistance is common and side effects can be severe, leading to treatment discontinuation (16). Other successful therapies include small molecule inhibitors such as vemurafenib and dabrafenib, which selectively target tumours harbouring BRAFV600 mutations (17). While these agents produce rapid and profound tumour regression, resistance and disease progression typically occur within months (18). Melanoma cells retain high plasticity and an ability to "phenotype switch"; one of the suspected mechanisms through which melanoma evades and develops resistance to these therapies is through dedifferentiation (19). Based on gene expression profiles, Tsoi et al. characterised melanoma cell lines and tumours into four subtypes along this differentiation spectrum from least differentiated or stem cell-like to most differentiated or melanocyte-like. The four subtypes are known as undifferentiated, neural crest-like, transitory and melanocytic, with distinct 'signatures' based on RNA sequencing data (19). It was also demonstrated that progressive dedifferentiation occurs with acquired resistance to standard melanoma therapies (19).

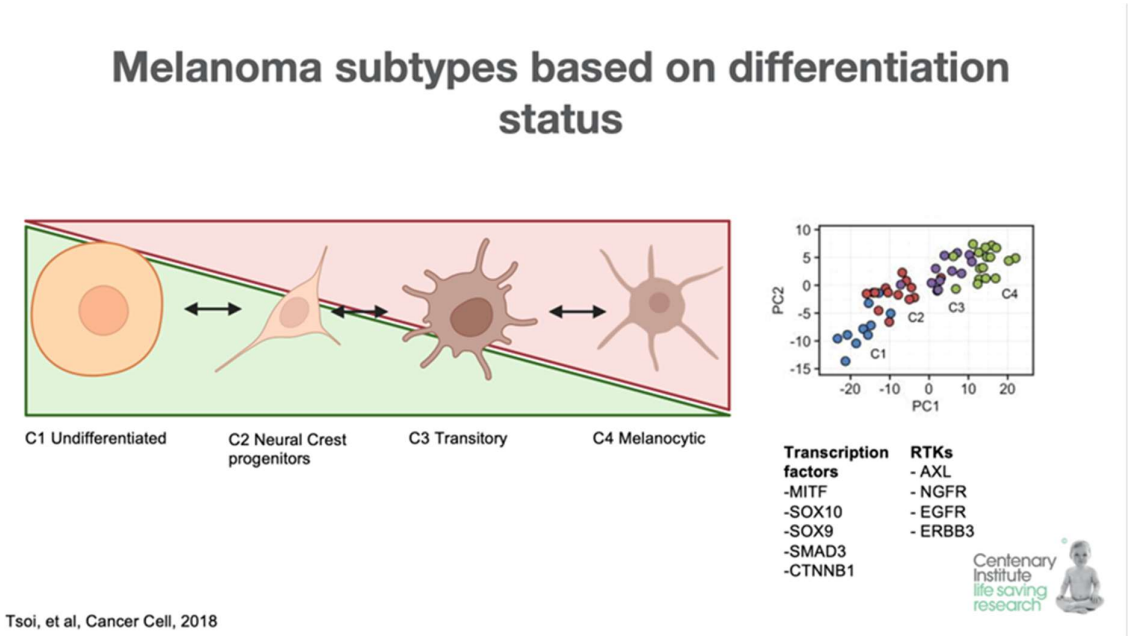


**FIGURE 1. MELANOMA SUBTYPES BASED ON DIFFERENTIATION STATUS.**

**Melanoma cells can be grouped into four major differentiation states: C1 (undifferentiated), C2 (neural crest progenitors), C3 (transitory), and C4 (melanocytic), arranged along a gradient from least to most differentiated. Arrows indicate potential plasticity between states. The right panel shows principal component analysis (PCA) of transcriptomic profiles, illustrating distinct clustering of the four subtypes. Key transcription factors (MITF, SOX10,**

**SOX9, SMAD3, CTNNB1) and receptor tyrosine kinases (AXL, NGFR, EGFR, ERBB3) associated with each state are listed. Adapted from Tsoi et al., *Cancer Cell*, 2018.**

### 1.1.3 The Role of Epigenetic Regulators

Beyond genetic drivers, epigenetic dysregulation plays a critical role in melanoma development, progression, and phenotype switching. Aberrations in DNA methylation, histone modification, and chromatin remodelling have been implicated in melanoma pathogenesis (20). Epigenetic regulators can influence broad transcriptional networks that govern key cancer hallmarks. Large-scale genomic analyses of melanoma patient samples reveal a high prevalence of mutations in genes encoding epigenetic regulators (21). Among these, the *MDS1* and *EVI1* complex locus *(MECOM)*, a known proto-oncogene, emerged as the most frequently mutated transcription factor in one study, present in 36.8% (14/38) of cases (21). The next sections will focus on the known mechanistic roles of *MECOM*, its roles in various cancers, and in melanoma specifically.

## 1.2 THE *MDS1* AND *EVI1* COMPLEX LOCUS

The *MDS1* and *EVI1* complex locus (*MECOM*) produces multiple protein isoforms that act as master transcriptional regulators in development and disease. More specifically, these isoforms have been extensively implicated in a variety of cancers as both proto-oncogenes and tumour suppressors, and yet the context-dependent, distinct and sometimes opposing functions of these isoforms, namely Ecotropic Viral Integration Site 1 *(EVI1)* and *MECOM* (also known as *MDS1-EVI1* and *PRDM3*), challenge our understanding of gene regulation. An exploration of the structure and function of these proteins better informs our understanding of their role in malignancy.

### 1.2.1 GENE STRUCTURE AND ISOFORMS

The *MECOM* locus encodes two main isoform subgroups from these two genes: *EVI1* and *MECOM* (1). The *EVI1* isoforms are characterised by a series of zinc finger motifs, with the most common isoform containing seven zinc finger domains towards the N-terminus and three distally. These zinc finger arrays recognise and bind distinct DNA consensus sequences (2, 3). Two C-terminal binding protein (CtBP) consensus sites lie in the intervening region (4), while a small acidic domain is found in the C-terminal region (5). The MECOM protein is synthesized from the *MDS1-EVI1* read-through transcript, encoding an N-terminal PR domain followed by the same array of zinc finger motifs and other described features of EVI1 (Figure 2).

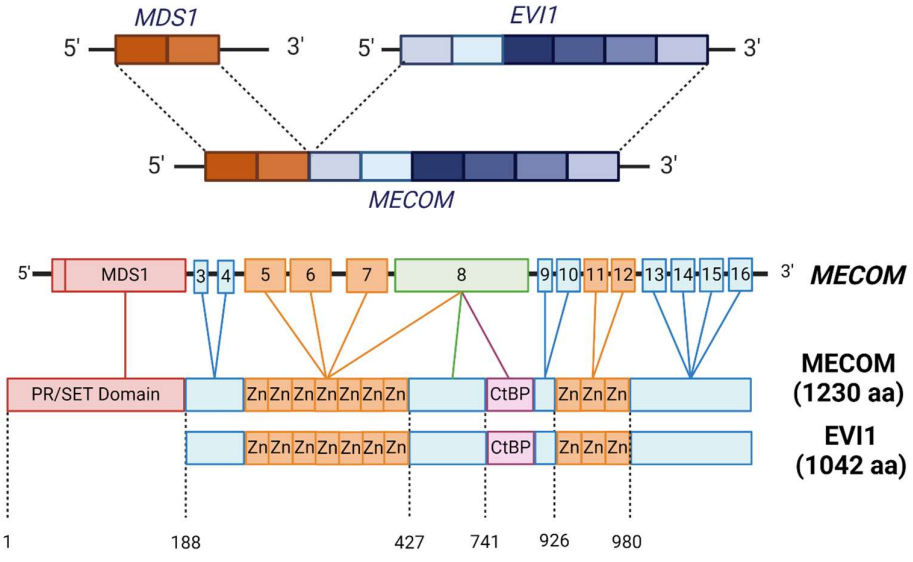


**FIGURE 2. THE ISOFORMS OF MDS-EVI1. The *MECOM* locus encodes multiple isoforms, including *MDS1*, *EVI1*, and the full-length *MECOM* transcript, which combines *MDS1* and *EVI1* exons. The schematic illustrates exon organization and corresponding protein domains. MECOM (1230 amino acids) contains an N-terminal PR/SET domain, two clusters**

**of zinc finger motifs (Zn), and CtBP-binding sites, while EVI1 (1042 amino acids) lacks the PR/SET domain. Exon numbers and amino acid positions are indicated below the diagram.**

### 1.2.2 MOLECULAR MECHANISMS AND PROTEIN INTERACTIONS

MECOM is a member of the PR/SET domain-containing (PRDM) protein family. This family consists of 19 proteins (in humans), characterised structurally by a *S*u(var)3-9, *E*nhancer-of-zeste and *T*rithorax (SET)-like PR domain followed by a variable array of zinc finger motif (22). MECOM and its closely related homolog PRDM16 are both conserved in *C. elegans* and *Drosophila* (23). Some PRDM proteins, most notably PRDM9 and PRDM7, have demonstrated lysine methyltransferase activity in line with their closer homology with the more ancient SET-domain enzymes, while the remainder are more accurately described as pseudomethyltransferases (24). The totality of evidence indicates that MECOM falls into the latter category. While there have been limited reports that MECOM may possess weak, cytosolic H3K9 methyltransferase activity (22), it lacks the highly conserved, key catalytic tyrosine residue which defines the known SET-domain methyltransferases (25), and sequence alignment thus indicates it would not possess direct methyltransferase function (24). *In vitro* assays failed to show that MECOM could methylate free histones (H3, H4) (26, 27). Moreover, knockdown of the established set of SET-domain H3K9-methylating enzymes (Suv39h1/Suv39h2, Eset1/Eset2, or G9a/Glp) in mouse embryonic fibroblasts abolished all detectable H3K9 methylation (28). MECOM was not targeted in these experiments, yet methylation was entirely lost, indicating that MECOM does not contribute to H3K9 methylation.

Intriguingly, several other PRDM proteins also have an isoform variant lacking their respective PR/SET domains. To further the analogy to MECOM and EVI1, many of these protein isoform pairs have been implicated in tumorigenesis, and have been postulated to possess different roles in their truncated vs full-length forms (Table 1). Many of these studies demonstrate that in the cancer state there is an imbalance in the ratio of Full-length PRDM to shorter isoforms, with higher levels of the shorter forms correlating with transformation (29).

**TABLE 1. MEMBERS OF THE PRDM FAMILY WHICH SHARE A COMMON DUALITY OF PR-CONTAINING AND PR-LACKING ISOFORMS.**

| Full-length Protein | Shortened Isoform | Proposed functions |
|---|---|---|
| PRDM1/BLIMP1 | PRDM1b/BLIMP1β | Full-length: Tumour suppressor in diffuse large B cell lymphoma (DLBCL) (30-33), Natural killer cell lymphoma (34)<br>Short: Oncogenic in DLBCL (35, 36), myeloma (37) |
| PRDM2/RIZ1 | RIZ2 | Full-length: Tumour suppressor in breast cancer (38), DLBCL (39), myeloid leukaemias (40, 41), endometrial cancer (42), colorectal cancer (43), hepatocellular carcinoma (44)<br>Short: May function as a negative regulator of RIZ1 (45), oncogenic in breast cancer (38) |
| PRDM3/MECOM | EVI1 | Full and short length: Conflicting reports on function discussed in detail in text |

| | | |
|---|---|---|
| PRDM6/PRISM | PRDM6/33# | Full-length: Suspected involvement in smooth muscle (46) and endothelial cell differentiation (47)<br>Short: Unknown |
| PRDM16/MEL1 | sPRDM16/MEL1S | Full-length: May function as a tumour suppressor in kidney (48), lung, and pancreatic cancers (49)<br>Short: Oncogene in AML (50) |

Although MECOM has not been shown to function directly as a methyltransferase, there is robust evidence that MECOM functions as an epigenetic regulator through extensive DNA and protein binding interactions. The C-terminal zinc finger domains bind to a GAAGATGAG consensus sequence (51). Missense mutations in these distal zinc finger sequences have been linked to haematologic and skeletal abnormalities including bone marrow failure, amegakaryocytic thrombocytopenia, and radio-ulnar synostosis (52-54), and may predispose to myeloid malignancies (55). The N-terminal zinc fingers recognise a consensus sequence of 15 nucleotides consisting of three elements of GA(T/C)AA, with the first three aiding in binding specificity and the remainder directly binding to DNA (56).

Together with the PR-domain, the N-terminal zinc finger domain has primarily been shown to be involved in recruitment to DNA via protein-protein interactions. Specifically, MECOM and its isoforms appear to act as transcriptional repressors through interactions of these domains with known histone methyltransferases, such as suppressor of variegation 3–9 homolog 1 (SUV39H1) and euchromatic histone-lysine N-methyltransferase 2 (G9a), histone deacetylases such as histone deacetylase complex 1 and 2 (HDAC1/2), and direct DNA methyltransferases such as DNA methyltransferase 3 alpha and beta (DNMT3A/B). Both MECOM and EVI1 coimmunoprecipitate with SUV39H1 and G9a (27, 57, 58). The interaction between EVI1 and SUV39H1 requires the proximal two zinc fingers of EVI1 and the C terminal domain of SUV39H1. Using GAL4 luciferase constructs, both the Nucifora and Delwel groups demonstrated that SUV39H1, via its SET domain, mediates the transcriptional repression activity of EVI1 in a dose-dependent manner (57, 58). This suggests that EVI1's function as a transcriptional repressor is significantly strengthened through recruitment of SUV39H1, likely through SUV39H1's ability to methylate histones at EVI1 target genes. The combination of forced expression of EVI1 and downregulation of SUV39H1 or G9a in mouse embryonic fibroblasts reduced the colony forming ability of these cells compared with forced EVI1 expression alone (27).

MECOM and EVI1 can also associate with HDAC1/2, while it appears that MECOM alone can interact with the full nucleosome remodelling and deacetylase (NuRD) complex (which is formed in part by HDAC1/2) (25). The NuRD complex is crucial to the epigenetic regulation of developmental genes, modulating the expression of genetic pathways critical for proliferation, differentiation and embryonic development. Abnormalities of NuRD signalling or function are associated with cancer and premature aging (59). The primary members of the NuRD complex include HDAC1/2, metastasis-associated proteins 1 or 2 (MTA1/2), RB Binding Proteins 4 or 7 (RBBP4/7), methyl-CpG-binding domain 2 or 3 (MBD2/3), chromodomain helicase DNA-binding protein 3, 4 or 7 (CHD3/4/7), and GATA zinc finger domain containing 2A or 2B (GATAD2A/B) (60). Using a proteomic IP-MS screen in an ovarian cancer cell line, Bard-Chapeau et al. showed that RBBP4, HDAC1, HDAC2 and CHD4 were likely interaction

partners of EVI1 (61). To clarify the differential binding partners of EVI1 and MECOM, Ivanochko et al. performed IP-MS assays using full-length mouse MECOM and EVI1. They found that only MECOM could pull down the full NuRD complex, while EVI1 had a more limited ability to bind only to RBBP4 and CHD4 (25). Their results suggest that the ability of EVI1 to guide the NuRD complex to chromatin and perform its regulatory functions may be impaired compared with that of MECOM.

MECOM and its isoforms may repress gene expression through promotion of DNA methylation. Analysis of DNA methylation patterns in AML patient samples revealed that high *EVI1* expression is associated with hypermethylation of more than 200 genes compared to normal CD34+ cells or other AML samples, with the strength of this hypermethylation signature correlating with EVI1 expression levels (62). Using a series of stably integrated luciferase reporter constructs containing different regions of the miR-124-3 regulatory sequence, Senyuk et al. demonstrated that EVI1 and DNMT3B cooperatively repress transcription (63). MiR-124-3 encodes a group of small genes involved in the regulation of differentiation and cell cycling across a range of tissue types, including haematopoietic (64), mesenchymal (65), and epithelial progenitors (66). Co-immunoprecipitation experiments demonstrated that EVI1 forms complexes with DNMT3A/B *in vivo* (63). The functional significance of these interactions was demonstrated through *in vitro* DNA methyltransferase assays, with this activity being enhanced by co-expression of EVI1 and DNMT3B (63). This N-terminal zinc finger domain of EVI1 appears essential for this interaction and function, as a double point mutant within zinc fingers 1 and 6 loses methyltransferase and repressive activity in this model (63, 64). The interaction between EVI1 and DNMT3A is itself regulated by phosphorylation of serine 436 of EVI1, with phospho-null mutations at this site showing reduced DNMT3A binding and altered DNA methylation patterns in hematopoietic stem and progenitor cells, suggesting a complex regulatory mechanism for EVI1-mediated DNA methylation (67).

MECOM has also been implicated in carcinogenesis by binding to tissue-type specific transcription factors and dysregulating differentiation. These interactions appear to occur primarily through direct protein-protein binding that alters transcription factor activity. For example, in hematopoietic tissues EVI1 has been shown to interact with and modulate the functions of key lineage determination factors such as GATA1/2, RUNX1, and PU.1 (68-70). EVI1 physically interacts with GATA1 via its N-terminal zinc fingers to displace it from DNA binding sequences, thereby preventing normal differentiation and potentiating malignant transformation (68). Similarly, EVI1 binds to RUNX1 to prevent its transcriptional activation of target genes and block granulopoiesis (69). While EVI1 also binds to PU.1, this does not appear to prevent PU.1 from binding to its consensus DNA sequences, but rather prevents it from binding necessary transcriptional co-activators and thus prevents myelopoiesis (70). Outside of haematopoiesis, MECOM interacts with transcriptional regulators in other tissues, including SMAD proteins in TGF-β signalling (discussed below). The outcomes of these interactions are highly context dependent.

The CtBP domain was demonstrated to be necessary for EVI1 to interact with CtBP1 *in vivo,* and this interaction appears to mediate repression of TGFβ signalling (71). The ability of EVI1 to transform Rat1 fibroblasts was abolished by site-directed mutagenesis of the CtBP domain (from PLDLS to

PLASS)(72). In a series of elegant experiments focusing specifically on the interactions between EVI1 and CtBP2, Pastoors et al. demonstrated that EVI1 interacts with CtBP1/2 in AML cells via the conserved PLDLS domain, and that the interaction is essential for leukaemia transformation across a range of mouse and human-derived models (73). They also showed that binding of CtBP2 to chromatin can be abolished by either knockdown of EVI1 or competitive inhibition with overexpression of a sequence of four PLDLS motifs (73). Previously, it had been shown that EVI1, but not MECOM, homo-oligomerizes, that this oligomerisation promotes its interaction with CtBP, and that thus MECOM has a significantly impaired ability to both bind CtBP and repress TGFβ signalling (74). A subsequent IP-MS pulldown of MECOM and EVI1 demonstrated that both isoforms bind CtBP1/2 (25). Conversely, the leukemia-associated fusion gene AML1/MDS1/EVI1 resulting from the (3;21)(q26;q22) translocation robustly interacts with CtBP1 (75). Together, these results suggest that the oncogenic potential of EVI1 isoform may in part be mediated by interactions with CtBP and the downstream signalling cascade of this interaction. The functional impact of MECOM and CtBP interactions have not been investigated. *CTBP* expression and activity is elevated in a variety of cancers, with overlap between those also implicating MECOM/EVI1: ovarian cancer (76, 77), colorectal and lung cancer (78), and AML (75).

In addition to evidence suggesting CtBP1/2 interact with MECOM's CtBP domain to repress TGFβ signalling, Kurokawa et al. have also shown that EVI1 binds to Smad3, an intracellular mediator of TGF-β signalling, via its N-terminal zinc finger domain in Mv1Lu cell lines to repress TGF-β signalling (79). To add complexity, TGFβ itself has a context-dependent role as both a tumour-promoter and tumour suppressor. In normal and pre-malignant cells, TGFβ functions as a negative regulator of cell proliferation and survival, and can induce terminal differentiation and apoptosis (80). However, in the cancer state it is coopted as a pleiotropic cytokine, and activation of this signalling pathway acts as a potent promoter of cell motility, invasion, metastasis and tumour plasticity (81). Both genetic and epigenetic alterations have been found to induce this switching mechanism across multiple cancer types (82). More research is required to fully characterise the impact of MECOM vs EVI1 on TGFβ signalling in both normal and malignant cells.

### 1.2.3 Additional isoforms and regulation of expression

Although *MECOM* and *EVI1* are the predominant transcripts arising from the *MDS1/EVI1* locus, multiple other transcripts have been annotated and are suspected to have distinct functions. EVI1Δ324 is a variant that is co-expressed with EVI1 but lacks the 6th and 7th zinc fingers from the N-terminal array (83). EVI1 and EVI1Δ324 overall appear to act similarly as transcription factors: ChIP arrays and sequencing in an ovarian cancer cell line demonstrated 71% overlap in their bound genes, and both isoforms lead to almost identical gene expression profiles in HeLa cells (84). Nonetheless, unlike EVI1, EVI1Δ324 lacks the ability to transform Rat1 fibroblasts (85) or murine haematopoietic stem cells (86). This suggests that EVI1 may also possess post-translational oncogenic effects.

The various transcripts arising from the *MECOM* locus appear to also differentially regulate each other's expression. Using ChIP and luciferase reporter assays in AML and HEK239 cells respectively, Maicas

et al. demonstrated that EVI1 activates its own transcription, whereas MECOM and EVI1Δ324 act as repressors of *EVI1* (86). The promoter regions they identified were not consistent with previously identified MECOM/EVI-1 DNA-binding motifs (86), suggesting that these isoforms may be binding and regulating transcription as part of a larger protein complex. This differential autoregulation may help to explain why different cancer types show varying patterns of MECOM isoform expression. The finding that regulation occurs through non-canonical binding sites supports other evidence that MECOM proteins often function through interactions with other proteins rather than binding DNA directly.

Chromosomal inversions and translocations, and locus amplification events, have been implicated in the over-expression of MECOM and tumourigenesis across a range of tissues. Common variants include inversions between two breakpoints on chromosome 3 (inv(3;3)), reciprocal translocations between chromosomes 3 and other chromosomes (t(3;3), t(3;12) and t(3;21)), and copy number increases at the chromosomal region 3q26.2. Using bone marrow biopsies from patients with confirmed over-expression of EVI1 and known myeloid malignancies or myelodysplastic syndrome, and human AML cell lines, Gröschel et al. detected characteristic breakpoint patterns involving both the inv(3) and t(3;3) rearrangements which lead to repositioning of an 18kb enhancer region (which they called the "commonly translocated segment") either upstream of *EVI1* (within the *MECOM* locus) or downstream of *EVI1* (87). They used chromosome conformation capture to show that this commonly translocated segment, originally located near *RPN1*, acts as an enhancer of aberrant *EVI1* expression by physically interacting with the *EVI1* promoter in these rearrangements, regardless of whether it was newly positioned up or downstream of the gene. The effect of these rearrangements appears specific to the EVI1 isoforms, which are considered the oncogenic isoform in this cancer type. Further, 3q26.2 amplification events are one of the earliest and most frequent chromosomal abnormalities in epithelial ovarian cancers. While these amplification events are associated with increased expression of both MECOM and EVI1, the relationship between CNV and gene expression is non-linear (26). This raises the possibility that rearrangements may again alter promoter or enhancer activity as an additional mechanism to induce over-expression of these genes.

### 1.2.4 Developmental functions and physiologic roles

Despite this extensive research using *in vitro* assays, cell lines, and animal and patient-derived cancer models which has revealed much of MECOM's molecular interactions and regulatory mechanisms, comparatively little is known of the physiological role of MECOM and EVI1 in normal tissue development and maintenance. Early work demonstrated a temporally distinct pattern of MECOM/EVI1 expression primarily within mesoderm-derived tissues of the developing mouse embryo, including the urinary system, the early limb buds, the heart, the bronchioles of the lung, and the nasal cavities (88). In the adult, MECOM is expressed at high levels in the ovary and kidney (89), and may be expressed to a lesser extent in the lung, uterus and heart (88). These studies did not differentiate between MECOM and its isoforms. An exonal deletion causing loss of both MECOM and EVI1 is embryonically lethal at day 10.5-13.5 post-fertilization in mice (90, 91). The impacts of its loss are pleiotropic, including

generalised hypocellularity, profoundly impaired brain and neuronal development, impairments of angiogenesis and vascular defects causing haemorrhaging, and distinct cardiac malformations which were the most likely cause of death (90). MECOM-/- zebrafish embryos display abnormalities of craniofacial development associated with decreased expression of markers of cartilage (COL2A1 and SOX9A) and bone (RUNX2A/B) (92), and deficits of angiogenesis (93). Together, these studies demonstrate that MECOM functions as a master transcriptional regulator essential for normal development across multiple tissue types, suggesting how its dysregulation could drive oncogenesis by coopting core developmental programs.

## 1.3 THE *MDS1* AND *EVI1* COMPLEX LOCUS AND CANCER

### 1.3.1 HAEMATOLOGICAL MALIGNANCIES

The *MECOM* locus was first identified as a common site of retroviral integration in murine myeloid leukemia models and later recognized as a critical oncogenic driver in human hematologic malignancies (94). In acute myeloid leukemia (AML) and myelodysplastic syndromes (MDS), MECOM overexpression frequently results from chromosomal rearrangements, and is strongly associated with poor prognosis and resistance to chemotherapy (95). The World Health Organization classifies AML with inv(3)(q21.3q26.2) or t(3;3)(q21.3;q26.2)/*GATA2–MECOM* (*EVI1*) mutations, as well as AML with other *MECOM* rearrangements, as major disease subtypes (96). Through different mechanisms, both the inv(3) and t(3;3) rearrangements lead to overexpression of the EVI1 isoform and, frequently, loss of the MECOM isoform (87, 97). These abnormalities are present in approximately 1–2.5% of AML and MDS cases (98, 99). Although these rearrangements consistently drive EVI1 overexpression, abnormal expression is also observed in 6–11% of adult AML cases and 9–28% of paediatric cases even in the absence of these specific chromosomal rearrangements (100). Collectively, MECOM dysregulation represents a defining feature of a subset of AML and MDS, with profound implications for disease classification, prognosis, and treatment strategies.

Despite its evident clinical significance, the precise oncogenic role of EVI1 in hematologic malignancies remains incompletely understood. EVI1 overexpression in experimental models profoundly perturbs hematopoietic programs, influencing both proliferation and differentiation. In murine embryonic stem cells, endogenous EVI1 is expressed in the undifferentiated state but is gradually silenced as the cells differentiate (101). Transient EVI1 overexpression in murine hematopoietic progenitors promotes accumulation of myeloblasts and promyelocytes while impairing differentiation; withdrawal of EVI1 expression triggers terminal myeloid differentiation and apoptosis (102). Mouse transplantation studies indicate that enforced EVI1 expression can induce fatal MDS and, in some cases, other malignancies such as acute B-lymphoblastic leukemia, but is insufficient alone to drive AML transformation (103, 104). When Cuenco et al. directly compared the outcome of EVI1 and MECOM overexpression, both were found to enhance the expansion of myeloid and immature progenitors while suppressing erythropoiesis in bone marrow; however, only EVI1 overexpression resulted in fatal outcomes (104). Consistent with these findings, clinical and genomic studies suggest that additional oncogenic “hits” are required for full leukaemic transformation. Most commonly, AML and MDS cases with inv(3)/t(3;3) harbour activating mutations in RAS pathway genes (NRAS, KRAS) or related signalling proteins, which promote dysregulated proliferation(94). Given its established role in hematopoietic malignancies, MECOM may similarly influence lineage plasticity and oncogenicity in solid tumours such as melanoma, which is explored in the following sections.

### 1.3.2 Solid Cancers

MECOM has also been implicated as a key transcription factor in a variety of solid malignancies. Overexpression of MECOM in ovarian cancer was first reported shortly after its identification in AML (105), although its biological and clinical significance remains incompletely understood. Chromosomal abnormalities leading to amplification of 3q26.2 are common in high-grade serous ovarian cancers; this region encompasses *MECOM* and *EVI1* (26, 106). High-resolution array CGH of 235 tumours identified a ~2 Mb amplicon at 3q26.2, with copy number gains correlating with ≥5-fold increases in *EVI1* and *MECOM* transcripts in the majority of advanced cases, confirmed at the protein level (26). Intriguingly, increased DNA copy number and *MECOM* expression were associated with improved patient outcomes, whereas high *EVI1* transcript levels predicted poor survival. Functional assays demonstrated that forced overexpression of either MECOM or EVI1 enhanced proliferation and migration in ovarian cancer cell lines, underscoring their oncogenic potential despite the contradiction in prognosis. This study specifically dissected and highlighted isoform-specific differences, suggesting distinct biological roles for MECOM and EVI1.

As previously discussed, MECOM often functions in concert with lineage-dependent transcription factors. In ovarian cancer, Bleu et al. showed that MECOM binds specifically to PAX8 (a key regulator of Müllerian lineage identity) via its PR/SET and zinc finger domains (107). ChIP-sequencing revealed that knockdown of PAX8 largely abolished MECOM binding to DNA, and the PAX8/MECOM complex co-occupied motifs distinct from canonical MECOM sites. This complex regulated a gene module involved in cell adhesion and extracellular matrix organization. Knockdown of *MECOM* and *EVI1* in ovarian cancer cell lines arrests cancer growth and reduces proliferation and migration (108, 109). Similarly, CRISPR-Cas9 deletion of the *MECOM* enhancer leads to decreased proliferation, migration, and colony formation in ovarian cancer cells and xenografts (110). These effects may in part be mediated by MECOM's regulation of KRAS expression and downstream MAP kinase signalling, with ChIP-qPCR confirming MECOM binding to the *KRAS* promoter (109). Collectively, the evidence highlights *MECOM* as a context-dependent oncogene in ovarian cancer, with implications for tumour maintenance and potential therapeutic targeting. Similar context-dependent roles have been reported in colorectal cancer, where MECOM/EVI1 influences both early tumourigenesis and metastatic behaviour.

MECOM/EVI1 have been implicated as key transcription factors in colorectal cancer, where they were found to be upregulated in 53% (8/15) of colorectal cancer samples and all 3 adenoma samples compared to adjacent normal mucosa, suggesting a role in early carcinogenesis (111). MECOM/EVI1 were detected in all five colon cancer cell lines tested and localized to the nucleus, consistent with their functions as transcription factors (111). MECOM/EVI1 are not typically expressed in normal colonic mucosa. Unexpectedly, MECOM/EVI1 have been shown to bind to the ΔNp63 promoter and downregulate its expression in colon cancer cell lines, thus delaying cell cycle progression and reducing proliferation, indicating that MECOM/EVI1 can exert growth-inhibitory effects under certain contexts (112).

Epithelial-mesenchymal transition (EMT) is a process by which epithelial cells lose polarity and adhesion, acquiring mesenchymal traits that enhance motility and invasion, and this is considered a key driver of metastasis in solid tumours. Depletion of MECOM/EVI in metastatic colon cancer cells increased invasion through Matrigel and caused spindle-shaped morphology, decreased E-cadherin, and increased N-cadherin expression (113). Despite these EMT-like changes, MECOM/EVI1-deficient cells failed to form metastatic foci in mice, whereas MECOM/EVI1-expressing cells metastasized to the intraperitoneal layer and formed micrometastases in lungs and spleen (113). More recently, MECOM/EVI1 were shown to activate the ETS2 oncogene via a distal super-enhancer in colorectal cancer and inflammatory bowel disease. Silencing MECOM/EVI1 downregulated ETS2 and impaired colony formation, sphere formation, and migration in colorectal cancer cells (114). This finding contrasts with earlier work suggesting that EVI1 loss enhances invasive features, underscoring the complexity of MECOM/EVI1 function in colorectal cancer. Although highly expressed in colorectal cancers, MECOM expression does not correlate with survival (115). In these studies, the MECOM and EVI1 isoforms were not differentiated, leaving their specific contributions unresolved.

*MECOM* and *EVI1* expression in breast cancer is more heterogeneous than in colorectal cancer, but its clinical impact is notable. High expression correlates with increased distant metastasis and poorer survival in estrogen receptor (ER)-negative and triple-negative breast cancers, subtypes associated with aggressive behaviour and limited treatment options (116). Knockdown of MECOM/EVI1 in breast cancer cell lines significantly reduced proliferation regardless of ER status, while oestradiol supplementation restored growth in ER-positive knockdown cells (116), suggesting that estrogen signalling may partially compensate for MECOM/EVI1 loss and explain the weaker prognostic effect in ER-positive disease.

Regulatory mechanisms also contribute to MECOM/EVI1 dysregulation. The tumour-suppressor microRNA miR-1, frequently downregulated in breast cancer, directly targets *MECOM/EVI1* transcripts in breast cancer stem cells (117). Restoration of miR-1 expression suppressed MECOM/EVI1, inhibited stem cell proliferation, and reversed EMT-like features, evidenced by increased E-cadherin and decreased N-cadherin expression (117). These findings implicate MECOM/EVI1 in maintaining stemness and invasive and metastatic potential. Again, the isoform-specific roles of MECOM versus EVI1 have not been characterised in breast cancer, representing a critical gap in current knowledge.

MECOM functions as a context-dependent oncogene in pancreatic cancer initiation, facilitating stress adaptation and lineage plasticity. While MECOM/EVI1 expression is virtually absent in normal pancreatic tissue, it is frequently overexpressed in pancreatic ductal adenocarcinoma (PDAC) precursors and established PDAC tumours (118). RNA-seq profiling of human pancreatic exocrine cells revealed that dedifferentiated acinar cells under stress activate cancer-related pathways with prominent *MECOM* expression, whereas duct cells do not (119). Under these conditions, MECOM is re-expressed during acute and chronic pancreatitis and correlates with, and is directly regulated by, SOX9 - a key transcription factor driving acinar-to-ductal metaplasia and PDAC initiation (119). In pancreatic cancer cell lines, MECOM depletion significantly reduced proliferation and migration (118), and as in ovarian cancer MECOM directly interacts with the KRAS pathway, through which it may

potentiate its oncogenic impact. Functional studies in mouse acinar cells demonstrated that MECOM/EVI1 knockdown impaired cell adhesion, increased acinar cell death, and suppressed dedifferentiation through reduced ERK signalling (119). These findings suggest that MECOM enables acinar cell survival under stress and promotes dedifferentiation, a critical step in PDAC initiation.

Although less well characterised, MECOM has also been implicated in more than 13 other cancer types, ranging from glioblastoma multiforme and lung adenocarcinoma to nasopharyngeal and urothelial cancers (120-132). Across these malignancies, higher MECOM/EVI1 expression generally correlates with adverse clinical features such as higher distant metastasis rates, therapy resistance, or poorer survival (122, 124, 127, 132). Conversely, in lung adenocarcinoma, MECOM downregulation was associated with poorer prognosis and links to immune cell infiltration, suggesting roles in tumour-immune crosstalk (120). Mechanistic studies consistently report that reducing MECOM/EVI1 expression reduces tumour growth by attenuating cancer stem cell properties (121), while overexpression promotes EMT, stemness, and therapy resistance (126, 127). Prostate cancer studies identify EVI1 as a driver of progression and therapy resistance, with knockdown impairing proliferation, migration and anchorage-independent growth (125). In glioblastoma, MECOM overexpression correlates with unfavourable prognosis (124); and in hepatobiliary cancers, EVI1 is linked to aggressive behaviour in intrahepatic cholangiocarcinoma (122) and antagonises TGF-β–mediated growth inhibition in hepatocellular carcinoma, implying escape from tumour-suppressive signalling (123). Collectively, these data point to a conserved oncogenic role in which inappropriate expression of MECOM/EVI1 supports lineage plasticity, EMT/cancer stem cell phenotypes, and stress-adaptive survival. Notably, most solid tumour studies do not resolve isoform-specific contributions (MECOM vs EVI1), potentially contributing to occasions of conflicting results across the literature. Given its established role in hematologic malignancies and emerging evidence in solid tumours, an important question is whether MECOM exerts similar context-dependent functions in melanoma, a cancer which can involve profound phenotypic switching and transcriptional reprogramming.

### *1.3.3 MELANOMA*

Building on its established role as a lineage-specific transcription factor that promotes dedifferentiation and plasticity in other solid tumours, MECOM may exert similar context-dependent functions in melanoma. As previously mentioned, *MECOM* was found to be the most frequently mutated gene in 36.8% (14/38) of melanoma cases (21). Similarly, it is one of the most commonly mutated genes in a cohort of publicly available melanoma samples with 24% (88/363) of samples bearing a *MECOM* mutation; *MECOM* is more commonly mutated in melanoma than other types of cancers across the large Project GENIE dataset (data publicly accessible via http://www.cbioportal.org/; Figure 3).

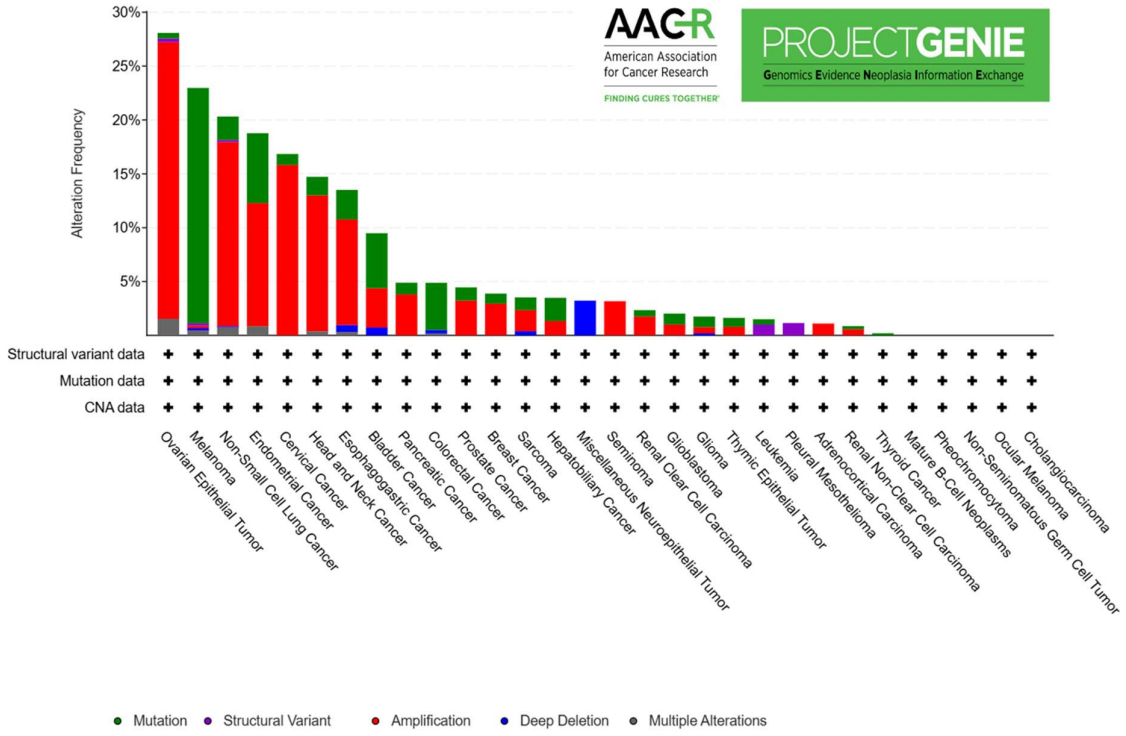


**FIGURE 3. FREQUENCY OF *MECOM* ALTERATIONS ACROSS CANCER TYPES IN AACR PROJECT GENIE DATASET. Bar plots depict the alteration frequency of *MECOM* in multiple cancer types, based on data from the AACR Project GENIE consortium. Alterations include mutations (green), structural variants (purple), amplifications (red), deep deletions (blue), and multiple alterations (grey). Cancer types are displayed along the x-axis, and alteration frequency (%) is shown on the y-axis. The presence of structural variant, mutation, and copy number alteration (CNA) data for each cancer type is indicated by plus signs below the bars. Data were obtained from cbioportal (https://www.cbioportal.org/) using the GENIE dataset.**

Consistent with this, large-scale mutation mapping from AACR Project GENIE demonstrates that *MECOM* mutations are dispersed across the coding sequence, with recurrent hotspots such as G799E (Figure 4). The predominance of missense variants and their wide distribution suggest functional heterogeneity, reinforcing the need to investigate context-dependent roles of MECOM in melanoma. Further, the sequenced mutations in *MECOM* predominately carried a UVB-signature of C → T transitions, providing a link between the primary environmental risk factor for melanoma (UV radiation) and epigenetic regulator mutations in the pathogenesis of melanoma (21).

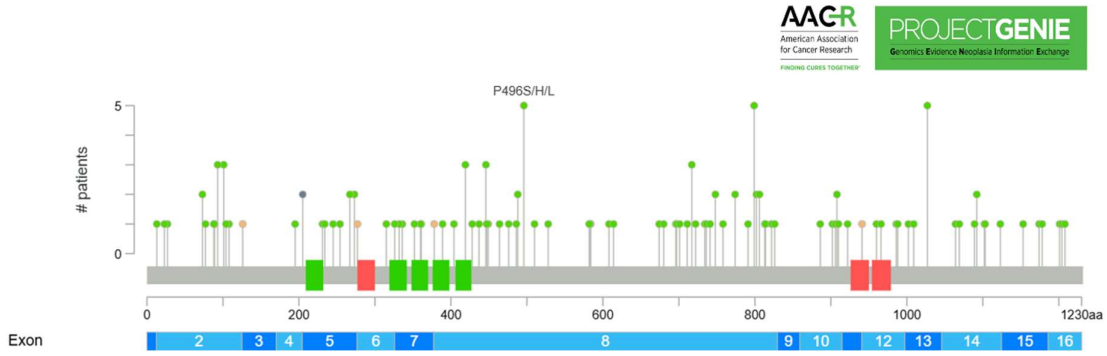


**FIGURE 4. LOLLIPOP PLOT ILLUSTRATING THE LOCATION AND FREQUENCY OF *MECOM* CODING MUTATIONS ACROSS THE PROTEIN (PROJECT GENIE).**

**Each vertical line represents a distinct variant, with the height corresponding to the number of patients harbouring that mutation (n = 134 mutations; n = 441 patients). Green circles denote missense mutations, orange circles indicate nonsense or splice-site variants, and red boxes highlight functional domains within *MECOM*. The corresponding exons are shown below. Data were aggregated from the AACR Project GENIE consortium.**

Unpublished results from the Tiffen lab utilising data from a collection of over 50 patient derived melanoma cell lines and The Cancer Genome Atlas (TCGA SKCM, http://www.cbioportal.org/) demonstrate significantly higher *MECOM* expression in dedifferentiated melanoma compared with the other subtypes (Figure 5). SOX10, another transcription factor and major driver of melanocyte differentiation from progenitor cells and melanoma phenotype switching (133), has been found to be poorly expressed in dedifferentiated melanoma, but highly expressed in the more differentiated subtypes (19). Again, drawing on expression data, preliminary results demonstrate the strongly inverse relationship between MECOM and SOX10 expression across the differentiation states of melanoma (Figure 5). This inverse relationship, coupled with emerging evidence of a physical interaction between MECOM and SOX10 (134), suggests a cooperative mechanism in promoting dedifferentiation.

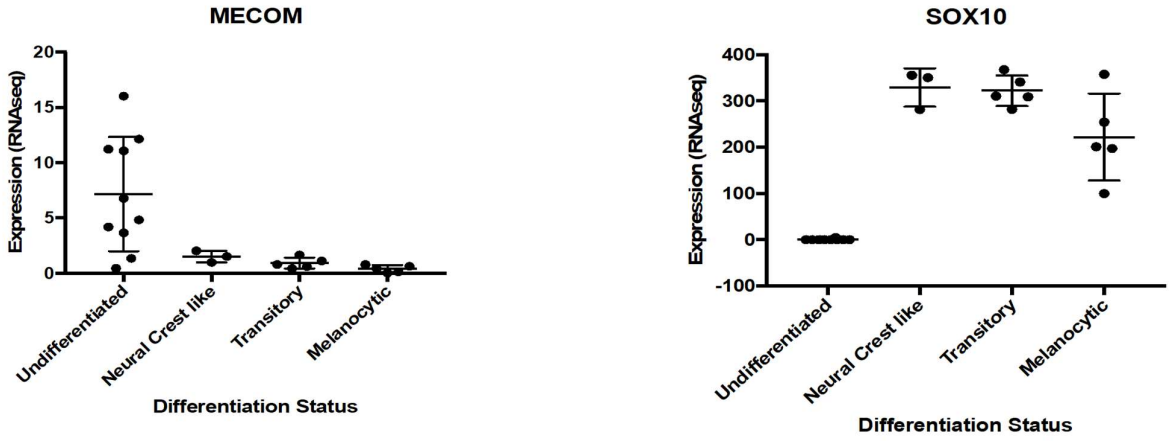


**FIGURE 5. *MECOM* AND *SOX10* EXPRESSION ACROSS MELANOMA DIFFERENTIATION STATES.**

**RNA-seq expression values (FPKM) from >50 patient-derived melanoma cell lines and TCGA SKCM samples were analysed to compare transcription factor expression across melanoma subtypes classified by differentiation state**

**(melanocytic, transitory, neural crest-like, and undifferentiated). *MECOM* is significantly higher in undifferentiated melanoma compared to other subtypes, while *SOX10* shows the opposite trend, being highest in melanocytic and lowest in undifferentiated states. Unpublished data, Tiffen Lab, Centenary Institute.**

A large-scale analysis of 1,048 melanomas identified *MECOM* as the most frequently co-mutated gene alongside *BRAF*, with co-mutation conferring improved clinical response to immunotherapy compared with wild-type *MECOM/BRAF* mutation (135). Across the entire cohort, MECOM mutations were associated with improved progression-free and overall survival, raising the possibility that MECOM status could serve as a biomarker for immunotherapy responsiveness. Despite these associations, the functional consequences of *MECOM* dysregulation in melanoma remain poorly defined.

## 1.4 Rationale, Hypotheses and Aims

Melanoma progression and therapeutic resistance are strongly influenced by cellular plasticity, whereby tumour cells adopt a spectrum of differentiation states ranging from melanocytic to dedifferentiated phenotypes. Transcriptional profiling studies have demonstrated that melanomas can be classified along this differentiation continuum, with distinct gene expression signatures corresponding to undifferentiated, neural crest-like, transitory, and melanocytic states (19). Importantly, progressive dedifferentiation has been associated with resistance to both targeted therapy and immunotherapy, suggesting that differentiation state modulates therapeutic vulnerability (19, 136).

While phenotype switching is most rigorously defined through transcriptional or epigenomic profiling, functional characteristics such as proliferation, migration, clonogenic capacity, and drug sensitivity have been shown to differ systematically between melanocytic and dedifferentiated melanoma states (19, 137). These phenotypic behaviours therefore provide informative, albeit indirect, readouts of differentiation-associated cell behaviour.

Epigenetic regulators are well positioned to influence melanoma plasticity by modulating broad transcriptional programs rather than single oncogenic pathways. Melanoma exhibits a high frequency of genetic alterations in epigenetic regulators, underscoring their potential contribution to disease progression and therapy resistance (21). Among these, the MDS1 and EVI1 complex locus (MECOM) has emerged as a recurrently altered transcriptional regulator, with mutations reported in melanoma patient samples (21). This is supported by analyses of publicly accessible datasets available via cBioPortal (Figure 3). In other cancer contexts, MECOM has been implicated in regulating cellular identity, differentiation, and survival (Section 1.3 The *MDS1* and *EVI1* complex locus and cancer); however, its functional relevance in melanoma remains poorly characterised.

Based on these observations, MECOM represents a plausible candidate regulator of melanoma differentiation-associated behaviour. However, whether MECOM actively drives melanoma phenotype switching, modulates specific functional traits associated with dedifferentiation, or acts in a highly context-dependent manner remains unknown. Addressing this knowledge gap requires functional

interrogation of MECOM perturbation across melanoma models representing diverse differentiation states, as well as examination of its clinical associations in patient-derived datasets.

### 1.4.1 Hypotheses

We hypothesise that MECOM contributes to differentiation-associated melanoma cell behaviour. Specifically, we propose that altering MECOM expression will modulate functional phenotypic traits linked to melanoma differentiation state, such as proliferation, migration, clonogenic capacity, and therapeutic sensitivity. Further, we hypothesise that MECOM expression or mutation status may associate with clinically relevant features in melanoma patient cohorts.

### 1.4.2 Aims

The overarching aim of this thesis is to investigate the functional and clinical relevance of MECOM in melanoma in the context of cellular phenotype and therapeutic response.

This will be addressed through the following objectives:

1) To develop melanoma cell line models with altered MECOM expression, using knockdown and overexpression approaches in cell lines representing diverse differentiation contexts.
2) To assess the impact of MECOM perturbation on differentiation-associated functional behaviours, including proliferation, migration, clonogenicity, anchorage-independent growth, and sensitivity to therapeutic agents with known differentiation-dependent effects.
3) To examine associations between MECOM expression or mutation status and clinical outcomes, immune-related features, and pathway-level signatures using publicly available melanoma datasets.

Together, these studies aim to clarify whether MECOM modulates phenotypic traits linked to melanoma differentiation state and to evaluate its potential relevance as a context-dependent biomarker.

# CHAPTER 2: METHODS

## 2.1 CELL LINES

The patient derived stage III and IV melanoma cell lines used in this study (Table 2) were provided by Professor Nicholas Hayward, QIMR Berghofer, Queensland (138, 139), and selected based on high or low *MECOM* expression (Chapter 3, Figure 8). *MECOM* expression had been previously characterised by RNA sequencing (GSE140673). Human embryonic kidney (HEK293T) cells were obtained from the Gene and Stem Cell Therapy lab at the Centenary Institute.

All human cell lines were authenticated by short tandem repeat profiling (Westmead Genomics Facility, Australia) and were confirmed mycoplasma-free prior to and during this work by in house PCR testing.

**TABLE 2. MELANOMA CELL LINES USED IN STUDY.**

| Cell Line | Primary Site | Cell Line Source | Patient Sex (age) |
|---|---|---|---|
| C001M | Right calf | Right calf nodule | F (50) |
| C002M | Right upper leg | Right thigh | M (60) |
| D22M | Right shoulder | Right shoulder | M (49) |
| D23M | N/A | Subcutaneous | M (30) |
| D38M | Occult primary | Right calf lymph node | M (50) |

## 2.2 CELL MAINTENANCE

Melanoma cell lines were cultured in monolayers in Roswell Park Memorial Institute Medium (RPMI) 1640 (Gibco, Thermofisher, North Ryde, Australia), supplemented with 10% (v/v) foetal bovine serum (FBS; Hyclone, GE Life Sciences, Australia) and 1% (v/v) penicillin (100 IU/mL)/streptomycin (100 µg/mL; Sigma-Aldrich, Australia). HEK293T cells were cultured in Dulbecco's modified Eagle's medium (DMEM; 4500 mg/L D-glucose, 110 mg/L sodium pyruvate, essential and non-essential amino acids), supplemented with 10% (v/v) FBS and 1% (v/v) penicillin (100 IU/mL)/streptomycin (100 µg/mL; Sigma-Aldrich, Australia). Cells were incubated at 37ºC in a humidified atmosphere of 5% $CO_2$ and 95% air in a cell culture incubator (Binder, Germany). Cells were trypsinised and sub-cultured every 4-10 days using 2.5% trypsin (10× stock; Thermo Fisher Scientific) when approximately 80% confluency had been reached, for a maximum of 20 passages.

## 2.3 GENERATION OF INDUCIBLE MECOM KNOCKDOWN IN MELANOMA CELL LINES

### *2.3.1 VECTOR CONSTRUCTS*

Customised lentiviral vectors expressing *MECOM*-specific short hairpin RNA (shRNA) constructs, along with a non-targeting control shRNA (scramble), were purchased from VectorBuilder (Chicago, IL). Each vector contains the shRNA sequence (Table 3) positioned downstream of LacO operator sites and upstream of a LacI repressor sequence, which is co-expressed with a puromycin resistance gene (Figure 6).

**TABLE 3. DETAILS OF SHRNA CONSTRUCTS USED IN KNOCKDOWN EXPERIMENTS.**

| Vector Name | shRNA Sequence | Target |
|---|---|---|
| Scramble shRNA | CCTAAGGTTAAGTCGCCCTCG | - |
| hMECOM shRNA#1 | GCACTACGTCTTCCTTAAATA | Exon 8 |
| hMECOM shRNA#2 | TTAACTGGAAGTCCAATTTAA | Exon 6 |
| hMECOM shRNA#3 | CTCAATCAATGTACCCATTTC | Exon 8 |

This inducible system leverages the interaction between LacI and LacO, derived from the bacterial lactose operon, to regulate shRNA expression. In the absence of the lactose analogue isopropyl-ß-D-thiogalactoside (IPTG), LacI binds to LacO and represses transcription. Upon IPTG addition, LacI dissociates from LacO, allowing transcription of the shRNA sequence. Puromycin selection enables enrichment of successfully transduced cells.

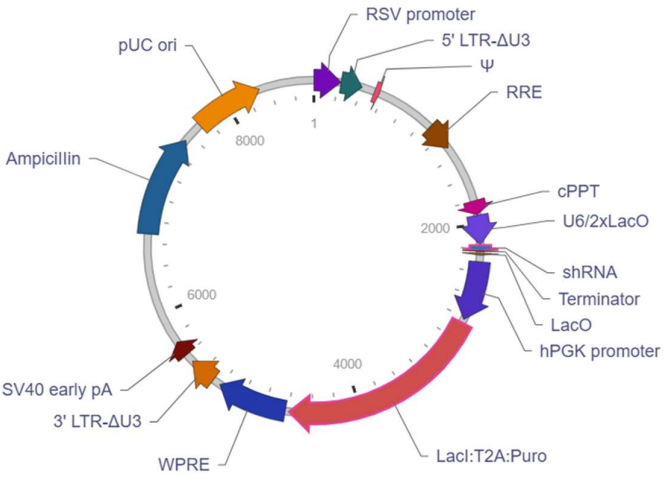


**FIGURE 6. REPRESENTATIVE VECTOR MAP OF PLASMIDS ENCODING IPTG-INDUCIBLE SHRNA CONSTRUCTS (ADAPTED FROM VECTORBUILDER.COM).**

### *2.3.2 Cell Transfection and Virus Packaging*

HEK293T cells (1 x$10^7$) were seeded into T175 flasks and transfected the following day using the calcium-phosphate method. One hour prior to transfection, cells were treated with 25μM chloroquine in antibiotic-free DMEM to enhance transfection efficiency (140). Lentiviral packaging plasmids pMD2-VSV-G (Addgene #12259), pRSV-Rev (Addgene #12253), and pMDLg/pRRE (Addgene #12251) along with each of the shRNA-expressing transfer vectors (Table 2.3) were heated at 65°C for 10 minutes to dissociate aggregates. Each of the transfer vectors along with the envelope/packaging vectors were then mixed with 2.5 M calcium chloride and 1/10 Tris-HCl/EDTA buffer and added dropwise to 300 mM phosphate/HEPES buffer under vortexing. The final mixture was added to cells and incubated overnight at 37°C, 5% $CO_2$.

After 16 hours incubation, the medium was replaced with complete DMEM containing 5 mM sodium butyrate and incubated for a further 48 h. Virus-containing supernatant was collected 72 h post-

transfection, centrifuged (5 min, 1,500 rpm), filtered (0.45 µm PVDF), and concentrated by ultracentrifugation (2 h, 26,000 rpm, 4°C). Viral pellets were resuspended in DMEM at 1/100th the original volume, incubated at 4°C for 2 hours, snap-frozen in liquid nitrogen, and stored at −80°C.

**TABLE 4. PLASMIDS USED IN TRANSFECTION FOR GENE KNOCKDOWN STUDIES.**

| Plasmid Type | Plasmid Name | Plasmid Amount (µg) | Functional Elements Encoded |
|---|---|---|---|
| Transfer | pLV[shRNA]-LacI/Puro-U6/2xLacO>Scramble_shRNA | 29.5 | Scramble shRNA |
| | pLV[shRNA]-LacI:T2A:Puro-U6/2xLacO >hMECOM[shRNA#1] | | hMECOM shRNA#1 |
| | pLV[shRNA]-LacI:T2A:Puro-U6/2xLacO >hMECOM[shRNA#2] | | hMECOM shRNA#2 |
| | pLV[shRNA]-LacI:T2A:Puro-U6/2xLacO >hMECOM[shRNA#3] | | hMECOM shRNA#3 |
| Envelope | pMD2-VSV-G | 4.9 | **VSV-G**: envelope G protein from vesicular stomatitis virus; enables pseudotyping for broad host cell entry |
| Packaging | pRSV-Rev | 3.9 | **Rev**: HIV-1 Rev protein (exons 2–3) under RSV U3 promoter; facilitates nuclear export of viral RNA via RRE binding |
| | pMDLg/pRRE | 12.7 | **gag**: core structural proteins of the virion<br>**pol**: retroviral enzymes (e.g., reverse transcriptase, integrase)<br>**RRE**: Rev Response Element; facilitates nuclear export of viral RNA via Rev protein |

### *2.3.3 Melanoma Cell Transduction*

Melanoma cells ($1.5 \times 10^5$) from the D22M, D38M, and D23M cell lines were seeded in quintuplicate T25 flasks and treated with 8 µg/mL polybrene (Sigma-Aldrich, Australia) to enhance viral uptake (141). Each cell line was transduced with 10 µL of lentiviral supernatant containing one of the following constructs: scramble shRNA, hMECOM shRNA#1, hMECOM shRNA#2 or hMECOM shRNA#3. One flask per cell line was retained as a polybrene-only negative control. Media was replaced 16 hours post-

transduction to mitigate polybrene-associated cytotoxicity. The scramble shRNA served as the primary matched control for all knockdown experiments performed under IPTG-induction conditions.

### *2.3.4 Cell Selection and Puromycin Dose Optimisation*

To determine the optimal puromycin concentration for selecting transduced cells, a kill curve assay was performed prior to transduction for each melanoma cell line. Cells ($1 \times 10^3$) were seeded into white 96-well plates and treated the following day with 100 µL of medium containing puromycin at 0, 0.5, 1, 2, 5, or 10 µg/mL (Sigma-Aldrich). After 72 hours of incubation, cell viability was assessed using CellTiter-Glo 2.0® (Promega, Alexandria, Australia), diluted 1:5 in 0.2% (w/v) Triton-X buffer. Plates were incubated for 10 minutes at room temperature, and luminescence was measured using a POLARstar Omega plate reader (BMG LABTECH, Australia). Growth curve analysis was performed in GraphPad Prism (v10.6.1), with luminescence values normalised to Day 0 readings.

Three days following transduction, cells were treated with puromycin at optimised concentrations (2 µg/mL for D38M, and 1 µg/mL for D22M and D23M) until death of all cells in the polybrene-only control flasks. Surviving cells were maintained in culture at half the optimised puromycin dose to maintain selective pressure and passaged upon reaching ~80% confluency.

### *2.3.5 IPTG Optimisation of Knockdown*

To optimise IPTG-induced shRNA expression, transduced melanoma cells ($1 \times 10^6$) were seeded into 6-well plates with 2 mL of medium containing 0, 0.5, or 1.0 mM IPTG. Fresh IPTG-containing medium was replenished every 48 hours. Cells were harvested at 48- and 96-hour timepoints, and pellets collected for downstream analysis (Section 2.4.1). Based on knockdown efficiency, 1.0 mM IPTG was selected for all subsequent experiments.

## 2.4 Generation of Inducible MECOM Overexpression in Melanoma Cell Lines

### *2.4.1 Vector Constructs*

Customised lentiviral vectors employing a dual tetracycline-inducible system were obtained from VectorBuilder (Chicago, IL). This system comprises two components (Table 5):

- Regulatory vector (Figure 7A): Encodes the tetracycline-controlled transcriptional silencer (Tts), the reverse tetracycline transactivator M2 (rtTA), and a hygromycin resistance gene. Transduction with this vector enables selection via hygromycin and facilitates inducible gene expression in response to tetracycline or its analogues.
- Expression vector (Figure 7B): Encodes either FLAG-tagged MECOM and mCherry under the control of a tetracycline response element (TRE) promoter, or FLAG-tagged mCherry alone (empty vector control). Transduced cells can then be selected by fluorescence-activated cell sorting (FACS) for mCherry expression using flow cytometry.

Successful overexpression requires co-transduction with both vectors and exposure to tetracycline or its analogues to activate transcription from the TRE promoter. The FLAG/mCherry-only construct was

used as a vector control to account for lentiviral transduction, antibiotic selection, and fluorescent sorting effects independent of MECOM expression.

**TABLE 5. VECTORS UTILISED IN INDUCIBLE MODELS OF MECOM OVEREXPRESSION.**

| Vector Type | Plasmid Name | Functional Elements Encoded |
|---|---|---|
| Regulatory | pLV[Exp]-CMV>tTS/rtTA/Hygro | **tTS**: Transcriptional silencer that binds TRE to suppress gene expression in the absence of tetracycline<br>**rtTA(M2)**: Activates TRE-driven transcription in the presence of tetracycline<br>**Hygro**: Hygromycin resistance gene for selection |
| Expression (MECOM) | pLV[Exp]-mCherry-TRE>FLAG/hMECOM[NM_004991.4] | **TRE**: Tetracycline-responsive promoter regulated by tTS/rtTA<br>**FLAG/hMECOM**: N-terminal FLAG-tagged human MECOM coding sequence<br>**mCherry**: Red fluorescent protein for selection via FACS |
| Expression (Control) | pLV[Exp]-CMV>FLAG/mCherry | **FLAG/mCherry**: N-terminal FLAG-tagged mCherry under constitutive CMV promoter; used as empty vector control |

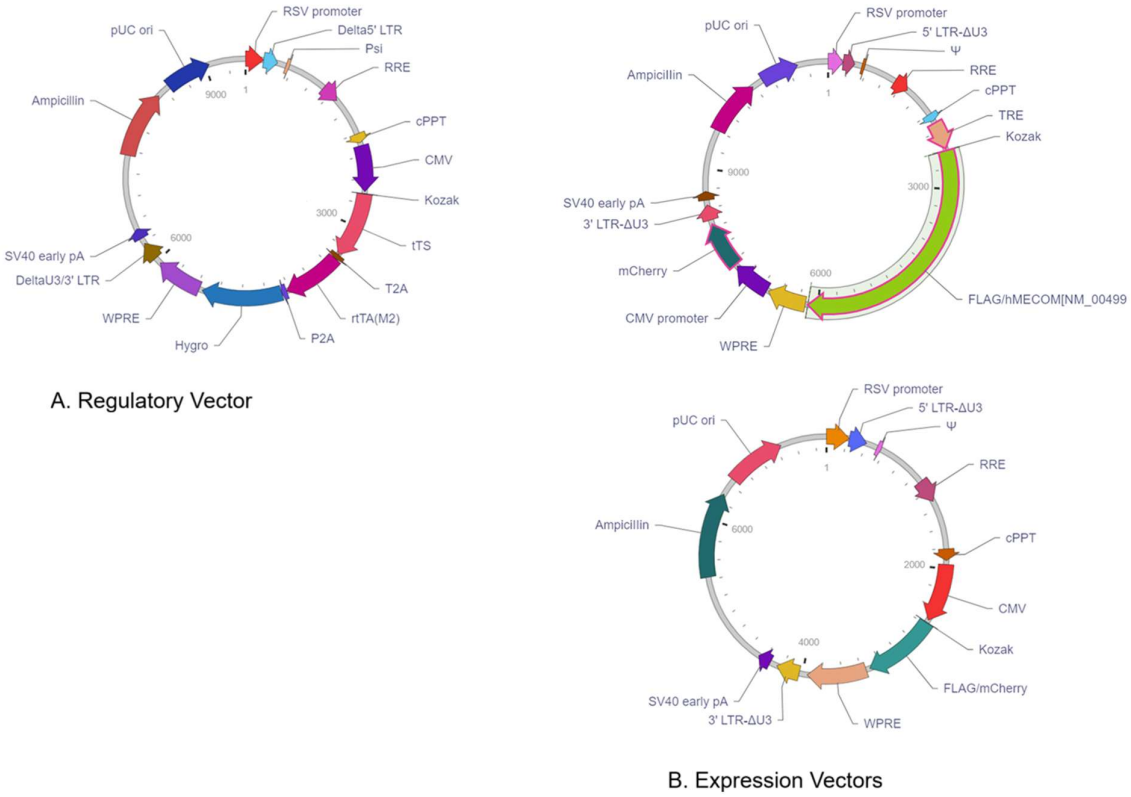


**FIGURE 7. VECTOR MAPS FOR INDUCIBLE OVEREXPRESSION VECTORS (ADAPTED FROM VECTORBUILDER.COM).**

Vectors were provided as glycerol stocks by the supplier and streaked for culture onto Luria Broth (LB)-agar plates containing 100 µg/mL ampicillin (15 g agar + 1 L LB medium). Plasmid DNA was extracted using the QIAprep Spin Miniprep Kit (QIAGEN) and submitted for Sanger sequencing (Macrogen, South Korea). Upon sequence confirmation, cultures were scaled up and plasmids extracted using the QIAGEN Plasmid Midi Kit. DNA yield was quantified by spectrophotometry at 260 nm using a Nanodrop (Thermo Fisher, Australia).

### *2.4.2 Cell Transfection and Virus Packaging*

Cell transfection and virus packaging was performed as described in Section 2.3.2 in HEK293T cells by the calcium phosphate precipitation method, with the transfer plasmids those outlined in Table 5 (Section 2.4.1).

### *2.4.3 Melanoma Cell Transduction*

Both sequential and co-transduction approaches were trialled using the dual tetracycline-inducible system. For sequential transduction, melanoma cells ($1.5 \times 10^5$) from the C001M and C002M cell lines were seeded in duplicate T25 flasks and treated with 8 µg/mL polybrene (Sigma-Aldrich, Australia). Each cell line was transduced with 10 µL of lentiviral supernatant containing the tTS/rtTA/Hygro construct, while the second flask served as a polybrene-only negative control. Following hygromycin

selection (Section 2.4.4), cells were re-seeded at the same density and transduced with 10 µL of lentiviral supernatant containing either the FLAG/hMECOM or FLAG/mCherry construct.

For co-transduction, melanoma cells ($1.5 \times 10^5$) from the same lines were seeded in triplicate T25 flasks and treated with polybrene. Two flasks were transduced with 10 µL of lentiviral supernatant containing the tTS/rtTA/Hygro construct, with one simultaneously receiving 10 µL of FLAG/hMECOM lentivirus and the other 10 µL of FLAG/mCherry lentivirus.

For all transductions, media was replaced 16 hours post-infection to mitigate polybrene-associated cytotoxicity.

### *2.4.4 Cell Selection and Hygromycin Dose Optimisation*

To determine the optimal hygromycin concentration for selecting transduced cells, a kill curve assay was performed for the C001M melanoma cell line. The hygromycin dose for C002M had been previously optimised within the same laboratory. C001M cells ($1 \times 10^3$) were seeded into white 96-well plates and treated the following day with 100 µL of medium containing hygromycin at 0, 50, 100, 200, or 500 µg/mL (Sigma-Aldrich). Treatments were refreshed every 48–72 hours. Cell viability was assessed at 7 and 14 days using CellTiter-Glo 2.0® (Promega, Alexandria, Australia), diluted 1:5 in 0.2% (w/v) Triton-X buffer. Plates were incubated for 10 minutes at room temperature, and luminescence was measured using a POLARstar Omega plate reader (BMG LABTECH, Mornington, Australia). Growth curve analysis was performed in GraphPad Prism (v10.6.1), with luminescence values normalised to Day 0 readings.

Three days post-transduction, cells were treated with hygromycin at the optimised concentrations of 200 µg/mL for C002M and 100 µg/mL for C001M. Selection was continued until complete cell death was observed in the polybrene-only control flask. Surviving transduced cells were maintained in culture under half the optimised hygromycin dose to preserve selective pressure and were passaged upon reaching ~80% confluency.

### *2.4.5 Fluorescence-activated cell sorting*

Following expansion, both sequentially and co-transduced melanoma cells were washed with PBS, detached using trypsin, and pelleted by centrifugation at 1,500 rpm at room temperature. Cell pellets were resuspended in cell sorting buffer containing 2 µM EDTA at a ratio of 1 mL buffer per $1 \times 10^7$ cells. Fluorescent cells (mCherry positive) were sorted using a 561 nm laser on a FACS Influx system (Becton Dickinson, BD). Sorted populations were expanded in culture and confirmed to exceed 90% purity based on post-sort analysis.

### *2.4.6 Tetracycline Optimisation of Overexpression*

Following the above transduction and sorting, C001M and C002M cells were seeded at a density of $3 \times 10^5$ in T25 flasks and allowed to adhere for 24 hours. Cells were then treated with tetracycline hydrochloride at 0, 1, or 2 µg/mL for 72 hours, with daily media changes and reapplication of the inducer. As no detectable MECOM overexpression was observed by Western blotting, alternative induction conditions were trialled. These included treatment with anhydrotetracycline hydrochloride at 50, 100, or

250 ng/mL, and co-treatment with either tetracycline hydrochloride or anhydrotetracycline hydrochloride (at the highest tested dose) combined with 1 mM sodium butyrate. Sodium butyrate has been demonstrated to improve expression of tetracycline-inducible vectors (142). The combination of 250 ng/mL anhydrotetracycline hydrochloride and 1 mM sodium butyrate produced the most consistent MECOM expression and was selected for all subsequent experiments.

Given the known pleiotropic effects of sodium butyrate on chromatin accessibility and gene expression, all phenotypic data generated using inducible overexpression models were interpreted cautiously and compared against matched vector controls exposed to identical induction conditions.

## 2.5 Generation of Constitutive MECOM Overexpression in Melanoma Cell Lines by Cloning

### *2.5.1 Primer Design*

Primers targeting the FLAG/hMECOM sequence in the VectorBuilder overexpression construct were designed using SnapGene software (www.snapgene.com). The construct had been previously validated by Sanger sequencing within the same laboratory to confirm the MECOM nucleotide sequence.

Primers were designed to amplify a 3,753 bp region encompassing the Kozak initiation sequence, N-terminal FLAG tag, and the full MECOM coding sequence. Restriction sites for EcoRI and HpaI were incorporated to facilitate directional cloning.

Two forward primers were designed:

MECOM_FWD_1: TAT TAC TAG AAT TCG ACT ACA AAG ACG ATG ACG ACA AGA TG

MECOM_FWD_2: TAT TAC TAG AAT TCG CCA CCA TGG ACT ACA AAG ACG

A single reverse primer was used for all reactions:

MECOM_HpaI_Rev: TAT TAC TAG TTA ACT CAT ACG TGG CTT ATG GAC TGG

Primers were complementary to the 5′ (forward) and 3′ (reverse) regions of the FLAG/hMECOM insert, enabling amplification for downstream validation and cloning applications. All primers were screened for secondary structures and GC content using the Integrated DNA Technologies (IDT) OligoAnalyzer™ Tool (https://sg.idtdna.com/pages/tools/oligoanalyzer) to optimise amplification efficiency. Primers were synthesized by IDT (Iowa, USA).

### *2.5.2 Polymerase chain reaction*

Polymerase chain reactions (PCR) were carried out in 20 µL volumes using Bio-Rad iProof High-Fidelity DNA Polymerase (0.02 U/µL), 1× iProof HF Buffer, 200 µM each dNTP, 0.5 µM forward and reverse primers (2.5.1 Primer Design), and 270 ng of plasmid DNA template (pLV[Exp]-mCherry-

TRE>FLAG/hMECOM[NM_004991.4]). Reactions were run in quintuplicate on a Bio-Rad MyCylcer thermalcycler with the following cycling conditions: initial denaturation at 98 °C for 1 min; 35 cycles of 98 °C for 10 s, 55 °C for 30 s, and 72 °C for 1 min; followed by a final extension at 72 °C for 10 min. A negative (no template) control was included.

### *2.5.3 Gel extraction of MECOM insert*

The PCR products from each primer set were pooled and electrophoresed alongside a negative control and GeneRuler 1 kb DNA ladder on a 1% agarose gel containing SybrSafe (1 µL/mL). Gels were run at 80 V for 1 hour and briefly visualised under UV light using a ChemiDoc system to confirm product size. Target bands were sharply excised with a scalpel.

DNA extraction from gel slices was performed using the Qiagen QIAquick Gel Extraction Kit, following the manufacturer's protocol. DNA yield and purity were assessed by spectrophotometry at 260 nm using a NanoDrop spectrophotometer (Thermo Fisher Scientific, North Ryde, Australia).

### *2.5.4 Digestion and Ligation of Insert and Vector*

Cloning was performed using the FUW lentiviral plasmid backbone (Addgene #14882), in-frame with an upstream mCherry-P2A sequence. Both the vector (2 µg) and MECOM insert (550 ng) were sequentially digested with *HpaI* (NEB, R0105S) and *EcoRI* (NEB, R0101S) in CutSmart and NEB EcoRI buffers, respectively, following manufacturer protocols. To prevent re-ligation, the vector was treated with calf intestinal alkaline phosphatase (CIP; NEB, M0290) in CutSmart buffer.

Digested products were purified after each step using the Qiagen QIAquick PCR Purification Kit. DNA yield and purity were assessed by spectrophotometry at 260 nm using a NanoDrop (Thermo Fisher Scientific).

Ligation reactions (20 µL) were set up using 1 µL T4 DNA ligase, 1 µL 40 µM ATP, and 2 µL T4 DNA Ligase Buffer, with vector:insert molar ratios of 1:3, 1:5, and 1:7, targeting a total DNA amount of ~100 ng. Reactions were incubated overnight at 16 °C on a Bio-Rad MyCycler and stored at 4 °C. Prior to transformation, ligase was heat-inactivated at 65 °C for 10 min.

### *2.5.5 Transformation*

Transformation was performed using α-Select Competent Cells (Bioline, BIO-85027). Cells were thawed on wet ice, and 5 µL of each ligation reaction was added to 25 µL aliquots of competent cells. Positive (pUC19) and negative controls were included.

Mixtures were incubated on ice for 30 min, heat-shocked at 42 °C for 35 s, then returned to ice for 2 min. Transformed cells were diluted in SOC medium (2% tryptone, 0.5% yeast extract, 0.4% glucose, 10 mM NaCl, 2.5 mM KCl, 10 mM $MgCl_2$, 10 mM $MgSO_4$) and incubated at 37 °C with shaking (220 rpm) for 1 h. Cultures were plated on LB agar containing 100 µg/mL ampicillin and incubated overnight at 37 °C in 5% $CO_2$.

### 2.5.6 Colony Selection and Screening

Single colonies were picked from overnight LB agar plates using sterile pipette tips and used to inoculate LB agar patch plates containing 100 µg/mL ampicillin. Each colony was also briefly inoculated into PCR tubes containing 10 µL ultrapure water, which were boiled at 100 °C for 5 min to lyse cells. One microlitre of lysate was used as template for PCR screening of the MECOM insert, using the same primers and thermocycling conditions described in Sections 2.5.1 and 2.5.2. Reactions were performed in 10 µL volumes using Qiagen HotStarTaq DNA Polymerase (#203203) and 10× PCR Buffer.

A total of 150 colonies were screened. No positive clones were identified using the MECOM_FWD_1 primer. Two positive clones were identified using MECOM_FWD_2, both derived from the 3:1 vector-to-insert ligation reaction. These colonies (pFUW 10-8 and pFUW 11-3) were picked from their respective patch plates and inoculated into LB medium containing 100 µg/mL ampicillin, followed by overnight incubation at 37 °C with shaking at 200 rpm.

### 2.5.7 Plasmid Isolation, Sequencing and Sequence Alignment

Overnight cultures were used to prepare glycerol stocks (1:1 mixture of sterile 50% glycerol and culture medium, stored at −80 °C) and for plasmid isolation using the QIAprep Spin Miniprep Kit (Qiagen, #27104). Purified plasmids were submitted for Sanger sequencing (Macrogen, South Korea).

Sequences were aligned to the human *MECOM* mRNA reference sequence (NM_004991.4) using SnapGene (www.snapgene.com). Only clone pFUW 11-3 showed no mutations across the coding sequence and was selected for downstream experiments.

### 2.5.8 Cell Transfection and Virus Packaging

Cell transfection and virus packaging were performed in HEK293T cells using the calcium phosphate precipitation method, as described in Section 2.3.2. The cloned pFUW 11-3 plasmid and unaltered control pFUW plasmid were used as transfer plasmids.

### 2.5.9 Melanoma Cell Transduction and FACS Sorting

Melanoma cells ($5 \times 10^4$) from the C001M and C002M cell lines were seeded into six wells each of a 12-well plate and treated with 8 µg/mL polybrene (Sigma-Aldrich). For each cell line:

- Two wells served as polybrene-only controls.
- Two wells were transduced with 10 µL of viral supernatant containing the pFUW construct.
- Two wells were transduced with 20 µL of viral supernatant containing the pFUW 11-3 (hMECOM) construct.

Media was replaced 16 h post-infection to mitigate polybrene-associated cytotoxicity. Transduced cells were expanded to T175 flasks and sorted for mCherry-positive cells using a MA900 Cell Sorter (Sony), as described in Section 2.4.5. Sorted populations were expanded in culture and confirmed to exceed 90% purity based on post-sort analysis.

## 2.6 Validation of *MECOM* Knockdown Or Overexpression in Melanoma Cell Lines

To confirm successful *MECOM* knockdown or overexpression, melanoma cell lines were seeded, treated, and harvested under conditions specific to each cell line and perturbation strategy. Validation was performed using Western blotting.

### *2.6.1 Experimental Setup, Treatment Conditions and cell harvesting*

Transduced melanoma cells were seeded at optimised cell densities as described in Table 6. Following the treatment and incubation periods, cells were harvested by aspirating the culture medium, washing with phosphate-buffered saline (PBS), and applying trypsin solution. After 5 minutes of incubation at 37°C in a humidified 5% $CO_2$ atmosphere, detachment was confirmed by light microscopy. An equal volume of complete medium was added to neutralise trypsin activity. Cell suspensions were centrifuged at 1,500 rpm for 5 minutes at room temperature. Supernatants were aspirated, and pellets were washed once with PBS, followed by a second centrifugation under the same conditions. Final cell pellets were either stored at −80°C or processed immediately for downstream applications.

**TABLE 6. EXPERIMENTAL SETUP FOR VALIDATION EXPERIMENTS INVOLVING MECOM PERTUBATION (ATET, ANHYDROTETRACYCLINE; NAB, SODIUM BUTYRATE; IPTG, ISOPROPYL B-D-1-THIOGALACTOPYRANOSIDE.) ALL OVEREXPRESSION CONDITIONS INCLUDE MATCHED VECTOR CONTROLS SUBJECTED TO IDENTICAL INDUCTION REGIMENS (ATET AND/OR NAB), AND ALL KNOCKDOWN CONDITIONS INCLUDE SCRAMBLE SHRNA CONTROLS UNDER CORRESPONDING IPTG TREATMENT CONDITIONS.**

| MECOM Manipulation | Constructs | Cell Lines | Seeding Density of Each Construct | Treatment | Duration |
|---|---|---|---|---|---|
| Knockdown | shRNA#1, shRNA#2, shRNA#3, scramble shRNA | D22M | 3 x$10^5$ in T25 | IPTG 0.5 mM, 1 mM | 48 hrs, 72 hrs, 1 week |
| | | D23M | 1.5 x$10^5$ in T25 | | 48 hrs, 72 hrs, 1 week |
| | | D38M | 3 x$10^5$ in T25 | | 48 hrs, 72 hrs, 1 week |
| Inducible overexpression | FLAG/hMECOM, FLAG/mCherry | C001M | 3 x$10^5$ in 6 well plate | aTet 50 ng/mL, 100 ng/mL, 250 ng/mL and NaB 0 mM, 1 mM | 72 hrs, 1 week |
| | | C002M | 3 x$10^5$ in 6 well plate | | 72 hrs, 1 week |
| Constitutive overexpression | FLAG/hMECOM, mCherry empty | C001M | 3 x$10^5$ in 6 well plate | Nil | 72 hrs |
| | | C002M | 3 x$10^5$ in 6 well plate | | 72 hrs |

### 2.6.2 Whole Cell Lysate Preparation

Cell pellets were resuspended in ice-cold radioimmunoprecipitation assay (RIPA) buffer containing 0.1% SDS, 0.5% sodium deoxycholate, 150 mM NaCl, 50 mM Tris (pH 8.0), 1% (w/v) Triton X-100, and phenylmethylsulfonyl fluoride (PMSF). Samples were incubated on ice for 30 minutes, then centrifuged at 15,000 rpm for 30 minutes at 4°C. The resulting supernatants were collected and used for downstream analysis.

### 2.6.3 Protein Quantitation

Protein concentration was determined using the DC Protein Assay (Bio-Rad), a colorimetric assay based on the Lowry method. Assay reagents A and S were combined in a ratio of 1 mL Reagent A to 20 µL Reagent S immediately prior to use. For each sample, 4 µL of whole cell lysate was mixed with 25 µL of the A+S reagent mixture in a 96-well plate.

Samples were incubated at room temperature for 15 minutes. Absorbance was measured at 650 nm using a Byonoy Absorbance 96 plate reader (Byonoy, Hamburg, Germany). Protein concentrations were calculated by interpolation from a standard curve generated using bovine serum albumin (BSA) standards prepared in RIPA buffer. All calculations were performed in Microsoft Excel, and technical triplicates were averaged for downstream analysis.

### 2.6.4 SDS-Polyacrylamide Gel Electrophoresis (SDS-PAGE)

Protein samples (40 µg) were mixed with 2× Laemmli buffer containing 5% β-mercaptoethanol (Sigma-Aldrich), then boiled at 95 °C for 5 minutes to denature proteins. Samples were loaded onto freshly cast 4–12% gradient SDS-PAGE gels alongside a molecular weight marker (Bio-Rad Precision Plus Protein™ Kaleidoscope™, #1610375) and electrophoresed at 108 V for 2 hours.

Protein transfer to 0.45 µm nitrocellulose membranes was performed in transfer buffer either for 90 minutes at 100 V on ice or overnight at 15 V at 4 °C. Transfer efficiency was assessed using Ponceau S staining (Sigma-Aldrich).

### 2.6.5 Western Blotting

Membranes were briefly rinsed with TBS-T to remove residual Ponceau stain, then blocked with 5% skim milk in TBS-T for 90 minutes at room temperature to prevent non-specific binding. Blots were incubated with primary antibodies (Table 7) for 1 hour at room temperature or overnight at 4 °C in either 5% (w/v) skim milk/TBS-T or 5% (v/v) bovine serum albumin (BSA)/TBS-T, depending on antibody requirements.

Following three 10-minute washes in TBS-T, membranes were incubated with the appropriate HRP-conjugated secondary antibodies for 90 minutes (Bio-Rad). After a second round of washes, signal was developed using a luminol-based detection system (Bio-Rad Clarity Western ECL Substrate, #1705060) and imaged using the ChemiDoc MP system (Bio-Rad). Band intensities were quantified using Image Lab software (Bio-Rad). When performing validation using the anti-MECOM antibody in the overexpression systems, anti-FLAG Westerns were performed in parallel as orthogonal validation.

**TABLE 7. PRIMARY ANTIBODIES USED FOR WESTERN BLOT EXPERIMENTS. Details include antibody specificity, working dilution, supplier, catalogue number, host species, clonality, and approximate molecular weight of the target protein(s). Sizes reflect expected bands for MECOM isoforms (MECOM, EVi1, EVI1) and flag-tagged constructs in kilodaltons (kDa).**

| Specificity | Dilution | Supplier | Catalogue # | Species | Clonality | Size (kDa) |
|---|---|---|---|---|---|---|
| MECOM | 1:1000 | Cell Signaling | 2593 | Rabbit | Monoclonal | ~190 (MECOM);<br>145 (EVI1);<br>105 (EVI1Δ) |
| FLAG | 1:5000 | Sigma | A8592 | Mouse | Monoclonal | 30<br>(FLAG/mCherry);<br>~190 (FLAG/hMECOM) |
| α-tubulin | 1:5000 | Sigma | T5168 | Mouse | Monoclonal | 50 |

### *2.6.6 Construct Identity Verification by PCR*

To confirm correct construct assignment following an unexpected expression pattern, genomic DNA was extracted from transduced cell lines using Qiagen DNeasy Mini Kit (#69504). PCR amplification was performed using primers specific for mCherry and FLAG-tagged MECOM sequences to distinguish vector-derived MECOM from endogenous expression. Amplicons were visualized by agarose gel electrophoresis.

## 2.7 Cell Proliferation Assay

To assess the impact of MECOM perturbation on cell proliferation, assays were performed using transduced melanoma cell lines under defined treatment conditions. Cell viability was assessed at multiple timepoints using the CellTiter-Glo® 2.0 assay (see Section 2.3). Luminescence readings were averaged and normalised to Day 0 values using GraphPad Prism (v10.6.1) for growth curve analysis. Multiple unpaired two-tailed t-tests were performed comparing controls versus overexpression or knockdown cells at each timepoint. P-values were adjusted for multiple comparisons using the two-stage step-up method of Benjamini, Krieger, and Yekutieli (FDR control, Q = 0.05). Data are presented as mean values; replicate numbers are indicated in figure legends. Given variable biological replication across assays, effect sizes and consistency of trends across cell lines were given priority over statistical significance alone when interpreting results.

### *2.7.1 Knockdown Cell Lines*

Knockdown cell lines were pre-treated with IPTG for one week prior to induce knockdown prior to assay setup. Cells were seeded at a density of $1 \times 10^3$ cells per well in white 96-well plates containing 100 µL of IPTG-supplemented medium. Biological and technical triplicates were included for each condition. Plates were incubated at 37 °C in a humidified 5% $CO_2$ atmosphere, and medium was refreshed every two days. Endpoints were set at Days 0, 2, 4, and 7.

### *2.7.2 Constitutive Overexpression Cell Lines*

For constitutive overexpression cell lines, the assay was performed identically to the knockdown protocol, except without pre-treatment or ongoing exposure to IPTG. Cells were seeded into RPMI medium, which was replaced every two days. Endpoints were set at Days 0, 3, 5, and 7.

## 2.8 Wound Healing Assay

To assess the impact of MECOM knockdown on cell migration, wound healing assays were performed using IPTG-treated melanoma cell lines.

Induced cells were seeded at a density of $2 \times 10^5$ cells per well in 6-well plates containing 2 mL of RPMI medium supplemented with IPTG. Biological and technical triplicates were included for each condition. Plates were incubated at 37 °C in a humidified 5% $CO_2$ atmosphere until confluency was reached.

Wounds were introduced by manually scratching each well with a sterile P200 pipette tip in a cross pattern. Medium was replaced immediately following the scratch to remove debris and maintain IPTG exposure. Images of the same field of view were captured at 0 h and 24 h post-scratch using a Nikon Eclipse TS100 microscope (4× objective; Nikon, Rhodes, Australia).

Wound area was quantified using ImageJ software and normalised to the 0 h timepoint to assess relative closure. Technical triplicates were averaged within each biological duplicate. Unpaired two-tailed t tests were performed per cell line, and false discovery rate (FDR) was controlled at Q = 0.05 using the two-stage Benjamini–Krieger–Yekutieli (BKY) procedure implemented in Prism (GraphPad Prism v10.6.1).

### *2.8.1 Constitutive Overexpression Cell Lines*

For constitutive overexpression cell lines, the assay was performed identically to the knockdown protocol, except without pre-treatment or ongoing exposure to IPTG. Cells were seeded into RPMI medium, which was replenished post-scratch.

## 2.9 Colony Formation Assay

Colony formation assays were performed to assess long-term proliferative capacity following MECOM perturbation.

Cells were seeded at densities ranging from $0.5 \times 10^3$ to $1 \times 10^3$ cells per well (depending on cell line) in 12-well plates containing 1 mL of RPMI medium supplemented with IPTG. Biological and technical triplicates were included for each condition. Plates were maintained at 37 °C in a humidified 5% $CO_2$ atmosphere for 14–21 days, with medium replaced every two days.

For the over-expression model, cells were pre-treated for one week with 250 ng/mL anhydrotetracycline hydrochloride (aTet; Sigma-Aldrich) and 1 mM sodium butyrate (NaB; Sigma-Aldrich). Following pre-treatment, cells were seeded into 12-well plates containing RPMI medium supplemented with the same

drug concentrations. Untreated controls were included for comparison. The assay was otherwise performed identically to the knockdown protocol, with medium replaced every two days and incubation continued for 14–21 days.

### *2.9.3 Staining and Quantification*

At endpoint, medium was aspirated and wells were washed with ice-cold PBS. Cells were fixed with ice-cold methanol (Thermo Fisher Scientific) for 10 minutes, then stained with 0.5% (w/v) crystal violet (Sigma-Aldrich) in methanol for 20 minutes at room temperature. Excess stain was removed by washing with distilled water, and plates were allowed to dry overnight.

Plates were imaged using the ChemiDoc MP Imaging System (Bio-Rad), and colony quantification was performed using ImageJ software and OpenCFU (143). Colony counts were normalized to matched scramble controls within each biological replicate and treatment condition to account for batch variability. Normalized values were $\log_2$-transformed, and technical replicates were averaged to yield one value per biological replicate per condition prior to statistical analysis. For IPTG-dependent effects, a ΔΔ analysis was performed by subtracting the $\log_2$ fold change under basal conditions from that under IPTG induction for each biological replicate. One-sample t-tests were used to assess whether mean $\log_2$ fold changes (or ΔΔ values) differed from zero. Geometric mean fold changes (GMFC) and 95% confidence intervals were obtained by back-transforming $\log_2$ means and confidence bounds (antilog base 2).

## 2.10 Soft Agar Assay

Anchorage-independent growth was assessed using a soft agar colony formation assay in D22M, D23M, and D38M melanoma cell lines following MECOM knockdown.

A 2% agar stock solution was prepared by dissolving agar in deionised water and autoclaving at 120 °C for 30 minutes. For the base layer, 0.5% agar was prepared by mixing liquefied 2% agar with warm RPMI medium at a 1:3 ratio. A volume of 1.5 mL was pipetted into each well of 6-well plates and allowed to solidify at room temperature.

Cells were pre-treated with 1 mM IPTG for one week prior to assay setup. For each condition (IPTG-treated and untreated controls), cells were suspended in RPMI and mixed with warm 1.2% agar to achieve a final concentration of 5,000 cells per 1.5 mL in 0.3% agar. The cell-agar mixtures were layered onto the base agar in technical triplicate.

Plates were incubated at 37 °C in 5% $CO_2$ for 14–21 days. Only D23M cells demonstrated the ability to form spheroids suspended in soft agar. As a result, anchorage-independent growth analyses were limited to this model, and conclusions regarding MECOM perturbation effects on anchorage independence were confined to this cellular context.

For each well, five non-overlapping fields were imaged at ×4 magnification using brightfield microscopy (Nikon, Australia). Colonies were counted manually, normalized to imaged area, and averaged to yield a per-well colony density. To account for variability in absolute colony numbers between experiments, per-well values were normalized to the contemporaneous scramble control and expressed as $\log_2$ fold-change. Statistical analysis was performed on per-well normalized values using one-sample t-tests against zero (no change), with Benjamini–Krieger–Yekutieli correction for multiple comparisons.

## 2.11 Drug Sensitivity Testing

Previous work has suggested that dedifferentiated melanoma cells are more sensitive to inducers of ferroptosis than melanocytic cell lines (19). Therefore, we assessed changes in sensitivity to inducers of ferroptosis (Erastin, RSL-3) following perturbation of MECOM by knockdown or overexpression. Other drugs with known or proposed efficacy in melanoma were also tested, including a histone deacetylase inhibitor (Vorinostat), Bromodomain and Extra-Terminal motif (BET) inhibitors (JQ1 and ABBV-744), and BRAF inhibitors (dabrafenib and vemurafenib).

Baseline $IC_{50}$ values were determined in non-transduced parental cell lines. Cells were seeded at 1,000 cells per well in 96-well plates and treated with each drug across eight half-log concentrations (0.003 μM to 30 μM), selected based on reported effective ranges in melanoma cell culture. Treatments were applied in technical triplicate. After 72 hours, cell viability was assessed using the CellTiter-Glo® 2.0 assay (Section 2.3). Dose–response curves were fit using a log(inhibitor) vs. response model with variable slope in GraphPad Prism (v10.6.1), and $IC_{50}$ values were calculated by nonlinear regression. These data established baseline sensitivity profiles for undifferentiated versus melanocytic subtypes. Baseline $IC_{50}$ values were derived from single biological experiments and are therefore interpreted as reference profiles rather than definitive estimates of inter-experimental variability.

Pairwise comparisons of $\log IC_{50}$ values between cell lines were performed using extra–sum-of-squares F tests in Prism. To quantify effect size, differences in $\log IC_{50}$ ($\Delta \log IC_{50}$) were calculated by subtraction of best-fit values. Standard errors (SE) for each $\log IC_{50}$ were estimated from Prism's 95% confidence intervals using the formula:

$$SE = \frac{\text{Upper limit} - \text{Lower limit}}{2 \times 1.96}$$

The SE for each difference was computed by error propagation:

$$SE_{\Delta} = \sqrt{SE_1^2 + SE_2^2}$$

The 95% confidence interval for $\Delta \log IC_{50}$ was then calculated as:

$$\Delta \pm 1.96 \times SE_{\Delta}$$

Multiple comparisons were controlled using the Bonferroni method within each drug's family of planned pairwise tests (α = 0.05). Knockdown cell lines were pre-treated with 1 mM IPTG for one week prior to assay setup and tested using the same drug panel and concentration range as described above.

To test the hypothesis that phenotype switching alters ferroptosis sensitivity, constitutive and inducible MECOM overexpression cell lines were selectively treated with Erastin and RSL-3. Two concentrations (3 µM and 30 µM) were chosen based on parental cell line sensitivity. Assays were performed as described above, with viability assessed after 72 hours using CellTiter-Glo® 2.0. Technical triplicates were averaged within each biological replicate (bio n = 2 per group). Unpaired two-tailed t-tests were performed for each drug–dose comparison within each cell line. False discovery rate (FDR) was controlled at Q = 0.05 using the two-stage Benjamini–Krieger–Yekutieli (BKY) procedure implemented in GraphPad Prism (v10.6.1). Given the limited biological replication, these experiments were used to assess directional changes and consistency of response rather than to make definitive quantitative claims regarding drug sensitivity shifts.

## 2.12 Analysis of Publicly Available Clinical and Omics Data

To assess the clinical relevance of *MECOM* in advanced melanoma, publicly available datasets were analysed. These analyses aimed to explore associations between *MECOM* expression, mutational status, and patient outcomes following immune checkpoint therapy, as well as to investigate links with metastatic patterns, immune contexture, and oncogenic signalling pathways. The following subsections describe the data sources, preparation steps, and statistical methods used.

### *2.12.1 Data Source and cohort selection*

Clinical, genomic, and transcriptomic data were obtained from the publicly available cohort published by Liu et al. (144), comprising 144 patients with advanced melanoma treated with anti–PD-1 therapy (nivolumab or pembrolizumab). RNA-seq expression profiles were available for 121 patients, and whole-exome sequencing (WES) data for 124 patients. Clinical endpoints included progression-free survival (PFS), overall survival (OS), and best overall response (BOR) assessed by RECIST v1.1 criteria.

### *2.12.2 Data Preparation*

RNA-seq expression values for *MECOM* were reported in transcripts per million (TPM). For analyses treating *MECOM* expression as a continuous variable, values were transformed using $\log_2(\text{TPM} + 1)$ to reduce skew and stabilize variance. For categorical analyses, patients were stratified into HIGH MECOM and LOW MECOM groups using a median split of TPM values. Mutation status was derived from WES data; melanomas with one or more *MECOM* missense mutations were classified as *MECOM*-

mutant, and all others as wild-type. Data were organized and cleaned in Microsoft Excel, including calculation of $\log_2(TPM + 1)$ values and preparation of analysis tables.

### *2.12.3 Statistical Analyses*

All statistical analyses were performed in GraphPad Prism v10.6.1. Specific approaches included:

**Survival Analysis**: Kaplan–Meier curves were generated for PFS and OS. Survival distributions were compared using the logrank (Mantel–Cox) test. Hazard ratios (HR) and 95% confidence intervals (CI) were calculated for HIGH vs LOW MECOM expression and *MECOM*-mutant vs wild-type groups. Subgroup analyses excluded patients with prior MAPK inhibitor (MAPKi) therapy and stratified by prior CTLA-4 blockade (ipilimumab-naïve vs ipilimumab-experienced).

**Response Analysis**: Objective response rates (CR/PR vs SD/PD) were compared between HIGH and LOW MECOM groups using contingency tables. Associations were tested using Chi-square and Fisher's exact tests, with odds ratios (OR) and 95% CI reported.

**Clinical and Demographic Associations**: Differences in *MECOM* expression by sex and melanoma subtype were assessed using Mann–Whitney and Kruskal–Wallis tests, respectively. Correlation between *MECOM* expression and age was evaluated using Spearman's rank correlation. Hodges–Lehmann median differences and confidence intervals were reported for Mann–Whitney tests where applicable.

**Metastatic Patterns**: *MECOM* expression was compared between patients with versus without metastases at six anatomical sites (brain, lung, bone, liver/visceral, lymph node, and any distant site [i.e. not locally invasive or lymph node only]) using two-sided Mann–Whitney tests. False discovery rate (FDR) correction was applied across site comparisons. Presence of metastasis was also tested against HIGH/LOW MECOM status using Chi-square and Fisher's exact tests.

**Pathway and Immune Correlation Analyses**: Single-sample gene set enrichment analysis (ssGSEA) scores for immune-related signatures (e.g., interferon response, antigen presentation) and oncogenic programs (e.g., PI3K–AKT–mTOR, KRAS, EMT, TGFβ) were correlated with MECOM expression using Spearman's rank method. Immune cell composition was inferred using CIBERSORT LM22 applied to RNA-seq TPM data. Correlations between *MECOM* expression and estimated immune fractions (including total immune infiltrate and individual cell subsets) were assessed using Spearman's rank method. FDR correction was applied for multiple testing in correlation analyses.

**Significance Thresholds:** All tests were two-sided. A p-value $< 0.05$ was considered statistically significant. For multiple comparisons, FDR-adjusted p-values were calculated using the Benjamini–Hochberg procedure.

# CHAPTER 3: IMPACT OF MECOM DEPLETION ON PHENOTYPIC TRAITS AND THERAPEUTIC VULNERABILITY IN MELANOMA

## 3.1 INTRODUCTION

Phenotype switching between melanocytic and dedifferentiated states is a hallmark of melanoma plasticity, influencing progression, therapeutic resistance, and metastatic potential. Previous literature and preliminary data have implicated *MECOM* as a potential regulator of this process, with elevated *MECOM* expression associated with dedifferentiated phenotypes (see Section 1.3.3 Melanoma). However, the functional contribution of *MECOM* to melanoma phenotype dynamics has not been characterised.

This chapter investigated whether *MECOM* modulates melanoma phenotype switching through gene knockdown strategies in patient-derived melanoma cell lines. Five lines were selected to represent distinct differentiation states and *MECOM* expression levels, enabling bidirectional perturbation experiments (see also Chapter 4: MECOM Overexpression Reveals Context-Dependent Effects on Melanoma Cell Behaviour). We first established IPTG-inducible *MECOM* knockdown in dedifferentiated, high *MECOM* lines and validated suppression at the protein level. Functional assays, including proliferation, migration, clonogenicity, and anchorage-independent growth, were performed to assess the consequences of MECOM depletion on cell phenotype. Dedifferentiated melanoma are characteristically more invasive, and less proliferative, than their melanocytic counterparts (136). Therefore, we hypothesised that a phenotype switch from dedifferentiated to melanocytic following MECOM knockdown would lead to increased proliferation rate, with decreased migration, clonogenicity, and anchorage independent growth.

Finally, we examined whether MECOM knockdown altered sensitivity to clinically relevant drugs, focusing on ferroptosis inducers and epigenetic modulators previously shown to exhibit differentiation-dependent effects (19). We hypothesised that inducing a phenotype switch from dedifferentiated to more melanocytic would therefore decrease sensitivity to these agents. Together, these experiments aimed to clarify whether MECOM acts as a driver of melanoma plasticity and therapeutic vulnerability.

## 3.2 CELL LINE CHARACTERISTICS AND DIFFERENTIATION STATUS

To investigate the role of MECOM in melanoma phenotype switching, five patient-derived melanoma cell lines were selected based on a combination of MECOM expression level and previously assigned differentiation status. Differentiation states (melanocytic, transitory, neural crest-like or dedifferentiated) had been defined using transcriptomic analyses of existing RNA sequencing data, employing a principal component analysis–based framework consistent with that described by Tsoi et al. (2018). MECOM expression was characterised independently by RNA sequencing.

Using these criteria, C001M and C002M were classified as melanocytic models, whereas D22M, D23M, and D38M were classified as dedifferentiated models. The two selected melanocytic cell lines (C001M,

C002M) exhibited extremely low MECOM expression (FPKM < 0.02), while the three dedifferentiated cell lines (D22M, D23M, D38M) displayed substantially higher MECOM expression (Figure 8). This selection facilitated testing whether MECOM knockdown in dedifferentiated, high *MECOM* lines could promote a shift toward a melanocytic phenotype, and conversely, whether MECOM overexpression in melanocytic, low *MECOM* lines could induce dedifferentiation.

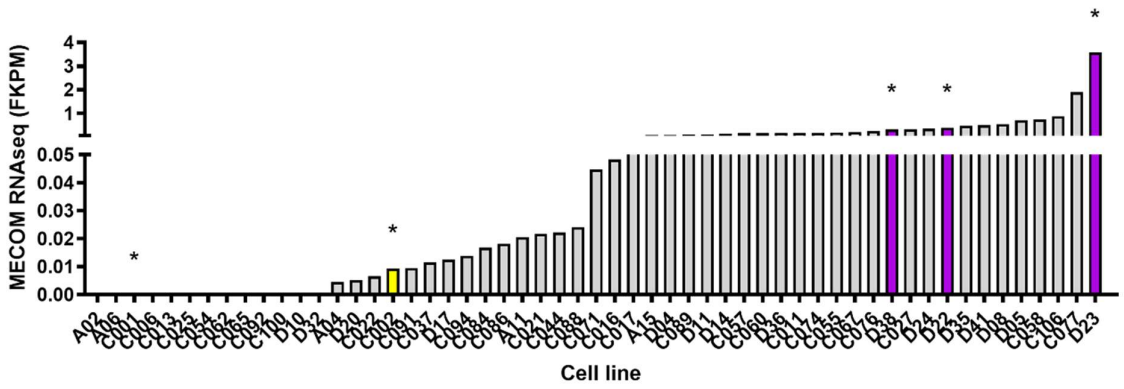


**FIGURE 8. *MECOM* EXPRESSION ACROSS MELANOMA CELL LINES AND SELECTED EXPERIMENTAL MODELS.Histogram showing *MECOM* RNA-seq expression (FPKM) in patient-derived melanoma cell lines. Each bar represents an individual cell line, ordered by increasing *MECOM* expression. Asterices indicate the five cell lines selected for functional studies: two melanocytic lines with low *MECOM* expression (C001M, C002M) and three dedifferentiated lines with high *MECOM* expression (D22M, D23M, D38M).**

## 3.3 Generation and Validation of Inducible MECOM Knockdown in Melanoma Cell Lines

Dedifferentiated melanoma cell lines D23M and D38M were transduced with lentiviral vectors encoding three *MECOM*-targeting shRNAs and a scramble control, followed by puromycin selection and IPTG induction to activate knockdown.

To expand the analysis, D22M was included as an additional high *MECOM* cell line with prior evidence of spheroid-forming capacity. While anchorage-independent growth assays were attempted in all three lines, spheroid formation was not observed under the conditions tested. The remaining cell biology assays designed to evaluate phenotype switching were completed in all three cell lines.

Despite careful optimisation, achieving robust and consistent MECOM knockdown across melanoma cell lines proved technically challenging, and variability in knockdown efficiency impacted downstream analyses.

### 3.3.1 *Optimisation of puromycin selection confirmed effective dose ranges for melanoma cell lines*

Prior to transduction, puromycin "kill curves" were generated to determine the optimal selection concentration for D22M and D23M cells. Cell viability declined in a dose-dependent manner, with complete cell death noted by 2 or 3 days of treatment with doses ≥1 µg/mL (Figure 9). Based on these results, 1 µg/mL was selected as the concentration for D22M and D23M, while 2 µg/mL was used for D38M based on previous optimisation.

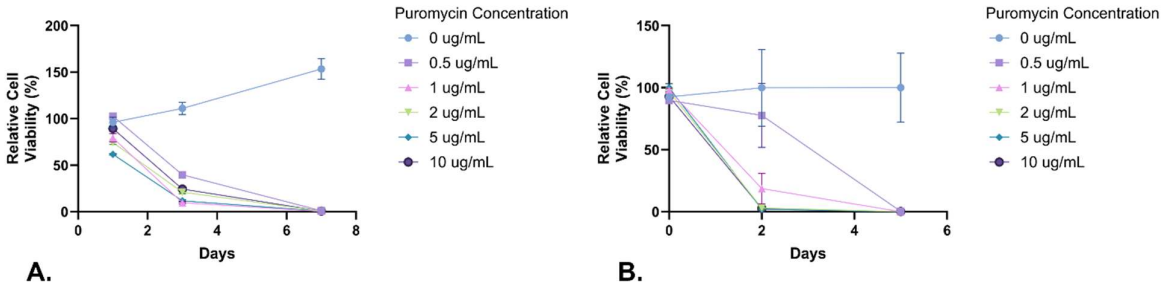


**FIGURE 9. PUROMYCIN "KILL CURVES" FOR D22M AND D23M CELLS.(A) D22M and (B) D23M cells were treated with increasing concentrations of puromycin (0–10 µg/mL) for up to 7 days. Relative cell viability was determined by luminescence measurements normalized to Day 0 readings. Data represent one biological replicate performed in technical triplicate. Error bars represent the standard error of the mean (SEM). Based on these findings, a concentration of 1 µg/mL puromycin was selected for post-transduction selection in both cell lines.**

### 3.3.2 *IPTG induction achieved variable knockdown of MECOM*

MECOM knockdown was assessed by Western blot following IPTG induction in melanoma cell lines transduced with scramble or MECOM-targeting shRNAs. While IPTG induction was well tolerated, knockdown efficiency varied markedly between cell lines and shRNA constructs, limiting reproducibility.

In D22M and D38M, representative blots are shown with fold-change values annotated below each lane (Figures 8A–B). MECOM expression was normalized to α-tubulin and expressed relative to IPTG-treated scramble control. In D22M, MECOM levels were substantially reduced across all shRNA constructs following IPTG induction (fold-changes 0.01-0.10). Further, shRNA#1 appeared to have poor knockdown effect of EVI1 compared with its strong knockdown of MECOM (fold-change 0.63 vs 0.01). Although the knockdown effect noted in D38M was overall less strong, the best reductions in MECOM expression were observed in shRNA#1 (fold-change 0.16) and shRNA#3 (fold-change 0.33) when treated with IPTG 1 mM.

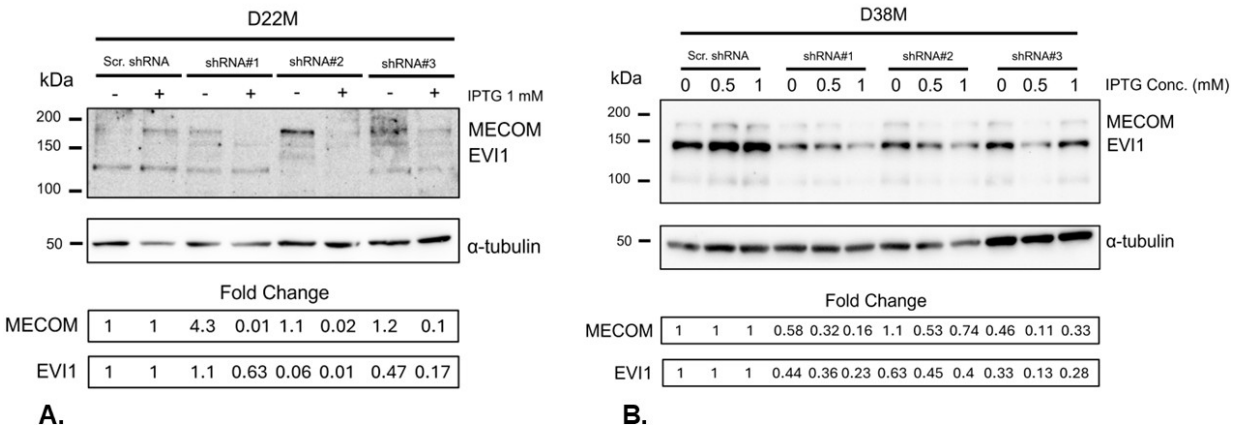


**FIGURE 10. VALIDATION OF IPTG-INDUCIBLE *MECOM* KNOCKDOWN IN D22M AND D38M MELANOMA CELL LINES.Western blot analysis of MECOM expression following IPTG induction in melanoma cells transduced with scramble control (Scr.) or *MECOM*-targeting shRNAs (#1–#3). α-tubulin served as a loading control. Fold-change values for MECOM (190 kDa) and EVI1 (145 kDa) were calculated relative to relevant scramble controls.**
**(A) D22M cells treated with 1 mM IPTG for 72 hours showed strong MECOM knockdown across all shRNAs, with fold-change values annotated below each lane. shRNA#1 exhibited minimal effect on *EVI1* compared to *MECOM*.**
**(B) D38M cells treated with IPTG at 0.5 or 1 mM demonstrated partial MECOM suppression, with the greatest reduction observed for shRNA#1 and shRNA#3 at 1 mM IPTG.**

For D23M, knockdown validation was performed in triplicate, and mean fold-change values are presented with error bars (Figure 10). While variability was high, a trend towards reduced MECOM expression was observed across the three constructs following IPTG induction, and additionally towards knockdown of EVI1 in shRNA#1 and shRNA#3. These findings indicate that MECOM knockdown was achievable but limited and inconsistent across cell lines and constructs, highlighting technical challenges in suppressing MECOM expression using inducible shRNA systems.

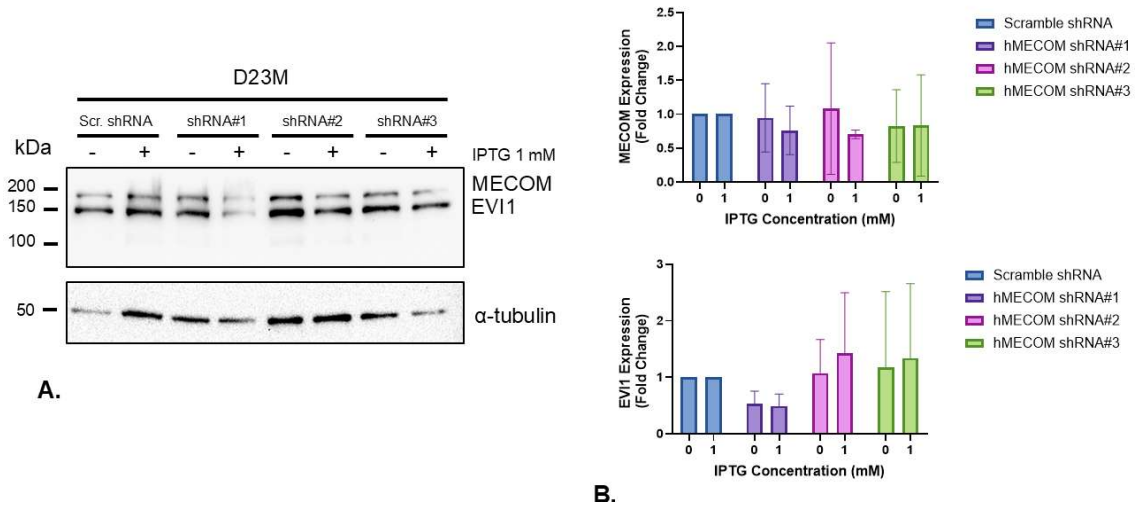


**FIGURE 11. VALIDATION OF IPTG-INDUCIBLE *MECOM* KNOCKDOWN IN D23M MELANOMA CELLS.**
**(A) Western blot analysis of MECOM expression following IPTG induction (1 mM, 72 hours) in D23M cells transduced with scramble control or *MECOM*-targeting shRNAs (#1–#3). α-tubulin served as a loading control.**
**(B) Quantification of MECOM and EVI1 expression (fold-change relative to IPTG-treated scramble control) across three**

**biological replicates. While variability was high, a trend toward reduced MECOM expression was observed for shRNA#1 and shRNA#2 following IPTG induction, with additional reduction in EVI1 for shRNA#1 and shRNA#3.**

For consistency across cell lines, shRNA#1 and shRNA#3 were selected for downstream knockdown experimentation, with limited experiments performed with all three knockdown vectors. All functional assays were performed on pooled populations following puromycin selection and IPTG induction, with knockdown efficiency validated at defined timepoints prior to assay initiation. Sustained MECOM suppression during the full assay duration was inferred from continued inducer exposure and selective pressure but was not independently revalidated at assay endpoints.

## 3.4 FUNCTIONAL ASSAYS AND DRUG SENSITIVITY FOLLOWING INDUCIBLE MECOM KNOCKDOWN

To determine whether MECOM influences melanoma cell behaviour and therapeutic response, we performed a series of functional assays following inducible MECOM knockdown in dedifferentiated melanoma cell lines. These assays assessed key phenotypic traits including proliferation, migration, clonogenicity, and anchorage-independent growth to evaluate potential shifts toward a melanocytic state. In parallel, drug sensitivity profiling was conducted using clinically relevant compounds, focusing on ferroptosis inducers and epigenetic modulators previously linked to differentiation-dependent vulnerabilities. This integrated approach aimed to clarify whether MECOM depletion modulates both intrinsic cellular properties and pharmacologic sensitivity, providing insight into its role in melanoma plasticity and treatment resistance.

### *3.4.1 MECOM KNOCKDOWN REDUCES CELL VIABILITY IN MELANOMA CELL LINES*

Proliferation assays following one-week IPTG induction revealed cell line–specific effects of *MECOM* knockdown. In D22M, no sustained differences in growth were observed between constructs, although all *MECOM*-targeting shRNAs showed a transient increase in viability at Day 3 compared to scramble control. In contrast, D23M exhibited a consistent reduction in proliferation with shRNA#3 across Days 3, 5, and 7, culminating in a ~42% decrease in viability at Day 7 compared to scramble (relative cell viability 2256% vs 1305%; q = 0.00009). Similarly, D38M showed a significant reduction in proliferation with shRNA#2 at Days 3, 5, and 7, with a ~21% decrease at Day 7 (relative cell viability 752.5% vs 595.8%; q = 0.00012). These findings suggest that MECOM suppression can impair melanoma cell growth in a subset of dedifferentiated lines, although the effects were variable and construct dependent. Additional induction regimes (no pre-treatment and 48-hour pre-treatment with IPTG in D23M and

D38M) did not demonstrate significant differences in proliferative potential, perhaps indicating that a phenotype switch requires a longer period of MECOM depletion (data not shown).

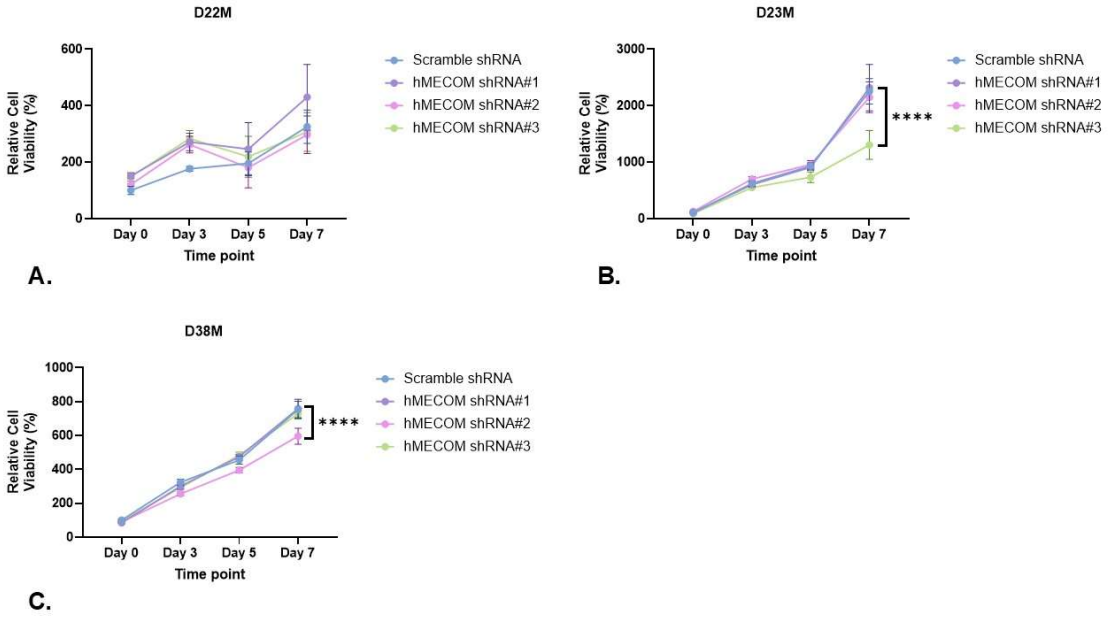


**FIGURE 12. EFFECT OF MECOM KNOCKDOWN ON MELANOMA CELL PROLIFERATION.Proliferation assays were performed in melanoma cell lines D22M (A), D23M (B), and D38M (C) following IPTG induction (1 mM) for 7 days prior to seeding. Cells were plated at 1,000 cells/well in 96-well plates and monitored over 7 days using CellTiter-Glo 2.0 luminescence assay. Relative cell viability was normalized to Day 0 readings. Each line represents the mean of three biological replicates, with error bars indicating standard deviation. In D22M, no sustained differences were observed between constructs, although all *MECOM*-targeting shRNAs showed transiently higher viability at Day 3 compared to scramble control. In D23M, shRNA#3 significantly reduced proliferation at Days 3, 5, and 7 compared to scramble (****q < 0.001). In D38M, shRNA#2 significantly reduced proliferation at Days 3, 5, and 7 compared to scramble (****q < 0.001). Statistical analysis was performed using multiple t-tests with Benjamini–Krieger–Yekutieli (BKY) correction for multiple comparisons.**

### *3.4.2 MECOM KNOCKDOWN DOES NOT SIGNIFICANTLY ALTER MELANOMA CELL MIGRATION IN WOUND HEALING ASSAYS*

Scratch assays were performed to assess whether *MECOM* knockdown affected melanoma cell migration. D22M and D38M cells were pre-treated with IPTG (1 mM) for 7 days prior to scratch induction, and wound closure was monitored over time. D23M was excluded from analysis due to poor adherence following scratch induction. Quantification of wound area revealed no statistically significant differences in migration between scramble and *MECOM*-targeting shRNAs in either cell line, although a non-significant trend toward increased wound closure was observed for D22M shRNA#3. These findings indicate that MECOM knockdown did not significantly alter the migratory capacity of dedifferentiated melanoma cells under the conditions tested.

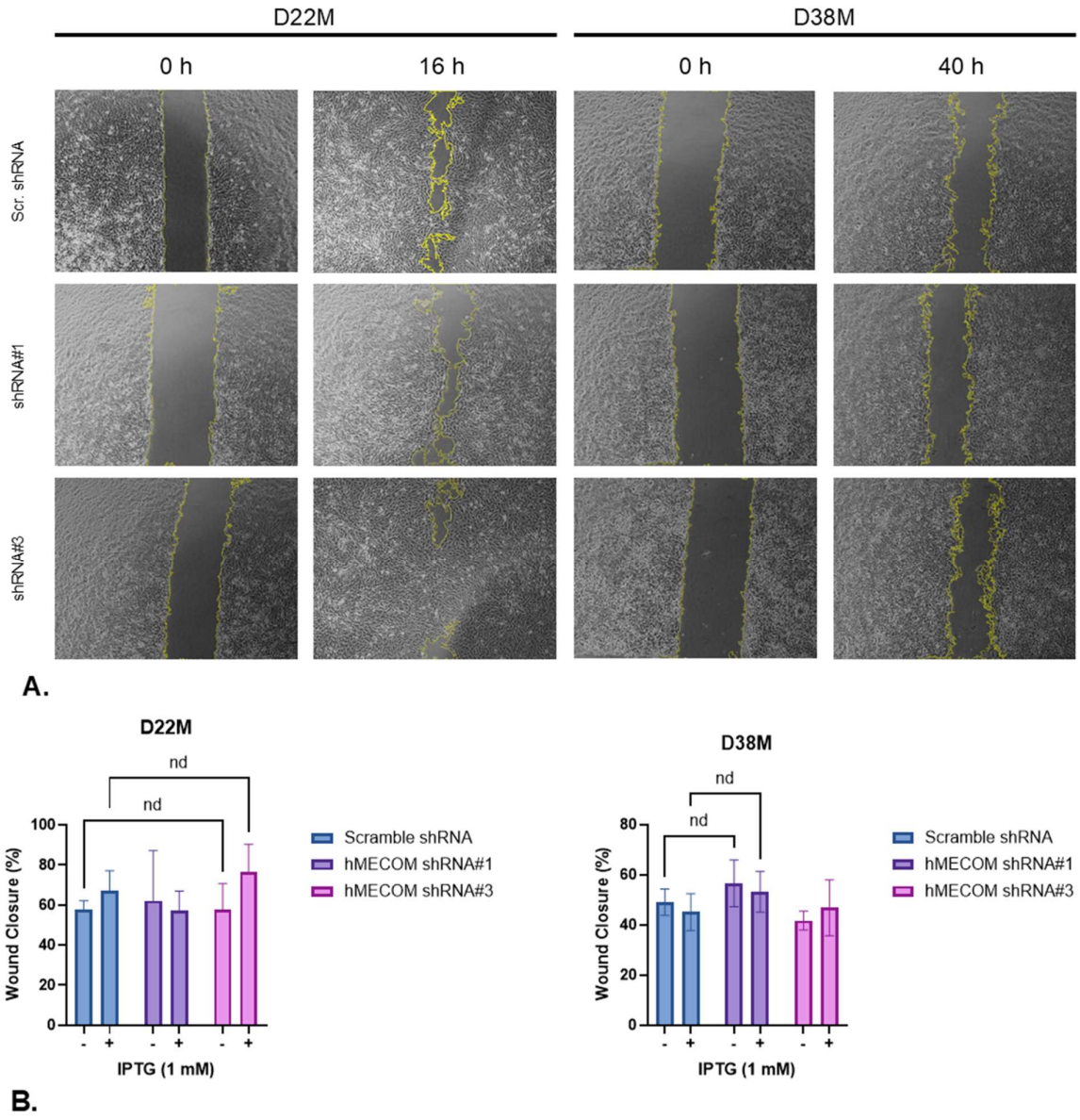


**FIGURE 13. EFFECT OF MECOM KNOCKDOWN ON MELANOMA CELL MIGRATION IN WOUND HEALING ASSAYS.(A) representative images of wound closure in D22M (0 h and 16 h) and D38M (0 h and 40 h) melanoma cell lines following IPTG induction (1 mM, 7 days) and transduction with scramble or *MECOM*-targeting shRNAs (#1 and #3). Images were captured at ×4 magnification, and wound margins are outlined in yellow. (B) Quantification of wound closure (%) normalized to 0 h, based on ImageJ analysis. Results represent means ± SEM from three biological replicates (technical duplicates per replicate). Statistical analysis was performed using multiple t-tests with Benjamini–Krieger–Yekutieli (BKY) correction for multiple comparisons. MECOM knockdown did not significantly influence wound closure in either cell line (nd = no difference).**

### *3.4.3 MECOM KNOCKDOWN HAS LIMITED EFFECT ON ANCHORAGE INDEPENDENT GROWTH*

Anchorage-independent growth was assessed using soft agar assays in the D23M melanoma cell line, as D22M and D38M did not form colonies under these conditions. Across all *MECOM*-targeting constructs, knockdown did not significantly alter colony formation compared to scramble controls, although a consistent trend toward reduced colony density was observed under IPTG-treated conditions (Figure 14). Due to high variation between biological replicates, normalization to contemporaneous scramble controls and $\log_2$ transformation was performed (raw counts available in Supplementary Data, Table 16). This revealed median fold-changes ranging from approximately −0.1 to −0.9, indicating modest reductions in colony growth that did not reach statistical significance. These findings suggest that MECOM knockdown may have a limited effect on anchorage-independent growth in D23M cells.

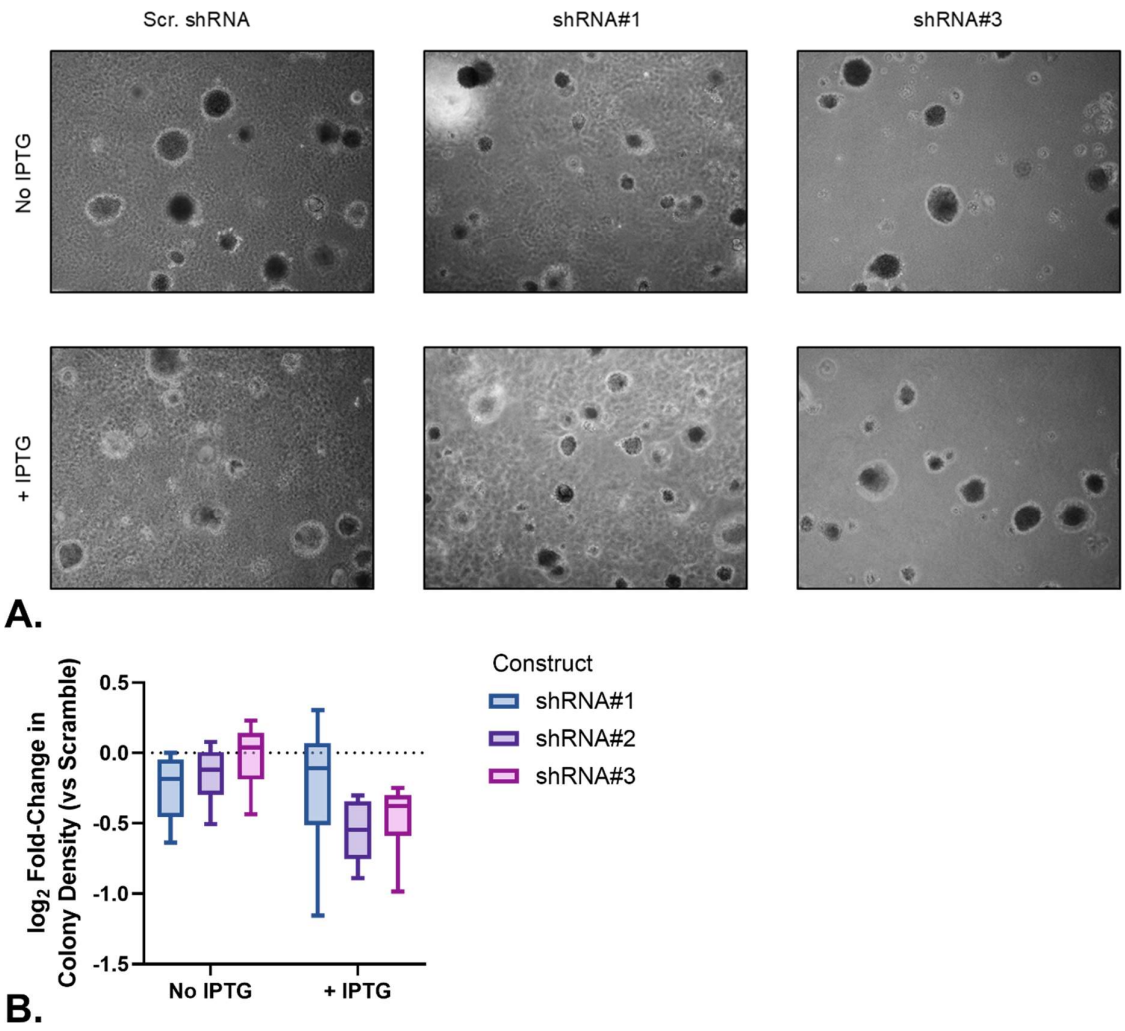


**FIGURE 14. EFFECT OF MECOM KNOCKDOWN ON ANCHORAGE-INDEPENDENT GROWTH IN MELANOMA CELLS.(A) Representative images of soft agar colonies formed by D23M melanoma cells transduced with scramble or *MECOM*-targeting shRNAs (#1, #2, #3) under untreated (No IPTG) and IPTG-treated (+IPTG) conditions. Images were captured at ×4 magnification after 3 weeks of incubation.**

**(B) Quantification of colony density expressed as $\log_2$ fold-change relative to the contemporaneous scramble control. Cells were pre-treated with IPTG (1 mM) for 7 days prior to seeding and maintained under the same conditions throughout the assay. For each well, five non-overlapping fields were imaged, and colonies were counted manually. Colony counts were normalized to imaged area and averaged per well. Box plots show per-well normalized values across biological replicates (n = 6 wells per condition). Statistical analysis was performed using one-sample t-tests against zero (no change) with Benjamini–Krieger–Yekutieli correction for multiple comparisons. *MECOM* knockdown did not significantly reduce anchorage-independent growth, although a non-significant trend toward decreased colony density was observed across constructs.**

### *3.4.4 MECOM KNOCKDOWN DOES NOT CONSISTENTLY ALTER CLONOGENIC POTENTIAL IN D23M OR D38M*

Colony formation assays in D23M and D38M cells showed no significant effect of MECOM knockdown on clonogenic growth under either basal or IPTG-induced conditions. D22M cells could not be assessed in this assay because the monolayer detached during preparatory washing, fixing, and staining steps. After normalization to scramble controls, $\log_2$ transformation, and averaging technical wells per biological replicate, one-sample t-tests versus zero on $\log_2$ fold changes revealed no significant differences for either shRNA construct in either cell line (Figure 15).

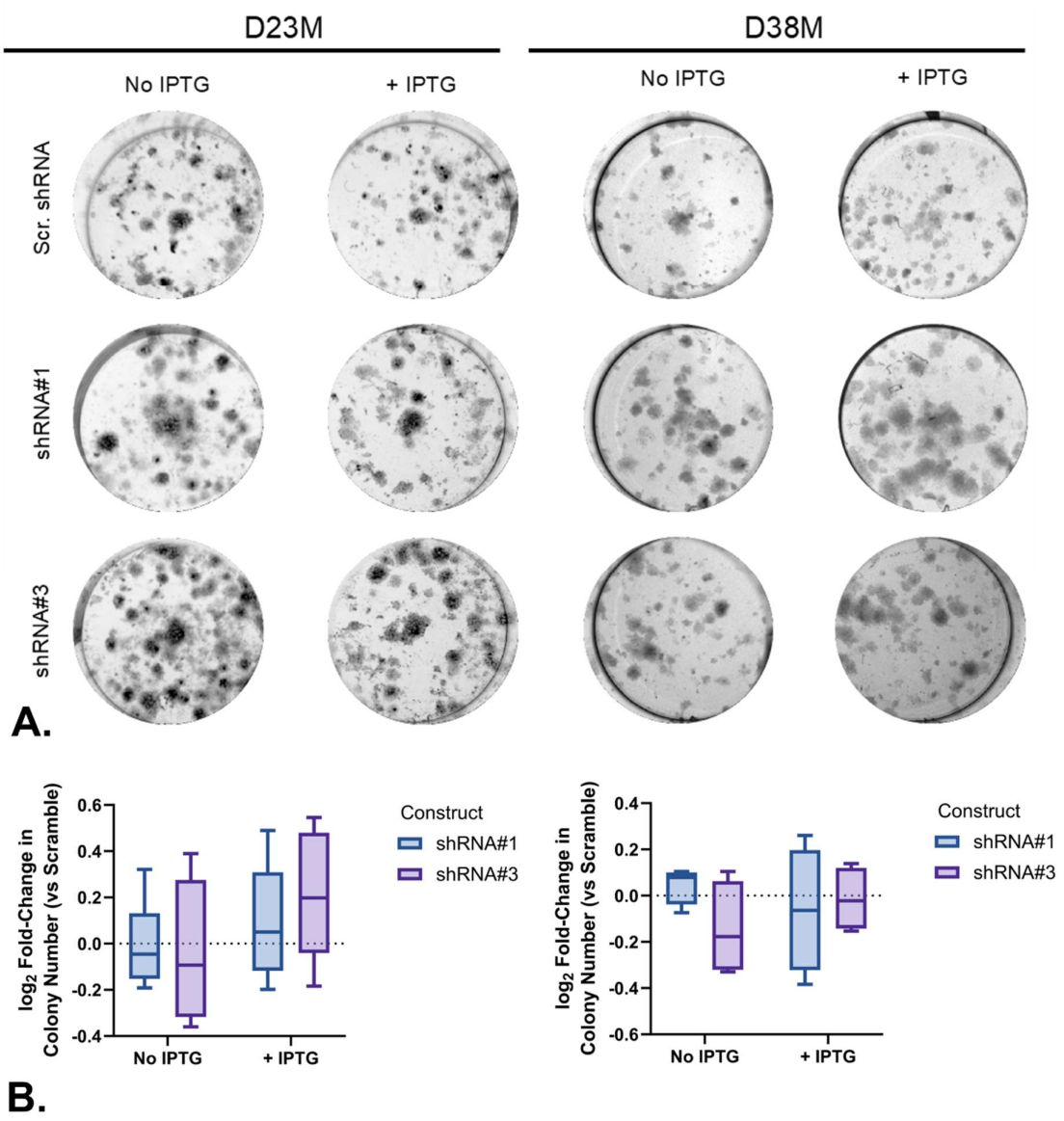


**FIGURE 15. MECOM KNOCKDOWN DOES NOT ALTER CLONOGENIC GROWTH IN MELANOMA CELL LINES.(A) Representative colony formation assay wells for D23M (left) and D38M (right) cells transduced with scramble control (scr.) or *MECOM*-targeting shRNAs (#1 and #3) under basal (no IPTG) and induced (+IPTG) conditions. Plates were stained and imaged after 14 days of growth.**

**(b) Box-and-whisker plots showing $log_2$ fold change in colony number relative to scramble controls for shRNA#1 (blue) and shRNA#3 (purple) under basal and IPTG-induced conditions. Each point represents a biological replicate (n = 3); technical wells were averaged prior to statistical analysis. The dotted line at zero indicates no difference from scramble. One-sample t-tests versus zero revealed no significant differences for either construct in either cell line.**

In D23M cells, ΔΔ analysis of IPTG-dependent effects yielded geometric mean fold change (GMFC) values of 1.07 (95% CI: 0.726–1.58; $p$ = 0.5314) for shRNA#1 and 1.18 (95% CI: 0.705–1.98; $p$ = 0.2984) (Table 8). Similarly, in D38M cells, IPTG-dependent GMFC values were 0.959 (95% CI: 0.144–6.37; $p$ = 0.8270) for shRNA#1 and 1.06 (95% CI: 0.849–1.32; $p$ = 0.1910; Table 8). These confidence intervals include unity and span both potential decreases and increases in colony number, indicating no reproducible IPTG-dependent effect in either cell line within the current sample size. The wide confidence intervals, particularly for shRNA#1 in D38M, reflect substantial variability and limited statistical power, suggesting that any true effect is likely small or absent.

**TABLE 8. IPTG-DEPENDENT EFFECTS OF MECOM KNOCKDOWN IN D23M AND D38M CELLS. ΔΔ analysis was performed by subtracting the $log_2$ fold change under basal conditions from that under IPTG induction for each biological replicate. Geometric mean fold changes (GMFC) and 95% confidence intervals were obtained by back-transforming $log_2$ means and confidence bounds. One-sample t-tests versus zero were used to assess significance.**

| Cell Line | Construct | GMFC | 95% CI | p-value |
|---|---|---|---|---|
| **D23M** | shRNA#1 | 1.07 | 0.726–1.58 | 0.5314 |
| | shRNA#3 | 1.18 | 0.705–1.98 | 0.2984 |
| **D38M** | shRNA#1 | 0.959 | 0.144-6.37 | 0.827 |
| | shRNA#3 | 1.06 | 0.849-1.32 | 0.191 |

### *3.4.5 PARENTAL CELL LINES DEMONSTRATE VARIABLE SUB-TYPE SPECIFIC SENSITIVITY TO MELANOMA DRUGS*

To establish baseline drug sensitivity profiles, parental melanoma cell lines representing dedifferentiated and melanocytic phenotypes were first tested against a panel of clinically relevant and mechanistically diverse compounds. This approach allowed us to determine whether intrinsic differences in drug response could distinguish these phenotypic states, providing a reference framework prior to re-testing in MECOM knockdown and overexpression models.

Dose–response analysis revealed marked heterogeneity in drug sensitivity among melanoma cell lines, consistent with differences in differentiation state (Figure 16). Ferroptosis inducers (Erastin and RSL-3) showed the most pronounced subtype-specific effects. D38M, a dedifferentiated line, exhibited dramatically lower $IC_{50}$ values for both agents compared to melanocytic lines C001M and C002M (all comparisons $p < 0.0001$ after correction), while D23M displayed intermediate sensitivity. These findings support previous reports that dedifferentiated melanomas are more vulnerable to ferroptosis (19).

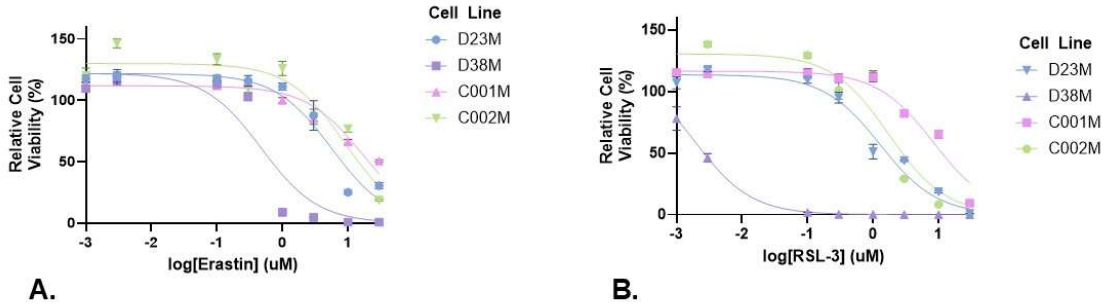


**FIGURE 16. DOSE–RESPONSE CURVES FOR FERROPTOSIS INDUCERS IN MELANOMA CELL LINES.(A) Erastin and (B) RSL-3 were tested across eight half-log concentrations (0.003–30 µM) for 72 h in four melanoma cell lines (D23M and D38M – dedifferentiated; C001M and C002M – melanocytic). Cell viability was measured using CellTiter-Glo® 2.0 and normalized to vehicle-treated controls. Data points represent the mean of technical triplicates, and error bars indicate the standard error of the mean (SEM). Curves were fit using a log(inhibitor) vs. response model with variable slope in GraphPad Prism (v10.6.1). Pairwise comparisons of log$IC_{50}$ values (extra–sum-of-squares F test) revealed significant differences among cell lines for both drugs. For Erastin (A), D38M was significantly more sensitive than D23M, C001M, and C002M (raw $p < 0.0001$; remained significant after Bonferroni correction), and D23M was significantly more sensitive than C001M (raw $p < 0.0001$; corrected significant) but not C002M (raw $p = 0.0751$; not significant after correction). For RSL-3 (B), the same pattern was observed.**

Epigenetic modulators with evidence of an association with MECOM also demonstrated subtype-dependent responses (Figure 17). For the BET inhibitor, JQ-1, D23M was significantly more resistant than C001M and C002M (corrected significant), whereas its difference from D38M did not remain significant after correction. HDAC inhibitors ABBV-744 and Vorinostat produced clearer patterns: D23M was consistently more resistant than all other lines ($p < 0.0001$), and D38M was more resistant than C001M for Vorinostat ($p < 0.0001$), but its difference from C002M was borderline (raw $p = 0.0129$; not significant after correction). These results suggest that dedifferentiated states may confer selective vulnerability to certain chromatin-targeting drugs.

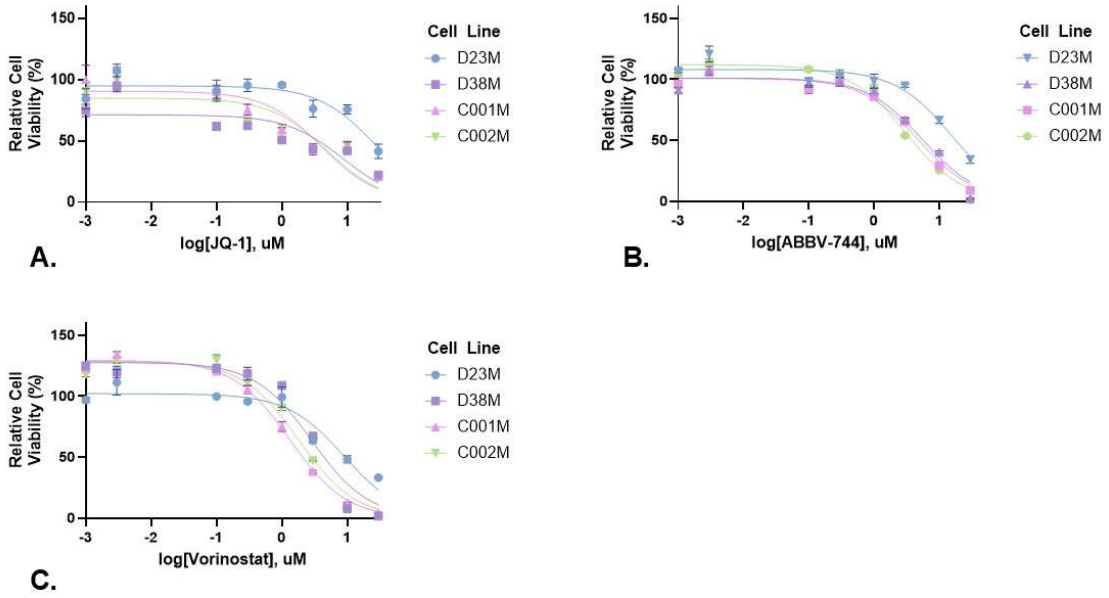


**FIGURE 17. DOSE–RESPONSE CURVES FOR EPIGENETIC MODULATORS IN MELANOMA CELL LINES.(A) JQ-1, (B) ABBV-744, and (C) Vorinostat were tested across eight half-log concentrations (0.003–30 µm) for 72 h in four melanoma cell lines (D23M, D38M, C001M, C002M). Data points represent the mean of technical triplicates, and error bars indicate the standard error of the mean (SEM). Curves were fit using a log(inhibitor) vs. Response model with variable slope in GraphPad prism (v10.6.1).**

**Pairwise comparisons of log$IC_{50}$ values (extra–sum-of-squares f test) revealed:**

**(A) JQ-1: D23M differed significantly from C001M (raw p = 0.0002) and C002M (raw p = 0.0009; both remained significant after Bonferroni correction), but the difference between D23M and D38M (raw p = 0.0189) was not significant after correction.**

**(B) ABBV-744: D23M was significantly more resistant than D38M, C001M, and C002M (all raw p < 0.0001; remained significant after correction).**

**(C) Vorinostat: D23M was significantly more resistant than D38M, C001M, and C002M (all raw p < 0.0001; corrected significant), and D38M differed significantly from C001M (raw p < 0.0001; corrected significant) but not C002M (raw p = 0.0129; not significant after correction).**

BRAF inhibitors showed the least consistent subtype effect (Figure 18). For Vemurafenib, D23M was significantly more resistant than C002M (corrected significant), while other comparisons were not significant after correction. Dabrafenib sensitivity was broadly similar across lines, except for D38M versus C002M ($p < 0.0001$). Importantly, no $IC_{50}$ could be determined for D23M with Dabrafenib, consistent with its classification as a BRAF wild-type melanoma cell line based on previous whole-exome sequencing. Overall, these data indicate that ferroptosis inducers and selected epigenetic drugs exhibit the strongest differentiation-dependent sensitivity shifts, whereas BRAF inhibitors remain largely unaffected by MECOM-driven phenotype changes. Full IC50 results are presented in

Table 9, and the relevant results of pairwise comparisons in Table 10.

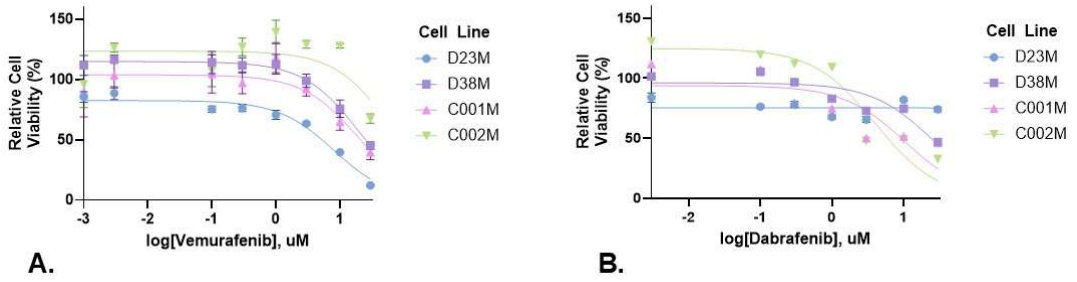


**FIGURE 18. DOSE–RESPONSE CURVES FOR BRAF INHIBITORS IN MELANOMA CELL LINES.(A) Vemurafenib and (B) Dabrafenib were tested across eight half-log concentrations (0.003–30 µM) for 72 h in four melanoma cell lines (D23M, D38M, C001M, C002M). Data points represent the mean of technical triplicates, and error bars indicate the standard error of the mean (SEM). Curves were fit using a log(inhibitor) vs. response model with variable slope in GraphPad Prism (v10.6.1).**

**Pairwise comparisons of log$IC_{50}$ values (extra–sum-of-squares f test) revealed:**

**(A) Vemurafenib: D23M differed significantly from C002M (raw p < 0.0001; remained significant after Bonferroni correction), but not from C001M (raw p = 0.0358; not significant after correction). D38M differed significantly from C002M (raw p = 0.0088; borderline after correction), and C001M vs. C002M was not significant after correction (raw p = 0.0379). (B) Dabrafenib: D38M differed significantly from C002M (raw p < 0.0001; corrected significant), but not from C001M (raw p = 0.1181).**

Taken together, the baseline panel establishes a phenotype-sensitivity signal: dedifferentiated lines, particularly D38M, show marked vulnerability to ferroptosis inducers and selective differences to epigenetic modulators, whereas BRAF inhibitors exhibit limited differentiation-dependent separation. The pattern is consistent across effect sizes ($\Delta$ log$IC_{50}$ with 95% CIs) and adjusted p-values (Table 10), with the strongest and most consistent shifts observed for Erastin/RSL-3 and ABBV-744/Vorinostat, and mixed findings for JQ-1. These baseline data therefore provide a robust comparison for assessing MECOM-associated phenotype switching and identify ferroptosis and chromatin-targeting agents as the most informative classes for follow-up testing.

**TABLE 9. $IC_{50}$ VALUES (μM) AND 95% CONFIDENCE INTERVALS FOR SEVEN DRUGS ACROSS FOUR MELANOMA CELL LINES.Dose–response curves were fit using a log(inhibitor) vs. Response model with variable slope in GraphPad prism (v10.6.1). $IC_{50}$ values represent the concentration (in μM) required to reduce cell viability by 50%, calculated from nonlinear regression. Confidence intervals (95% CI) were derived from the best-fit parameter estimates. Missing values (–) indicate no measurable $IC_{50}$ within the tested concentration range.**

| | **Melanoma Cell Line** | | | |
|---|---|---|---|---|
| | **D23M** $IC_{50}$ (μM, 95% CI) | **D38M** $IC_{50}$ (μM, 95% CI) | **C001M** $IC_{50}$ (μM, 95% CI) | **C002M** $IC_{50}$ (μM, 95% CI) |
| **Erastin** | 5.64 (4.02 to 8.03) | 0.476 (0.307 to 0.753) | 16.8 (13.0 to 22.1) | 9.04 (6.04 to 13.7) |
| **RSL-3** | 1.288 (0.957 to 1.75) | 0.00189 (0.00101 to 0.00341) | 8.51 (6.46 to 11.3) | 1.74 (1.14 to 2.66) |
| **JQ-1** | 26.4 (16.4 to 45.3) | 8.61 (3.72 to 19.9) | 4.08 (1.86 to 9.39) | 4.83 (1.97 to 12.0) |
| **ABBV-744** | 15.42 (11.7 to 20.6) | 5.58 (4.25 to 7.36) | 4.82 (3.98 to 5.84) | 3.09 (2.53 to 3.79) |
| **Voronistat** | 8.90 (5.90 to 13.7) | 2.85 (2.15 to 3.81) | 1.31 (1.16 to 1.49) | 1.81 (1.46 to 2.26) |
| **Dabrafenib** | - | 26.2 (15.5 to 47.4) | 10.6 (3.46 to 34.4) | 4.02 (2.38 to 7.16) |
| **Vemurafenib** | 8.07 (6.08 to 10.8) | 19.6 (14.1 to 27.8) | 19.5 (9.88 to 43.6) | 61.4 (29.5 to 214) |

**TABLE 10. PAIRWISE COMPARISONS OF LOGIC$_{50}$ VALUES BETWEEN MELANOMA CELL LINES FOR EACH DRUG.Differences in logIC$_{50}$ (Δ) and corresponding 95% confidence intervals were calculated from nonlinear regression estimates in GraphPad Prism (v10.6.1). Positive Δ indicates the first cell line is more resistant (higher logIC$_{50}$) than the second; negative Δ indicates greater sensitivity. Raw p-values were obtained using extra–sum-of-squares F tests, and Bonferroni-adjusted p-values were computed within each drug's family of planned comparisons (α = 0.05). Significant comparisons after correction are indicated in bold.**

| Drug | Comparison | Δ logIC$_{50}$ (95% CI) | Raw *p* | Bonferroni-adjusted *p* |
|---|---|---|---|---|
| **Erastin** | D23M vs D38M | 1.07 (0.83 to 1.32) | <0.0001 | **<0.0005** |
| | D23M vs C001M | -0.47 (-0.66 to -0.29) | <0.0001 | **<0.0005** |
| | D23M vs C002M | -0.21 (-0.44 to 0.03) | 0.0751 | 0.3755 |
| | D38M vs C001M | -1.55 (-1.77 to -1.32) | <0.0001 | **<0.0005** |
| | D38M vs C002M | -1.28 (-1.54 to -1.01) | <0.0001 | **<0.0005** |
| **RSL-3** | D23M vs D38M | 2.83 (2.54 to 3.13) | <0.0001 | **<0.0005** |
| | D23M vs C001M | -0.82 (-1.00 to -0.64) | <0.0001 | **<0.0005** |
| | D23M vs C002M | -0.13 (-0.36 to 0.10) | 0.2848 | 1.000 |
| | D38M vs C001M | -3.65 (-3.94 to -3.36) | <0.0001 | **<0.0005** |
| | D38M vs C002M | -2.96 (-3.29 to -2.64) | <0.0001 | **<0.0005** |
| **JQ-1** | D23M vs D38M | 0.49 (0.06 to 0.91) | 0.0189 | 0.0567 |
| | D23M vs C001M | 0.81 (0.40 to 1.23) | 0.0002 | **0.0006** |
| | D23M vs C002M | 0.74 (0.29 to 1.19) | 0.0009 | **0.0027** |
| **ABBV-744** | D23M vs D38M | 0.44 (0.27 to 0.61) | <0.0001 | **<0.0003** |
| | D23M vs C001M | 0.51 (0.36 to 0.65) | <0.0001 | **<0.0003** |
| | D23M vs C002M | 0.70 (0.55 to 0.85) | <0.0001 | **<0.0003** |
| **Vorinostat** | D23M vs D38M | 0.49 (0.27 to 0.71) | <0.0001 | **<0.0005** |
| | D23M vs C001M | 0.83 (0.64 to 1.02) | <0.0001 | **<0.0005** |
| | D23M vs C002M | 0.69 (0.49 to 0.90) | <0.0001 | **<0.0005** |
| | D38M vs C001M | 0.34 (0.20 to 0.47) | <0.0001 | **<0.0005** |
| | D38M vs C002M | 0.20 (0.04 to 0.35) | 0.0129 | 0.0645 |
| **Vemurafenib** | D38M vs C002M | -0.5 (-0.95 to -0.04) | 0.0088 | **0.0352** |
| | D23M vs C001M | -0.38 (-0.73 to -0.04) | 0.0358 | 0.1432 |
| | D23M vs C002M | -0.88 (-1.33 to -0.43) | <0.0001 | **<0.0004** |
| | C001M vs C002M | -0.50 (-1.04 to 0.04) | 0.0379 | 0.1516 |
| **Dabrafenib** | D38M vs C001M | 0.39 (-0.16 to 0.95) | 0.1181 | 0.2362 |
| | D38M vs C002M | 0.81 (0.47 to 1.15) | <0.0001 | **<0.0002** |

### *3.4.6 MECOM KNOCKDOWN CONFERS REDUCED ERASTIN SENSITIVITY IN D38M BUT MINIMAL EFFECTS ON OTHER DRUG CLASSES*

Guided by these findings, we next evaluated whether MECOM knockdown alters drug sensitivity in a manner consistent with phenotype switching. Because the baseline analysis revealed the clearest differentiation-dependent effects for ferroptosis inducers (Erastin, RSL-3) and epigenetic modulators (JQ-1, ABBV-744, Vorinostat), we focused the knockdown experiments on these drugs. Parental and knockdown cells were assayed under identical dosing and timing conditions; dose–response curves were fit as before, and primary endpoints were defined as the change in $\log IC_{50}$ ($\Delta \log IC_{50}$) relative to matched parental lines, with pairwise extra–sum-of-squares F tests and per-drug multiple-comparisons correction applied. This design directly tests whether perturbation of MECOM shifts sensitivity along the dedifferentiated to melanocytic axis for the drug classes most sensitive to phenotype state.

We hypothesized that knockdown would decrease sensitivity to inducers of ferroptosis and increase sensitivity to epigenetic regulators in the event of a phenotype switch from dedifferentiated to melanocytic. In D23M, Erastin and RSL-3 responses were unchanged, with overlapping dose–response curves and no significant $IC_{50}$ differences between constructs (Figure 19). By contrast, D38M knockdown lines displayed a marked reduction in Erastin sensitivity, with $IC_{50}$ values increasing from 9.65 μM in scramble controls to 19.36 μM and 22.14 μM for shRNA#1 and shRNA#3, respectively (raw $p = 0.0013$ and $<0.0001$; both remained significant after Bonferroni correction). These shifts were not observed for RSL-3, where curves remained similar across constructs. This pattern suggests that MECOM depletion can reduce vulnerability to certain ferroptosis inducers, but the effect is drug-specific and context-dependent, consistent with partial modulation of the dedifferentiated phenotype rather than a uniform switch.

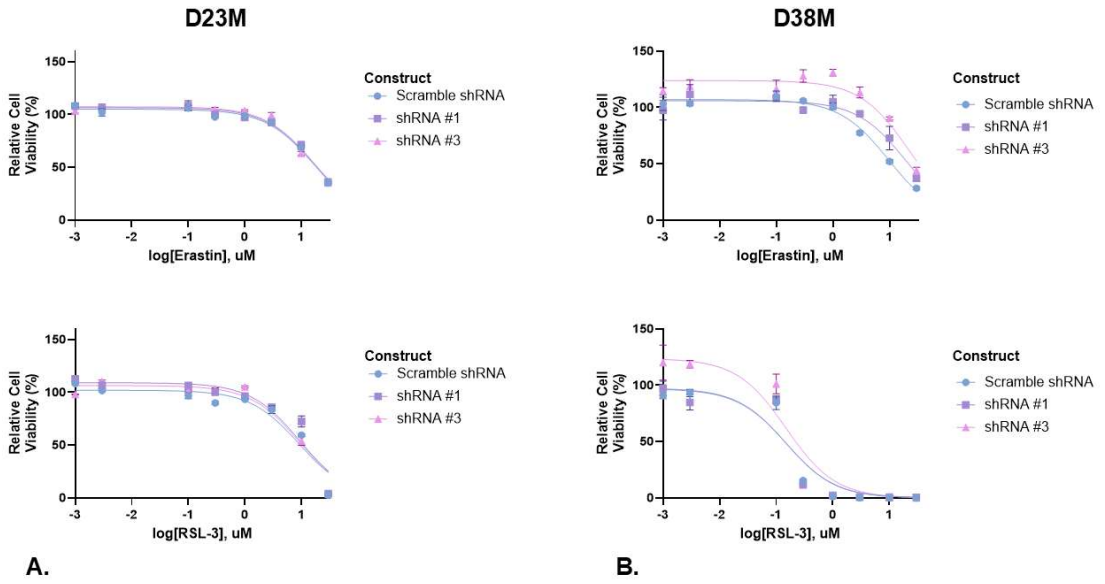


**FIGURE 19. DOSE–RESPONSE CURVES FOR FERROPTOSIS INDUCERS FOLLOWING MECOM KNOCKDOWN.(A) D23M and (B) D38M cells were treated with Erastin (top panels) or RSL-3 (bottom panels) across eight half-log concentrations (0.003–30 µM) for 72 h. Constructs included scramble shRNA (blue), shRNA#1 (purple), and shRNA#3 (pink). Data points represent the mean of technical triplicates, and error bars indicate the standard error of the mean (SEM). Curves were fit using a log(inhibitor) vs. Response model with variable slope in GraphPad prism (v10.6.1). Pairwise comparisons of log$IC_{50}$ values (extra–sum-of-squares f test) revealed:**
**(A) D23M: no significant differences between constructs for either drug.**
**(B) D38M: Erastin sensitivity was significantly reduced in knockdown lines compared to scramble (scramble vs shRNA#1: raw p = 0.0013; scramble vs shRNA#3: raw p < 0.0001; both remained significant after Bonferroni correction). No significant differences were observed for RSL-3.**

For epigenetic modulators, D38M constructs showed no significant differences in sensitivity to JQ-1, ABBV-744, or Vorinostat (Figure 20). In D23M, global comparison of fits indicated significant differences for ABBV-744 (shRNA#1 vs shRNA#3, raw p = 0.0034) and Vorinostat (shRNA#1 vs shRNA#3, raw p = 0.0087), but pairwise $IC_{50}$ comparisons revealed no consistent pattern: ABBV-744 differences did not involve scramble controls, and for Vorinostat, scramble vs shRNA#3 reached nominal significance (raw p = 0.0225) but was not significant after Bonferroni correction .

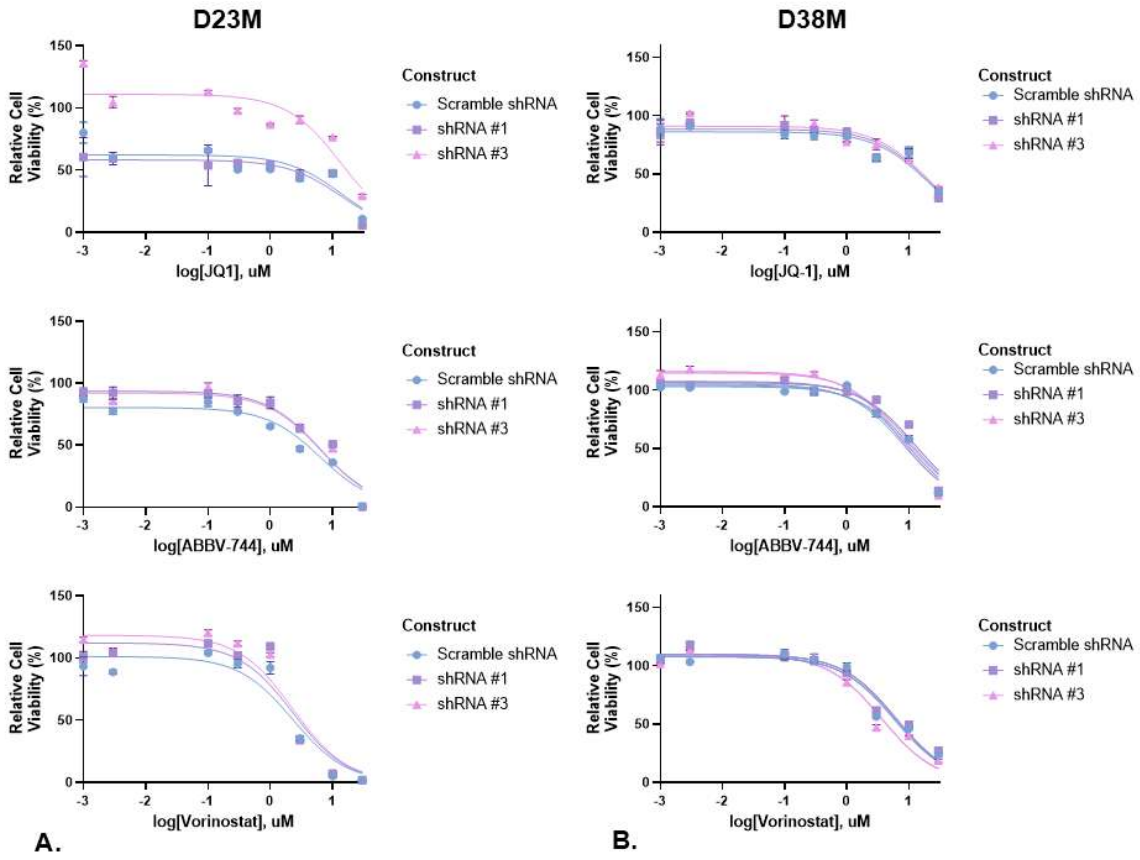


**FIGURE 20. DOSE-RESPONSE CURVES FOR EPIGENETIC MODULATORS FOLLOWING MECOM KNOCKDOWN.(A) D23M and (B) D38M cells were treated with JQ-1 (top panels), ABBV-744 (middle panels), or Vorinostat (bottom panels) across eight half-log concentrations (0.003–30 µM) for 72 h. Constructs included scramble shRNA (blue), shRNA#1 (purple), and shRNA#3 (pink). Data points represent the mean of technical triplicates, and error bars indicate the standard error of the mean (SEM). Curves were fit using a log(inhibitor) vs. Response model with variable slope in GraphPad prism (v10.6.1).**

**Global then pairwise comparison of fits revealed:**

**(A) D23M: significant differences for ABBV-744 (shRNA#1 vs shRNA#3, raw p = 0.0034) and Vorinostat (shRNA#1 vs shRNA#3, raw p = 0.0087). Pairwise $IC_{50}$ comparisons showed no significant differences between scramble and knockdown constructs for ABBV-744, and for Vorinostat, scramble vs shRNA#3 reached nominal significance (raw p = 0.0225) but was not significant after Bonferroni correction.**

**While global comparison of fits only demonstrated:**

**(B) D38M: no significant differences between constructs for any drug.**

Taken together, these findings suggest that MECOM depletion does not uniformly shift drug sensitivity along the dedifferentiated–melanocytic axis. Instead, effects are drug-specific and cell line–specific, with the most robust signal being reduced Erastin sensitivity in D38M, consistent with partial modulation of ferroptosis vulnerability rather than a global phenotype switch.

**TABLE 11. $IC_{50}$ VALUES (MM) WITH 95% CONFIDENCE INTERVALS FOR MECOM KNOCKDOWN CONSTRUCTS ACROSS FERROPTOSIS INDUCERS AND EPIGENETIC MODULATORS.D23M and D38M melanoma cell lines were treated with Erastin, RSL-l 3, JQ-1, ABBV- 744, or Vorinostat for 72 h following *MECOM* knockdown (shRNA#1, shRNA#3) or scramble control. $IC_{50}$ values were estimated by nonlinear regression using a log(inhibitor) vs. Response model with variable slope in GraphPad prism (v10.6.1). Values represent best-fit $IC_{50}$ with 95% confidence intervals derived from prism output.**

| | Melanoma Cell Line | | | | | |
|---|---|---|---|---|---|---|
| | D23M | | | D38M | | |
| | Scramble shRNA $IC_{50}$ (μM, 95% CI) | shRNA#1 $IC_{50}$ (μM, 95% CI) | shRNA#3 $IC_{50}$ (μM, 95% CI) | Scramble shRNA $IC_{50}$ (μM, 95% CI) | shRNA#1 $IC_{50}$ (μM, 95% CI) | shRNA#3 $IC_{50}$ (μM, 95% CI) |
| Erastin | 17.6 (15.0-20.7) | 17.7 (14.9-21.1) | 16.0 (13.6 to 18. 7) | 9.65 (7.92 to 11.8) | 19.3 (13.5 to 28. 6) | 22.1 (16.3 to 30.7) |
| RSL-3 | 9.12 (6.5 to 12.9 ) | 10.3 (7.10 to 15.0) | 8.33 (6.17 to 11. 3) | 0.160 (0.103 to 0.25 1) | 0.159 (0.0951 to 0.265) | 0.139 (0.0854 to 0.2 24) |
| JQ-1 | 23.2 (15.9 to 34. 9) | 19.0 (12.7 to 29.1) | 19.9 (13.7 to 29. 9) | 11.7 (5.93 to 23.6) | 14.3 (6.23 to 35. 8) | 14.3 (9.08 to 22.9) |
| ABBV-744 | 9.63 (7.60 to 12. 3) | 12.5 (9.42 to 16.6) | 7.34 (5.93 to 9.1 2) | 4.50 (3.29 to 6.18) | 7.18 (5.06 to 10. 2) | 7.20 (5.12 to 10.2) |
| Vorinostat | 5.84 (2.73 to 4.9 3) | 6.29 (4.75 to 8.40) | 3.65 (2.73 to 4.9 3) | 2.43 (1.63 to 3.66) | 2.43 (1.61 to 3.7 4) | 2.10 (1.49 to 2.99) |

**TABLE 12. PAIRWISE COMPARISONS OF MECOM KNOCKDOWN CONSTRUCTS FOR SELECTED DRUGS: Δ log$IC_{50}$, 95% CONFIDENCE INTERVALS, AND SIGNIFICANCE.Planned comparisons were performed between scramble and knockdown constructs (shRNA#1, shRNA#3) and between knockdown constructs within each drug family (Erastin, ABBV-744, Vorinostat). Δ log$ic_{50}$ values were calculated as Construct A − construct B, where positive δ indicates construct a has a higher $IC_{50}$ (reduced sensitivity) relative to construct B.**

| Drug | Comparison | Δ log$IC_{50}$ (95% CI) | Raw *p* | Bonferroni-adjusted *p* |
|---|---|---|---|---|
| | **D38M** | | | |
| Erastin | Scramble shRNA vs shRNA#1 | -0.303 (-0.487 to -0.118) | 0.0013 | **0.0026** |
| | Scramble shRNA vs shRNA#3 | -0.361 (-0.523 to -0.199) | <0.0001 | **<0.0002** |
| | **D23M** | | | |
| ABBV-744 | Scramble shRNA vs shRNA#1 | -0.112 (-0.274 to 0.049) | 0.1577 | 0.4731 |
| | Scramble shRNA vs shRNA#3 | 0.118 (-0.022 to 0.258) | 0.0859 | 0.2577 |
| | shRNA#1 vs shRNA#3 | 0.230 (0.075 to 0.385) | 0.0034 | **0.0102** |
| | **D23M** | | | |
| Voronistat | Scramble shRNA vs shRNA#1 | -0.032 (-0.208 to 0.144) | 0.7047 | 2.114 |
| | Scramble shRNA vs shRNA#3 | 0.205 (0.025 to 0.384) | 0.0225 | 0.0675 |
| | shRNA#1 vs shRNA#3 | 0.237 (0.059 to 0.415) | 0.0087 | **0.0261** |

## 3.5 CONCLUSION

This study provides the first functional evidence linking MECOM expression to melanoma cell behaviour, though the effects observed were modest and context dependent. Inducible MECOM knockdown was technically feasible but variable across cell lines, limiting reproducibility. While suppression of MECOM reduced proliferation in a subset of dedifferentiated model cell lines, other phenotypic traits such as migration, clonogenicity, and anchorage-independent growth, were largely unaffected. The alteration to proliferation rate is contrary to what we had anticipated if a phenotype switch were to occur and combined with the lack of impact on other cell characteristics this suggests that MECOM alone may not be driving a switch. Drug sensitivity profiling revealed an effect in D38M cells, where MECOM depletion significantly reduced vulnerability to Erastin, a ferroptosis inducer. However, this result did not generalise to the other tested ferroptosis inducer (RSL-3) or the other tested cell line (D23M). These findings indicate that MECOM may contribute to ferroptosis sensitivity and cellular phenotype but does not uniformly govern melanoma plasticity. Future work should explore combinatorial approaches and longer-term MECOM suppression to determine whether its role is modulatory rather than deterministic, and whether MECOM-targeted strategies could complement existing therapies in dedifferentiated melanoma.

A key limitation of this chapter is the absence of direct transcriptional or marker-based assessment of melanoma cell-state identity following MECOM knockdown. While functional assays were selected based on well-established behavioural differences between melanocytic and dedifferentiated states, these readouts provide indirect insight into differentiation-associated behaviour rather than definitive evidence of phenotype switching. Therefore, the results presented here support a role for MECOM in modulating specific functional traits and drug vulnerabilities in a context-dependent manner, but do not demonstrate MECOM as a sole driver of melanoma cell-state transitions.

# CHAPTER 4: MECOM OVEREXPRESSION REVEALS CONTEXT-DEPENDENT EFFECTS ON MELANOMA CELL BEHAVIOUR

## 4.1 INTRODUCTION

This chapter describes the development of experimental models to investigate *MECOM* overexpression in melanoma cell lines and assess its impact on cellular phenotype. This provides a complementary approach to MECOM knockdown as discussed in Chapter 3: Impact of MECOM Depletion on Phenotypic Traits and Therapeutic Vulnerability in Melanoma. We first optimized a dual-inducible lentiviral system to enable controlled MECOM expression, evaluating transduction strategies, induction conditions, and technical limitations. Due to persistent challenges, including unreliable induction, undetectable FLAG-tagged MECOM, and cytotoxicity associated with induction regimens, we transitioned to a constitutive overexpression approach. Using this system, we performed functional assays to determine whether MECOM overexpression influences proliferation, migration, clonogenic potential, and sensitivity to ferroptosis inducers. These experiments aim to clarify whether MECOM contributes to phenotype switching and aggressive behaviour in melanoma, providing mechanistic insight into its potential role in disease progression.

## 4.2 GENERATION AND VALIDATION OF INDUCIBLE MECOM OVEREXPRESSION IN MELANOMA CELL LINES

Initial experiments sought to establish an inducible model of MECOM overexpression, which would therefore minimize potential confounding effects of constitutive expression on cell viability and phenotype during model development. The dual-inducible lentiviral system was selected for its flexibility, enabling temporal regulation of MECOM expression via tetracycline-based induction. The following sections detail the optimization of selection conditions, evaluation of transduction strategies, and validation of MECOM induction under various treatment regimens. The rationale for the choice of cell line (C001M, C002M) is described in Chapter 3, Section 3.2.

### *4.2.1 OPTIMIZATION OF HYGROMYCIN SELECTION CONFIRMED EFFECTIVE DOSE RANGES FOR MELANOMA CELL LINES*

Prior to transduction, a hygromycin “kill curve” was generated to determine the optimal selection concentration for C001M cells. Cell viability declined in a dose-dependent manner, with complete cell death noted by day 7 of treatment with doses ≥100 µg/mL (Figure 21). Based on these results, 100 µg/mL was selected as the selection concentration for C001M, while 200 µg/mL was used for C002M based on previous optimisation.

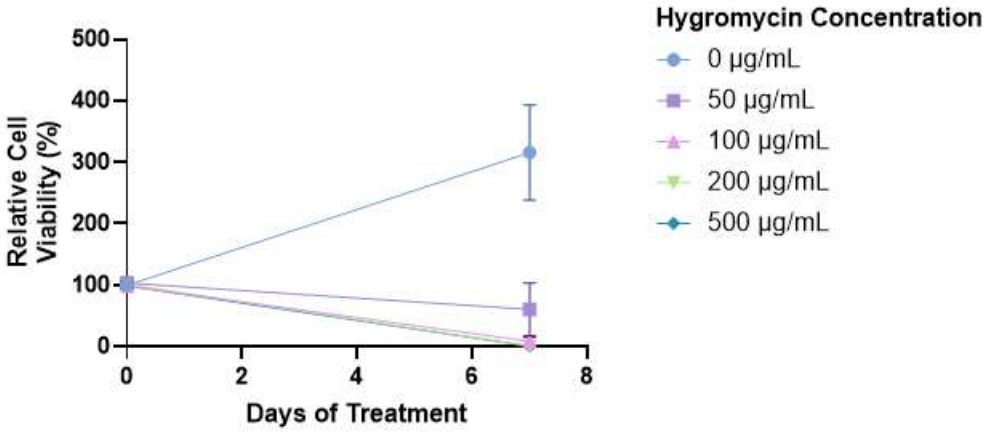


**FIGURE 21. HYGROMYCIN "KILL CURVE" FOR C001M CELLS.**

**Relative cell viability was determined by luminescence values normalized to day 0 readings. Data represent one biological replicate performed in triplicate technical replicates. Error bars represent the standard error of the mean (SEM).**

### *4.2.2 SEQUENTIAL AND CO-TRANSDUCTION APPROACHES YIELDED COMPARABLE ENRICHMENT OF TRANSDUCED POPULATIONS*

Establishing inducible MECOM overexpression required a dual lentiviral tetracycline-inducible system comprising two vectors:

- Regulatory vector encoding the tetracycline-controlled transcriptional silencer (Tts), reverse tetracycline transactivator M2 (rtTA), and a hygromycin resistance gene.
- Expression vector encoding either FLAG-tagged MECOM and mCherry under a tetracycline response element (TRE) promoter, or FLAG-tagged mCherry alone (empty vector control).

Co-transduction of both vectors was therefore necessary to achieve inducible MECOM overexpression. Both sequential and co-transduction methods were evaluated for establishing inducible MECOM overexpression. In both approaches, populations were established by hygromycin selection followed by enrichment of mCherry-positive cells by Fluorescent Activated Cell Sorting (FACS). Both the empty vector control and MECOM overexpression cell lines were sorted, and two rounds of sorting were required before post-sort analysis confirmed >90% purity (Figure 22). No significant differences in cell viability or enrichment were noted between sequential and co-transduction methods.

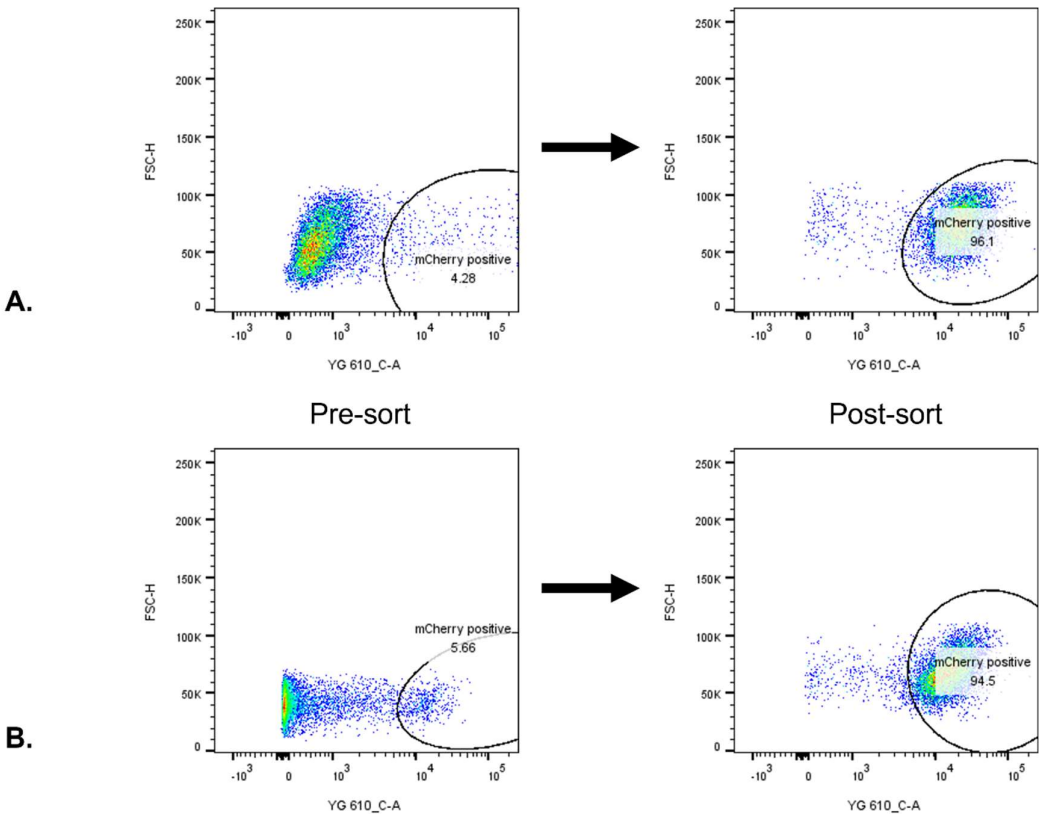


**FIGURE 22. REPRESENTATIVE PLOTS DEMONSTRATING ENRICHMENT OF MCHERRY-POSITIVE MELANOMA CELLS BY FACS IN C002M MELANOMA CELL LINE. (A) Sequential transduction: pre-sort (left) and post-sort (right) plots. (B) Co-transduction: pre-sort (left) and post-sort (right) plots.**
**Numbers indicate % mCherry-positive cells within the gate.**

### *4.2.3 Initial tetracycline-based induction failed to produce reliable MECOM overexpression*

Induction of MECOM expression was initially attempted using tetracycline hydrochloride (0–2 µg/mL), but no detectable upregulation of the MECOM protein was observed in the FLAG/hMECOM transduced cells by Western blotting (Figure 23A). Paradoxically, MECOM expression was detected in cells transduced with the FLAG/mCherry empty vector control in the C002M cells (Figure 23A). To exclude sample misidentification, PCR amplification of vector-specific sequences (mCherry and FLAG-tagged MECOM) was performed, confirming correct construct assignment. This unexpected finding did not replicate upon repeated transduction, selection, and FACS enrichment (Figure 23B).

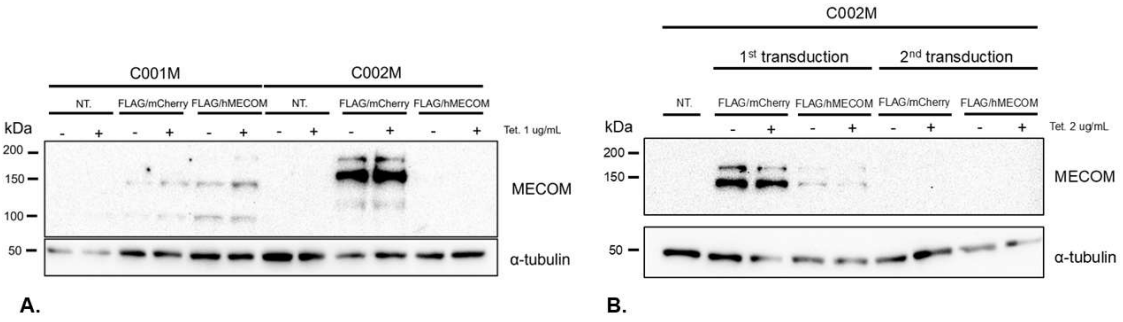


**FIGURE 23. OPTIMISATION OF INDUCIBLE OVEREXPRESSION OF MECOM. C001M and C002M melanoma cells transduced with either FLAG/hMECOM or FLAG/mCherry constructs were treated with tetracycline hydrochloride (0–2 µg/mL) for 72 hours. MECOM overexpression was not reliably detected in FLAG/hMECOM-transduced cells, whereas paradoxical MECOM expression was observed in FLAG/mCherry empty vector-transduced C002M cells (7A). Following repeat transduction, selection, and FACS enrichment under identical conditions, MECOM expression was not detected in FLAG/mCherry empty vector-transduced cells, confirming the initial anomaly was not reproducible (7B). Western blotting of whole cell lysates (C001M, C002M) was performed with anti-MECOM antibody. α-tubulin was used as a loading control.**

### *4.2.4 Robust MECOM expression required combined anhydrotetracycline and sodium butyrate treatment*

Alternative conditions were tested, including anhydrotetracycline hydrochloride (50–250 ng/mL) and co-treatment with sodium butyrate (1 mM). Anhydrotetracycline was chosen as the inducer because it binds the reverse tetracycline transactivator (rtTA) with higher affinity than tetracycline, ensuring efficient activation of the Tet-On system (145, 146). Sodium butyrate, a histone deacetylase inhibitor, was included to counteract epigenetic silencing of the TRE promoter, which can occur over time in lentivirally transduced cells (142). The combination of 250 ng/mL anhydrotetracycline and 1 mM sodium butyrate produced the most consistent and robust MECOM expression across both C001M and C002M cell lines (Figure 24A). No overexpression was induced under these conditions in the C002M sequentially transduced cell lines (Figure 24B). Consequently, only co-transduced cell lines were retained for subsequent experiments using the optimized induction conditions.

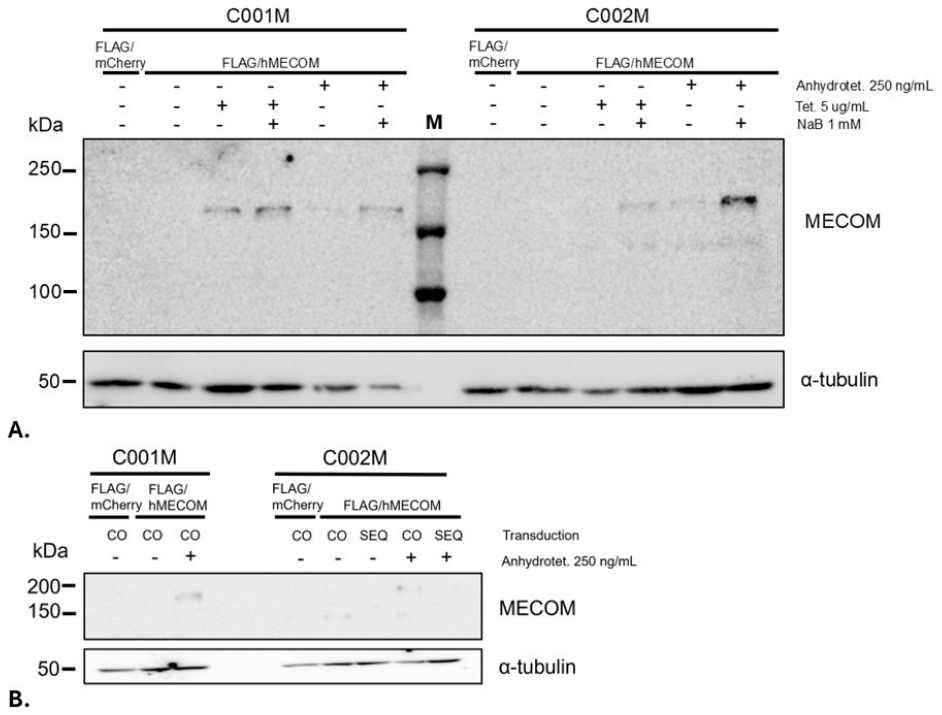


**FIGURE 24. OPTIMISATION OF INDUCTION CONDITIONS FOR MECOM OVEREXPRESSION.Western blot analysis of C001M and C002M melanoma cells treated with anhydrotetracycline hydrochloride (Anhydrotet.; 0-250 ng/ml) with or without sodium butyrate (NaB; 1 mM) for 72 hours. MECOM expression was observed under combined treatment with 250 ng/ml anhydrotet. and 1 mM NaB in co-transduced cell lines (A). No MECOM expression was detected in sequentially transduced C002M cells under the same conditions (B). Western blotting of whole-cell lysates was performed using anti-MECOM antibody, with α-tubulin as a loading control, and a protein marker for reference (M).**

### *4.2.5 FLAG-TAG DETECTION WAS UNRELIABLE DESPITE CONFIRMED MECOM EXPRESSION*

Despite successful generation and enrichment of transduced populations, MECOM induction in the dual tetracycline-inducible system was unreliable. Western blotting with anti-FLAG failed to detect FLAG-tagged MECOM (Figure 25B), despite robust detection of MECOM (Figure 25A) and FLAG-tagged mCherry (Figure 25B). The detection of MECOM with the anti-MECOM antibody under optimised conditions (anhydrotet. + NaB; Figure 25A), but undetectable FLAG, indicated that FLAG detection was unreliable in this system.

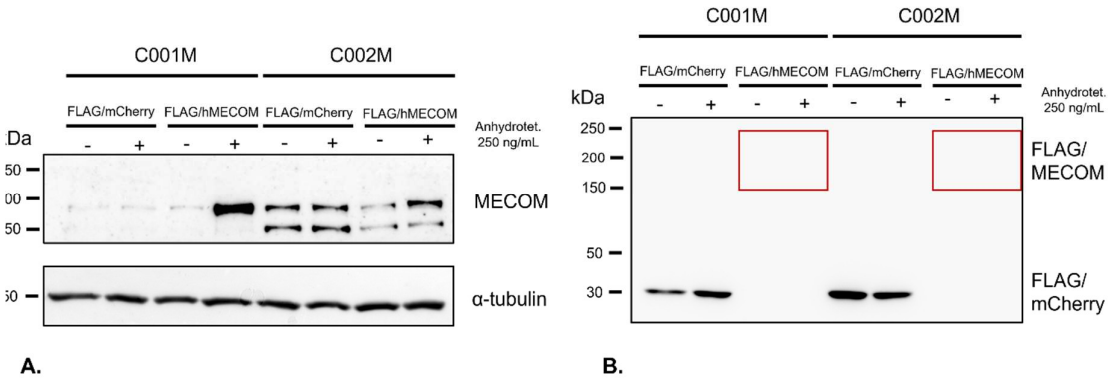


**FIGURE 25. DETECTION OF MECOM AND FLAG UNDER OPTIMISED INDUCTION CONDITIONS. Western blot analysis of C001M and C002M melanoma cells treated with anhydrotetracycline hydrochloride (anhydrotet.; 250 ng/mL) and sodium butyrate (NaB; 1 mM) for 72 hours. MECOM expression was confirmed under these optimised conditions using anti-MECOM antibody (9A). Detection of FLAG-tagged constructs was attempted using anti-FLAG antibody; FLAG-tagged mCherry was detected, whereas FLAG-tagged MECOM was not observed (9B). Squares indicate the expected position of FLAG-tagged MECOM. Western blotting of whole-cell lysates was performed with α-tubulin as a loading control.**

## 4.3 FUNCTIONAL ASSAYS AND DRUG SENSITIVITY FOLLOWING INDUCIBLE MECOM OVEREXPRESSION

To explore the role of MECOM over-expression within these cell lines and assess for a potential phenotype switch, colony formation assays and drug sensitivity assays focusing on inducers of ferroptosis were performed following one week of MECOM induction. Melanoma cell sensitivity to inducers of ferroptosis has been demonstrated to correlate with differentiation subtype, as shown by Tsoi et al. and in Chapter 3 Section 3.4.5 Parental cell lines demonstrate variable sub-type specific sensitivity to melanoma drugs). Drug concentrations for screening were determined based on IC50 testing in parental C001M and C002M cell lines.

### *4.3.1 INDUCTION CONDITIONS PREVENTED COLONY FORMATION INDEPENDENTLY OF MECOM EXPRESSION*

Induction conditions proved cytotoxic or cytostatic when cells were seeded at low densities for functional assays. While cells reached confluency in T25 flasks under induction, growth was markedly impaired in colony formation assays (1,000 cells/well in 12-well plates) and drug sensitivity assays (1,000 cells/well in 96-well plates). Colony formation was completely abrogated in wells pre-treated with sodium butyrate alone or sodium butyrate + anhydrotetracycline across both FLAG/mCherry and FLAG/hMECOM populations, indicating that the biological impact was driven by the induction regimen rather than MECOM overexpression (Figure 26). Co-treatment with sodium butyrate (1 mM), with or without anhydrotetracycline (250 ng/mL), prevented colony initiation and significantly reduced viability, precluding reliable performance of these assays, particularly after prolonged exposures (Figure 26).

The observed cytotoxicity affected both control and MECOM-overexpressing populations, indicating that growth inhibition was attributable to the induction regimen rather than MECOM expression itself.

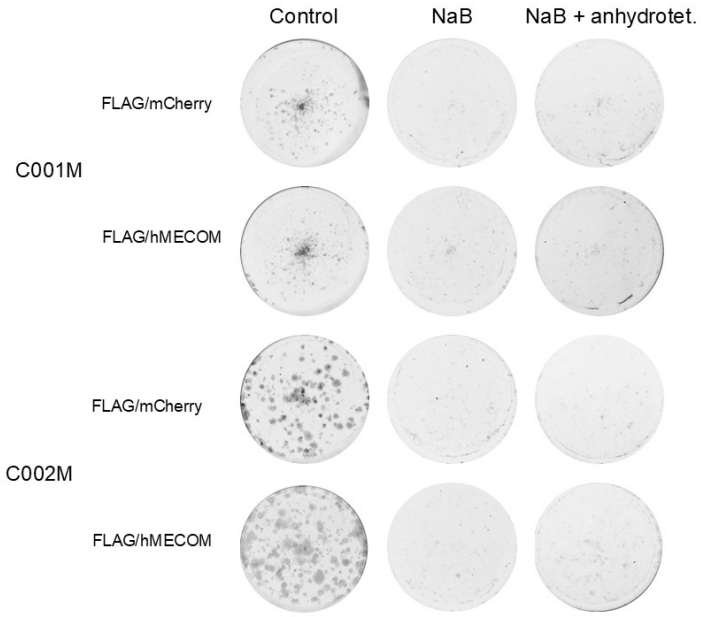


**FIGURE 26. IMPACT OF INDUCTION REGIMENS ON COLONY FORMATION IN MELANOMA CELLS. Representative images of colony formation assays in C001M (top rows) and C002M (bottom rows) melanoma cells transduced with either FLAG/mCherry (control) or FLAG/hMECOM constructs. Cells were seeded at low density (1,000 cells/well) and pre-induced under three conditions: no induction drug (control), sodium butyrate (NaB; 1 mM), or NaB combined with anhydrotetracycline (anhydrotet; 250 ng/ml). Colony formation was completely inhibited in wells treated with NaB alone or NaB + anhydrotet. across both vector types, indicating that cytotoxicity was attributable to the induction regimen rather than MECOM overexpression. Technical triplicates and biological replicates were performed.**

### *4.3.2 Induction conditions confounded or contributed to drug sensitivity independent of MECOM overexpression*

These effects were further characterized through drug sensitivity testing (Figure 27). At 48 h pre-induction, both cell lines showed mildly reduced sensitivity to Erastin in FLAG/hMECOM populations compared to FLAG/mCherry, independent of sodium butyrate or anhydrotetracycline exposure (Figure 27A). After 1 week of pre-induction, C001M cells exhibited increased sensitivity to high-dose Erastin (30 μM) in FLAG/hMECOM populations, particularly with sodium butyrate alone, and this effect was partially ameliorated by concurrent anhydrotetracycline treatment. In contrast, C002M cells demonstrated paradoxical resistance to Erastin following prolonged sodium butyrate ± anhydrotetracycline exposure, regardless of vector (Figure 27B). These patterns suggest that prolonged exposure to sodium butyrate, and especially sodium butyrate combined with anhydrotetracycline, may confer treatment resistance to Erastin at high doses, independent of *MECOM* overexpression.

For RSL-3, at 48 h pre-induction, low-dose treatment (3 μM) markedly reduced viability in NaB-treated cells (with or without anhydrotetracycline) across both FLAG/mCherry and FLAG/hMECOM

populations (~40–50%), compared to untreated controls (~85–115%), while high-dose RSL-3 (30 μM) resulted in near-complete loss of viability (<10%) across all conditions (Figure 27C). After 1 week of pre-induction, untreated cells exhibited good survival at low-dose RSL-3 (~100% normalized to vehicle-only control), while high-dose treatment reduced viability to ~40% in FLAG/mCherry cells but not in FLAG/hMECOM cells (~100%). The basis for this discrepancy is unclear. Importantly, NaB ± anhydrotetracycline pre-treatment uniformly sensitized cells to RSL-3, reducing viability to <10% at both doses across both cell lines, while untreated controls maintained high viability at low dose (Figure 27D). Any apparent differences between FLAG/hMECOM and FLAG/mCherry were minor and inconsistent.

Given the cytostatic and cytotoxic effects of sodium butyrate at assay seeding densities, inducible MECOM overexpression could not be reliably evaluated for phenotypic or drug sensitivity outcomes.

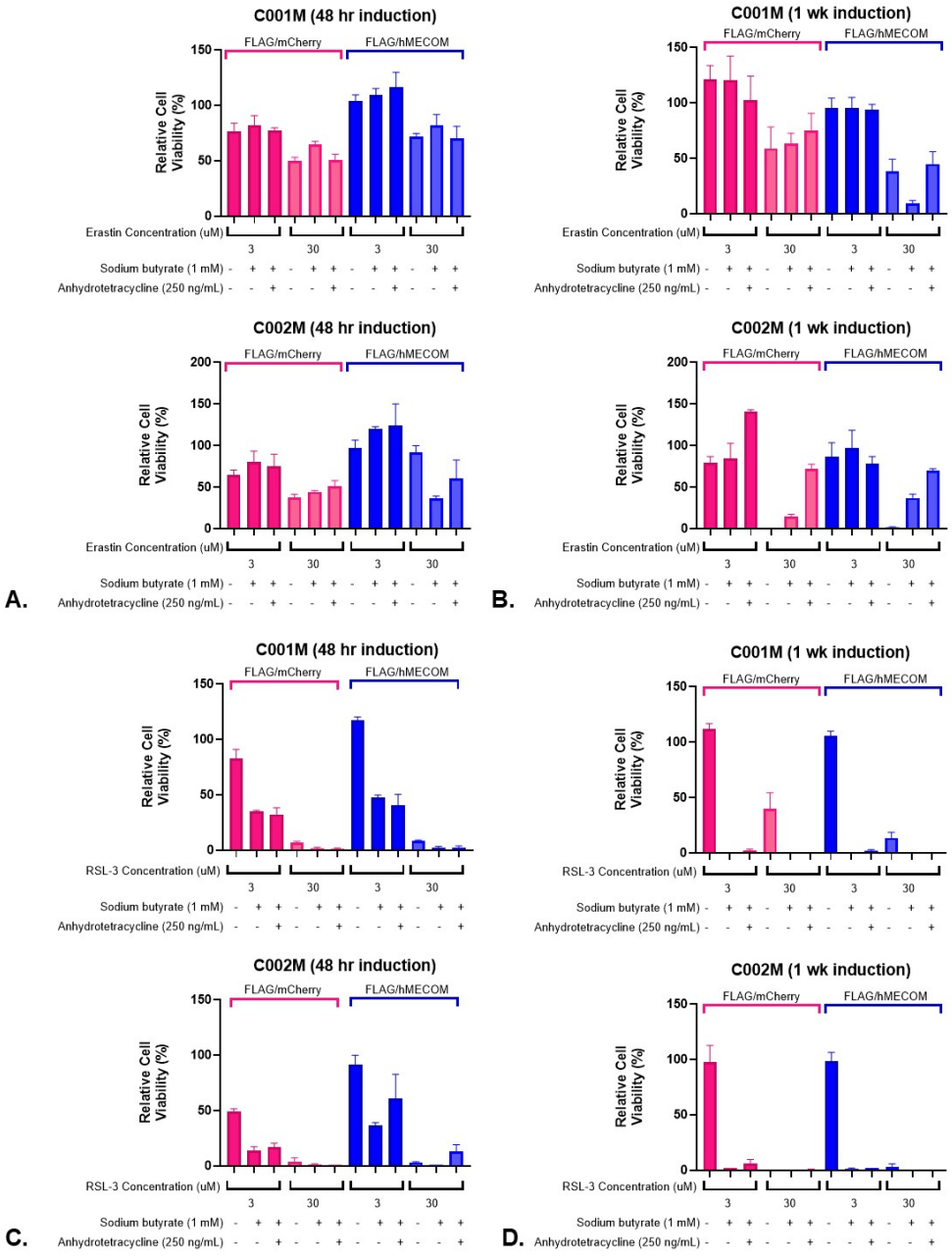


**FIGURE 27. VIABILITY OF MELANOMA CELLS FOLLOWING ERASTIN OR RSL-3 TREATMENT AFTER PRE-INDUCTION. C001M and C002M melanoma cells were pre-induced for either 48 hours or 1 week under three conditions: no induction, sodium butyrate (NaB; 1 mM), or NaB combined with anhydrotetracycline (anhydrotet; 250 ng/mL). Following pre-induction, cells were treated for 48 hours with either Erastin (3 µM or 30 µM) or RSL-3 (3 µM or 30 µM).**

**(A) Erastin treatment following 48-hour pre-induction.**

**(B) Erastin treatment following 1-week pre-induction.**

**(C) RSL-3 treatment following 48-hour pre-induction.**

**(D) RSL-3 treatment following 1-week pre-induction.**

**Graphs show viability normalized to vehicle-only controls, measured by CellTiter-Glo® 2.0 assay Data represent mean ± standard deviation of technical replicates. No formal statistical comparisons were performed due to the large**

**number of conditions and the dominant cytotoxic effect of induction regimens. Trends indicate that prolonged NaB ± anhydrotetracycline exposure strongly influenced drug sensitivity, overshadowing any MECOM-specific effects.**

## 4.4 Generation and validation of constitutive MECOM overexpression in melanoma cell lines

To overcome the evident limitations of the dual-inducible system, namely weak *MECOM* induction, undetectable FLAG signal, and cytotoxicity associated with sodium butyrate ± anhydrotetracycline, we designed and synthesised a constitutive MECOM overexpression vector. This approach aimed to achieve robust, tag-detectable expression without exposure to cytotoxic induction conditions, enabling downstream immunoprecipitation mass spectrometry and functional assays.

A constitutive MECOM overexpression construct (pFUW 11-3) was successfully cloned, sequence-validated, packaged, and stably expressed in C001M and C002M melanoma cell lines. MECOM was robustly detected by Western blot, while FLAG detection remained unreliable. Nevertheless, the constitutive system enabled progression to functional assays without sodium butyrate/anhydrotetracycline exposure.

### *4.4.1 Cloning strategy and PCR amplification of the MECOM insert*

A 3,753 bp FLAG/hMECOM insert encompassing the Kozak initiation sequence, N-terminal FLAG tag, and the full MECOM coding sequence was amplified from the previously validated VectorBuilder template. Two forward primers were evaluated (MECOM_FWD_1 and MECOM_FWD_2), paired with a common reverse primer (MECOM_HpaI_Rev), to flank the insert and create EcoRI/HpaI cloning sites to facilitate directional insertion into the FUW lentiviral backbone upstream of mCherry-P2A. Target-sized amplicons were visualised by agarose gel electrophoresis and excised for purification (Figure 28).

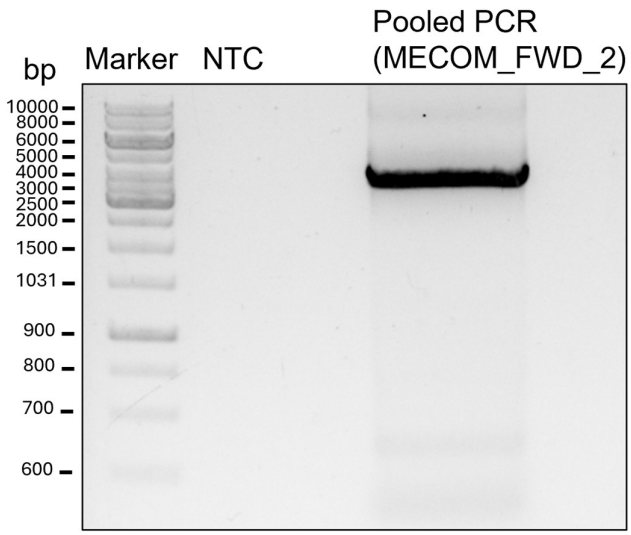


**FIGURE 28. PCR AMPLIFICATION OF FLAG/hMECOM INSERT.**

**Agarose gel electrophoresis showing amplification of the 3,753 bp FLAG/hMECOM insert using MECOM _FWD_2 with MECOM_HpaI_REV. Target band was excised and purified. No positive colonies were generated using the product amplified using the alternative MECOM_FWD_1 forward primer.**

The purified insert and FUW backbone were sequentially digested with EcoRI and HpaI, with calf intestinal phosphatase (CIP) treatment to prevent vector re-ligation. Ligation reactions were performed at 1:3, 1:5, and 1:7 vector:insert ratios and incubated overnight. Following transformation and plating on ampicillin selection, colonies were screened by PCR using the primer sets described above. A schematic of the resultant vector is shown in Figure 29.

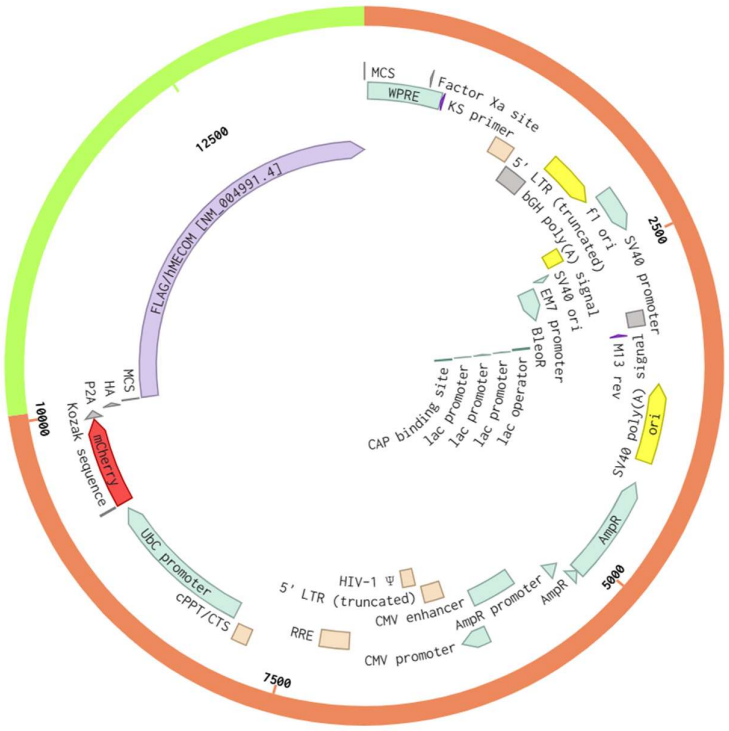


**FIGURE 29. SCHEMATIC REPRESENTATION OF THE ENGINEERED PFUW 11-3 VECTOR.The successful vector was generated following EcoRI/HpaI digestion of FUW backbone and MECOM insert, CIP dephosphorylation of the vector, and ligation in a 1:3 vector:insert ratio. The control vector lacks the FLAG/hMECOM insert but is otherwise identical. Diagram produced using benchling.com.**

### *4.4.2 Colony Screening and Sanger Validation of Insert*

Of 150 colonies screened over multiple rounds of cloning, two positives were identified using MECOM_FWD_2, both derived from the 1:3 ligation condition (Figure 30). Sanger sequencing confirmed a fully intact *MECOM* coding sequence in clone pFUW 11-3, which was selected for downstream work; the companion clone showed sequence deviations and was not pursued (Figure 31).

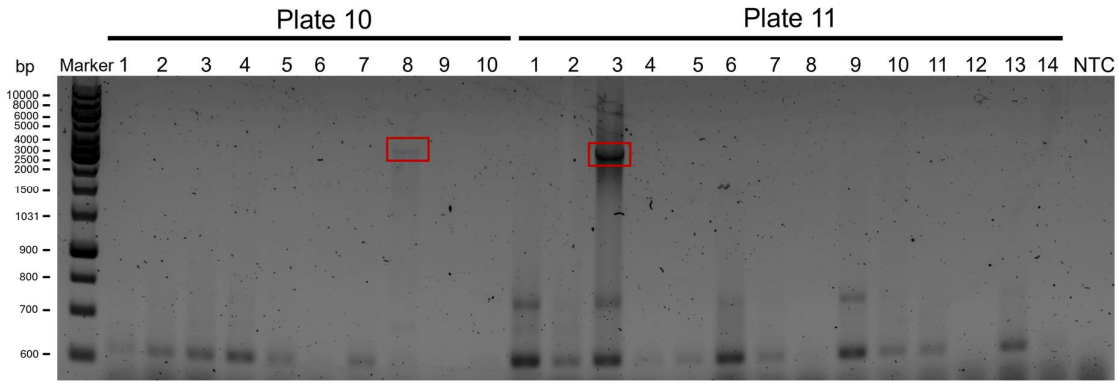


**FIGURE 30. PCR SCREENING OF TRANSFORMANTS.PCR screening identified two colonies positive for the *MECOM* insert. Red boxes highlight the identified transformants (10-8 and 11-3) which were subsequently purified and submitted for Sanger sequencing. NTC; no template control.**

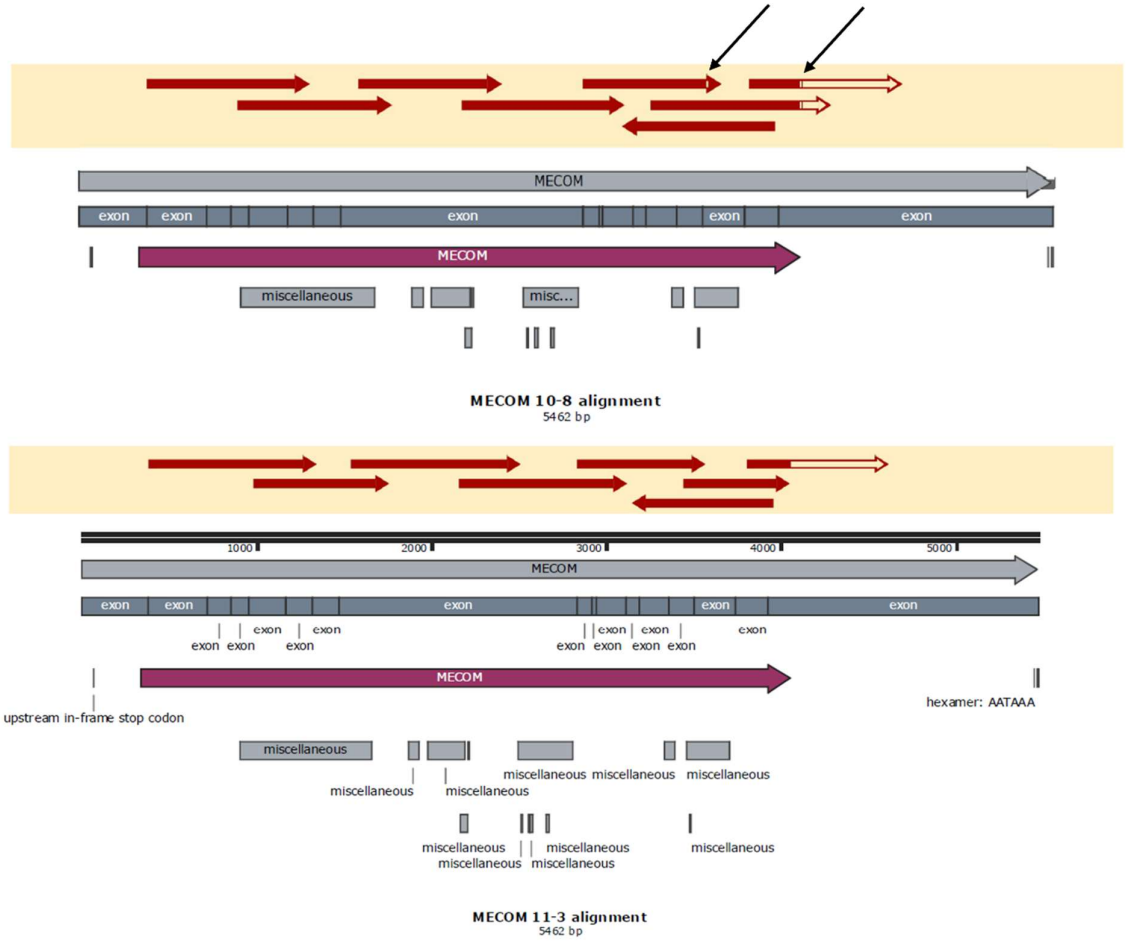


**FIGURE 31. SEQUENCE ALIGNMENT/SANGER SEQUENCING VALIDATION OF CLONES. Sanger sequencing confirmed an intact *MECOM* coding sequence in clone pFUW 11-3, which was advanced to downstream applications; the second clone (pFUW 10-8) contained sequence deviations and was excluded.**

### 4.4.3 *Lentiviral packaging, melanoma cell transduction, and enrichment*

The pFUW 11-3 (FLAG/hMECOM) and pFUW control transfer plasmids were packaged into lentivirus in HEK293T cells using calcium phosphate precipitation and used to transduce C001M and C002M melanoma cells. Post-transduction, mCherry-positive populations were enriched by FACS.

### 4.4.4 *Validation of constitutive expression by Western Blotting*

Western blotting of whole-cell lysates confirmed robust MECOM protein expression in pFUW 11-3-transduced cells across both melanoma lines (Figure 32A). In contrast, FLAG-tagged MECOM was undetectable, despite reliable detection of the FLAG/mCherry positive control under the same conditions, indicating persistent FLAG detection limitations in this system or with the use of this template (Figure 32B). α-Tubulin served as a loading control.

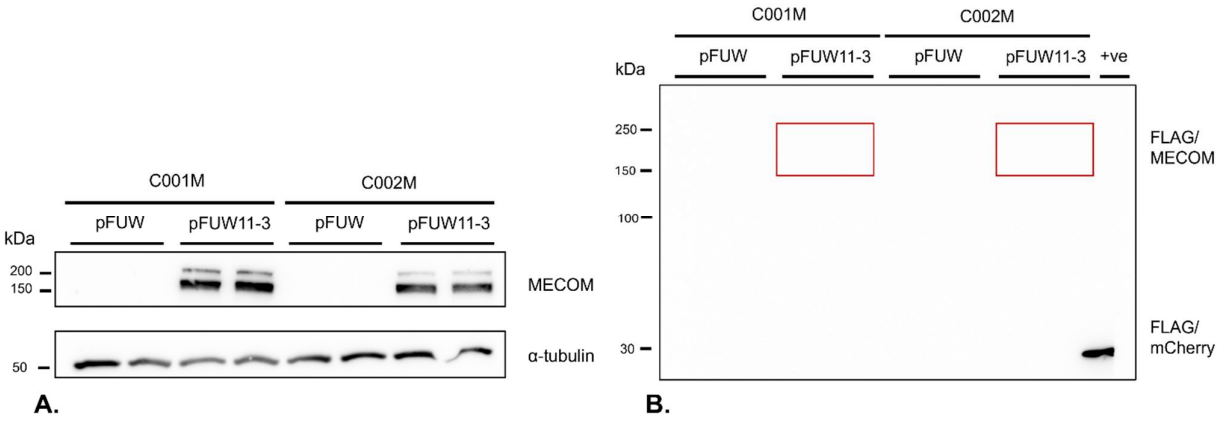


**FIGURE 32. VALIDATION OF CONSTITUTIVE MECOM OVEREXPRESSION AND FLAG DETECTION. Western blot analysis of C001M and C002M melanoma cells transduced with pFUW control (empty vector) or pFUW 11-3 (FLAG/hMECOM). MECOM expression was robustly detected in constitutive overexpression lines (A), while FLAG-tagged MECOM was not detected under the same conditions (B); FLAG/mCherry from the inducible system was readily detected as a positive control (+ve). α-Tubulin served as a loading control. Biological replicates of the transduction and enrichment process are shown side-by-side.**

With constitutive MECOM expression established without the need for exposure to inducing agents (sodium butyrate, anhydrotetracycline), we proceeded to functional characterization: scratch (wound-healing) assays, proliferation assays, colony formation assays (CFA), and drug sensitivity assays.

## 4.5 Functional assays and drug sensitivity following constitutive *MECOM* overexpression

To determine whether MECOM overexpression promotes phenotypic plasticity in melanoma, we performed functional assays and drug sensitivity tests in the two melanocytic cell lines (C001M and C002M) following establishment of constitutive MECOM overexpression. Our aim was to assess whether MECOM could drive a shift toward a less differentiated, more aggressive state. We evaluated proliferation, migration, clonogenic potential, and ferroptosis sensitivity. MECOM overexpression

produced clear phenotypic changes in C001M, including enhanced proliferation, accelerated wound closure, increased clonogenic capacity and increased sensitivity to ferroptosis inducers, whereas C002M remained largely unaffected. These findings suggest that *MECOM*-driven phenotype modulation is context-dependent, and melanoma plasticity may vary across differentiation states and cell lines.

### *4.5.1 Constitutive MECOM overexpression enhanced proliferation in C001M cells but not C002M*

In C001M, constitutive MECOM overexpression significantly increased viability compared to pFUW controls from Day 3 onward, with differences persisting through Day 7 (Figure 33A). At baseline (Day 0), viability was equivalent between groups (adjusted $p > 0.05$). By Day 3, *MECOM* overexpression cells exhibited ~30% higher viability (adjusted $p = 6.0\times10^{-6}$), increasing to ~56% at Days 5 and 7 (adjusted $p \leq 7.3\times10^{-5}$).

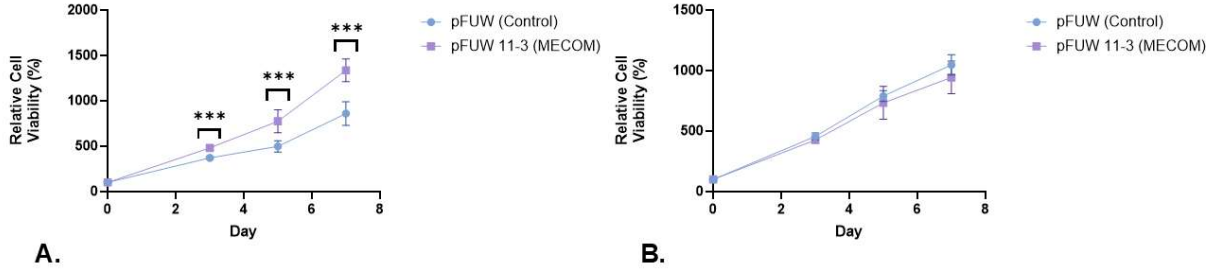


**FIGURE 33. PROLIFERATION OF MELANOMA CELLS UNDER CONSTITUTIVE MECOM OVEREXPRESSION. Time-course viability of pFUW control versus pFUW 11-3 (FLAG/hMECOM) transduced cells measured at Day 0, Day 3, Day 5, and Day 7 using the CellTiter-Glo® 2.0 luminescence assay.**
**(A) C001M: MECOM overexpression significantly increased viability at Days 3–7 compared to control (multiple unpaired two-tailed t-tests with Benjamini, Krieger, and Yekutieli FDR correction; Day 3 $p = 6.0\times10^{-6}$, Day 5 $p = 7.0\times10^{-4}$, Day 7 $p = 7.3\times10^{-5}$), with no difference at baseline (Day 0, adjusted $p > 0.05$).**
**(B) C002M: No significant differences were observed between groups at any timepoint (all adjusted $p > 0.05$).**
**Data shown as mean values normalised to Day 0 readings, encompassing technical triplicates and biological replicates of the transduction and enrichment process.**

In contrast, C002M cells showed no difference in proliferation between pFUW and pFUW *MECOM* populations across all time points (Figure 33B), indicating that MECOM-driven growth enhancement is context-dependent. Viability was measured via CellTiter-Glo® 2.0 luminescence assay; values reported are relative luminescence units (RLU).

### *4.5.2 Constitutive MECOM overexpression accelerated wound closure in C001M cells but had no detectable impact on C002M*

In C001M, MECOM overexpression significantly increased wound closure at 48 h (86.5% ± 9.86%) compared to pFUW control (56.6% ± 17.9%), a mean difference of 29.9% (Figure 34). In C002M, closure rates were similar between MECOM overexpression (40.6% ± 5.1%) and control (36.3% ± 13.0%; adjusted p > 0.05). Values represent mean percent closure at 48 h relative to Day 0 wound area.

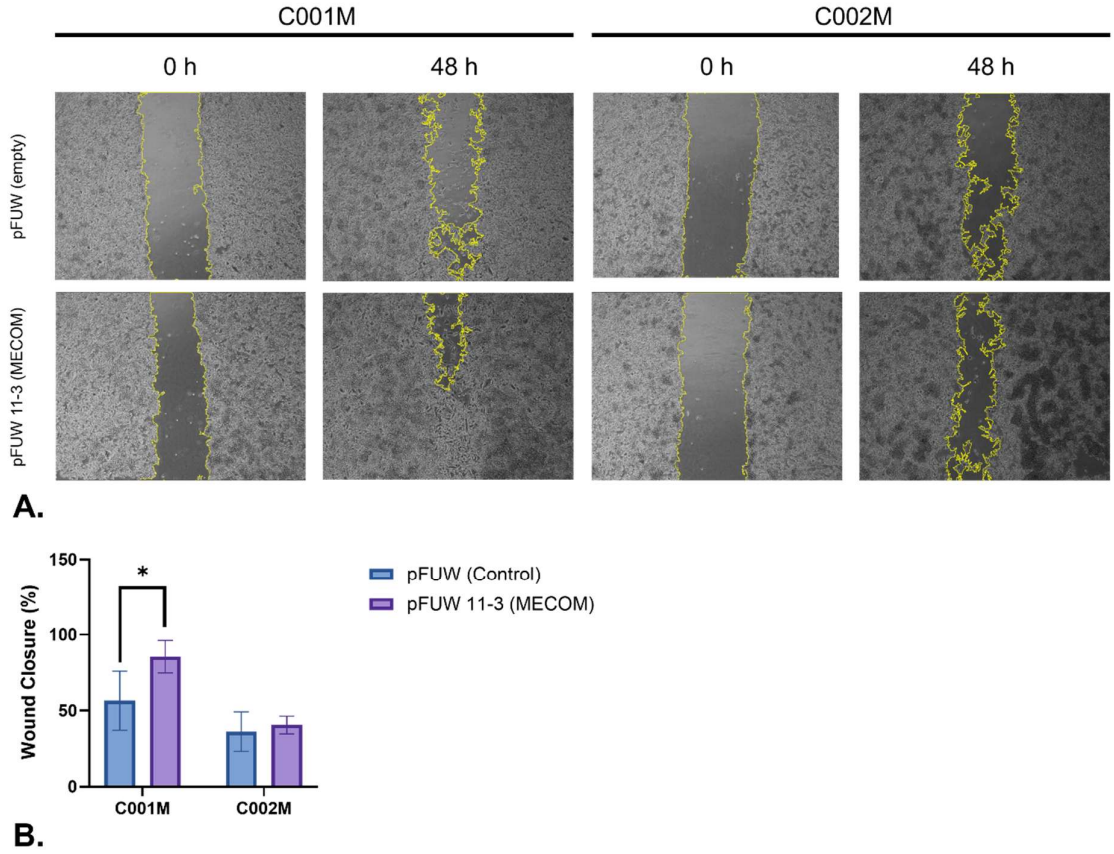


**FIGURE 34. WOUND HEALING (SCRATCH) ASSAY UNDER CONSTITUTIVE MECOM OVEREXPRESSION. MEAN PERCENT WOUND CLOSURE AT 48 HOURS RELATIVE TO DAY 0 IN PFUW CONTROL AND PFUW 11-3 (FLAG/hMECOM).**

**(A) Representative images of wound closure in C001M and C002M (0 h and 48 h) melanoma cell lines following transduction with pFUW (empty) or pFUW 11-3 (MECOM overexpression) vectors. Images were captured at ×4 magnification, and wound margins are outlined in yellow.**

**(B) Quantification of wound closure (%) normalized to 0 h, based on ImageJ analysis. Results represent means ± SEM from two biological replicates (technical triplicates per replicate). Statistical analysis was performed using multiple t-tests with Benjamini–Krieger–Yekutieli (BKY) correction for multiple comparisons. Quantification revealed:**

**- C001M: MECOM overexpression increased closure (86.5% ± 9.86% vs 56.6% ± 17.9%; q = 0.0194).**

**- C002M: no significant difference (40.6% ± 5.1% vs 36.3% ± 13.0%; adjusted p > 0.05).**

### *4.5.3 Constitutive MECOM overexpression increased clonogenicity in C001M cells but not C002M*

After 14 days, MECOM overexpression markedly increased colony number in C001M (99.7 ± 21.7 vs 34.0 ± 10.5 colonies; $q = 5.6\times10^{-5}$). In C002M, colony numbers were similar between MECOM overexpression samples and controls (58.3 ± 14.6 vs 62.7 ± 6.19 colonies; $q = 0.262$). Values represent mean ± SD from technical triplicates within each biological replicate (bio $n = 2$ per group). Increased clonogenicity has been associated with the dedifferentiated state in melanoma (147, 148), supporting the hypothesis that MECOM contributes to a more aggressive phenotype in a context-dependent manner.

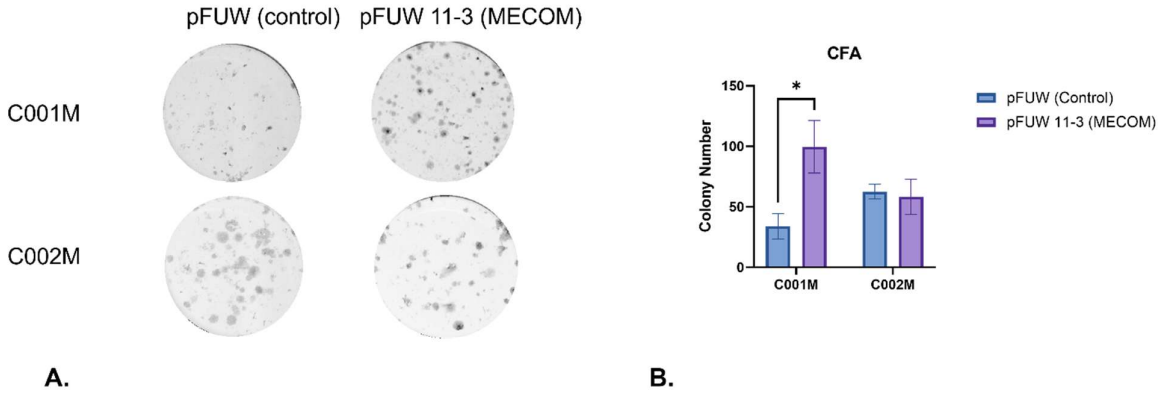


**FIGURE 35. COLONY FORMATION UNDER CONSTITUTIVE MECOM OVEREXPRESSION.(A) Representative wells from colony formation assays after 14 days in pFUW control and pFUW 11-3 (FLAG/hMECOM) lines.**
**(B) Quantification of colony counts (mean ± SD) for C001M and C002M under pFUW control versus MECOM OE. MECOM OE significantly increased colony number in C001M (99.7 ± 21.7 vs 34.0 ± 10.5; $q = 5.6\times10^{-5}$), while no significant difference was observed in C002M (58.3 ± 14.6 vs 62.7 ± 6.19; $q = 0.262$). Bars indicate mean ± SD; data reflect technical triplicates within each biological replicate (bio $n = 2$/group). Statistical comparisons were performed using multiple unpaired two-tailed *t*-tests with two-stage BKY FDR control at Q = 0.05.**

### *4.5.4 Constitutive MECOM overexpression increases sensitivity to inducers of ferroptosis in C001M cells but not C002M*

To test whether MECOM modulates ferroptosis sensitivity, constitutive overexpression lines were treated with Erastin and RSL-3 at 3 µM and 30 µM for 72 h, with viability normalized to vehicle (DMSO). In C001M, MECOM overexpression significantly decreased viability (i.e., increased sensitivity) for Erastin at 30 µM (56.0%±2.76% vs. 67.3%±4.32%; q = 0.000297) and RSL-3 at 3 µM (87.5%±4.28% vs. 100%±7.90%; q = 0.00225) and 30 µM (12.5%±2.35% vs. 16.3%±1.03%; q = 0.00220), with no significant change at Erastin 3 µM (q = 0.1547; Figure 36). In C002M, MECOM overexpression did not alter sensitivity to Erastin (3 µM, 30 µM) or RSL-3 at 3 µM (all q > 0.05). At RSL-3 30 µM, MECOM overexpression yielded slightly higher residual viability (2.67%±0.516% vs. 1.17%±0.408%; q = 0.000708), indicating a small, statistically significant resistance but with limited magnitude.

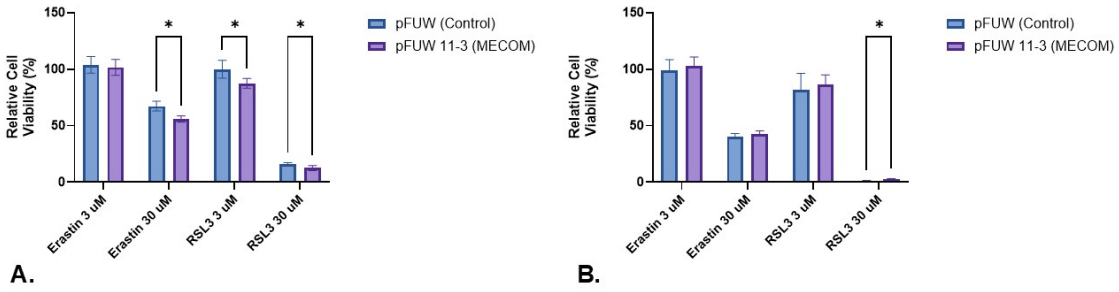


**FIGURE 36. FERROPTOSIS SENSITIVITY UNDER CONSTITUTIVE MECOM OVEREXPRESSION.Mean percent viability at 72 h relative to DMSO in pFUW (control) and pFUW 11-3 (FLAG/hMECOM) lines treated with Erastin or RSL-3 at 3 µM and 30 µM.**
**(A) C001M: MECOM overexpression increased sensitivity (lowered viability) for Erastin 30 µM, and RSL-3 3 µM and 30 µM (all q < 0.01, indicated by asterisks); no difference at Erastin 3 µM (q = 0.1547).**
**(B) C002M: no significant differences at Erastin 3 µM, 30 µM and RSL-3 3 µM (all q > 0.05). At RSL-3 30 µM, MECOM overexpression showed slightly higher residual viability (q = 0.000708).**
**Data represent means from technical triplicates within each biological duplicate, with error bars representing ± SD percent viability at 72 h relative to DMSO.**

## 4.6 Conclusion

This chapter describes the development and functional characterization of MECOM overexpression in melanoma cell lines. Initial attempts at establishing a dual-inducible system were limited by weak induction, unreliable FLAG detection, and cytotoxicity from sodium butyrate and anhydrotetracycline, which precluded meaningful functional assays or the planned IP-MS. To overcome these constraints, a constitutive overexpression system was engineered, enabling robust MECOM expression without exposure to toxic induction regimens. The persistent technical limitation encountered in both inducible and constitutive overexpression systems was the inability to detect the N-terminal FLAG epitope by immunoblotting, despite robust detection of MECOM protein. While this precluded planned FLAG-based interactome studies, several technical explanations are plausible. These include epitope masking due to protein folding or complex formation, instability or cleavage of the N-terminal tag, or steric occlusion arising from high-order protein–protein interactions. Importantly, functional assays were based on confirmed MECOM overexpression detected using MECOM-specific antibodies and did not rely on epitope tag detection.

MECOM overexpression promoted proliferation, accelerated wound closure, increased clonogenicity, and enhanced sensitivity to ferroptosis inducers in C001M cells, whereas C002M cells exhibited minimal changes. Although both C001M and C002M are classified as melanocytic based on prior transcriptomic analyses, these models differ in baseline MECOM expression and functional responsiveness, highlighting heterogeneity within melanocytic-state melanomas and cautioning against interpreting differentiation state as a uniform predictor of MECOM dependence. These findings indicate that MECOM driven phenotype modulation is highly context-dependent, supporting a

potential role for MECOM in modulating melanoma cell behaviour, and suggesting that intrinsic cellular state influences MECOM's functional impact. Given these experimental observations, the subsequent chapter focuses on leveraging publicly available datasets (TCGA and others) to examine MECOM expression patterns, mutation status, and their association with clinical outcomes in melanoma.

# CHAPTER 5: CLINICAL CORRELATES OF MECOM IN ADVANCED MELANOMA: ANALYSIS OF PUBLICLY AVAILABLE COHORTS

## 5.1 INTRODUCTION

The preceding chapters explored MECOM's functional role in melanoma cell phenotype through knockdown and overexpression strategies, revealing context-dependent effects on proliferation, migration, and ferroptosis sensitivity. While these findings suggest that MECOM may influence melanoma plasticity, they were derived from in vitro models and therefore require validation in clinically relevant settings.

This chapter shifts focus from experimental systems to patient-derived data, leveraging publicly available cohorts to examine *MECOM* expression and mutation status in advanced melanoma. Specifically, we analysed the Liu et al. dataset of patients treated with PD-1 blockade (144), enabling direct assessment of MECOM in the context of immunotherapy outcomes. Correlative analyses addressed demographic factors, survival, treatment response, metastatic patterns, and immune or oncogenic pathway signatures. To evaluate reproducibility, we performed a secondary analysis using The Cancer Genome Atlas Skin Cutaneous Melanoma dataset (TCGA-SKCM), which provides comprehensive genomic and transcriptomic profiles but lacks treatment-response data.

Together, these analyses aim to determine whether MECOM is associated with clinical outcomes or immune contexture in melanoma and to assess the extent to which experimental observations translate to patient cohorts.

## 5.2 ANALYSIS OF THE LIU ET AL. COHORT

To investigate the clinical relevance of MECOM in advanced melanoma, we analysed a publicly available, clinically annotated dataset published by Liu et al. This cohort comprises 144 patients with metastatic melanoma who received anti-PD-1 therapy (nivolumab or pembrolizumab), with comprehensive genomic, transcriptomic, and clinical data. RNA-sequencing expression profiles were available for 121 patients, and whole-exome sequencing data for 124 patients, enabling integrated analyses of *MECOM* expression and mutation status in relation to survival outcomes, treatment response, and melanoma biology.

The primary objectives of this analysis were:

- To explore the relationship between *MECOM* expression and melanoma subtype, baseline metastatic patterns, and demographic factors (age and sex).
- To assess whether *MECOM* expression is associated with progression-free survival (PFS), overall survival (OS), and response to anti–PD-1 therapy.

- To determine whether *MECOM* missense mutations confer prognostic significance in this setting.
- To evaluate the immune and oncogenic context of *MECOM* expression using pathway enrichment scores and immune cell deconvolution.

Analyses included Kaplan-Meier survival curves comparing HIGH MECOM versus LOW MECOM expression groups (median split) and *MECOM*-mutant versus wild-type tumours, with hazard ratios (HR) and logrank p-values reported. $Log_2$(TPM+1) transformation was applied to *MECOM* expression data to reduce skew. Response associations were tested using contingency tables and Fisher's exact tests. Non-parametric tests (Mann-Whitney) were used for comparisons of *MECOM* expression across subtypes, metastatic sites, and demographic groups. Correlation analyses employed Spearman's rank method for continuous variables and Single Sample Gene Set Enrichment Analysis (ssGSEA)-derived pathway scores, with false discovery rate (FDR) correction applied for multiple testing. Immune cell composition was inferred using CIBERSORT LM22 signatures (149).

This multi-dimensional approach allowed us to characterise MECOM's potential role in immune modulation, phenotype switching, and clinical outcomes in the context of PD-1 blockade.

### *5.2.1 MECOM EXPRESSION DOES NOT CORRELATE WITH AGE, SEX, OR TUMOUR TYPE*

We first examined whether *MECOM* expression varied by demographic or melanoma sub-type before assessing its association with clinical outcomes. *MECOM* expression did not differ by sex (Mann-Whitney, ns; Hodges-Lehmann median difference in $log_2$(TPM+1): Δ = 0.125, 95% CI -0.239 to 0.553; Figure 37A). Across patients with recorded age (n = 74), *MECOM* expression was not correlated with age (Spearman r = 0.058, p = 0.6238; Figure 37B). These findings indicate that variation in *MECOM* expression in this cohort is not explained by sex or age.

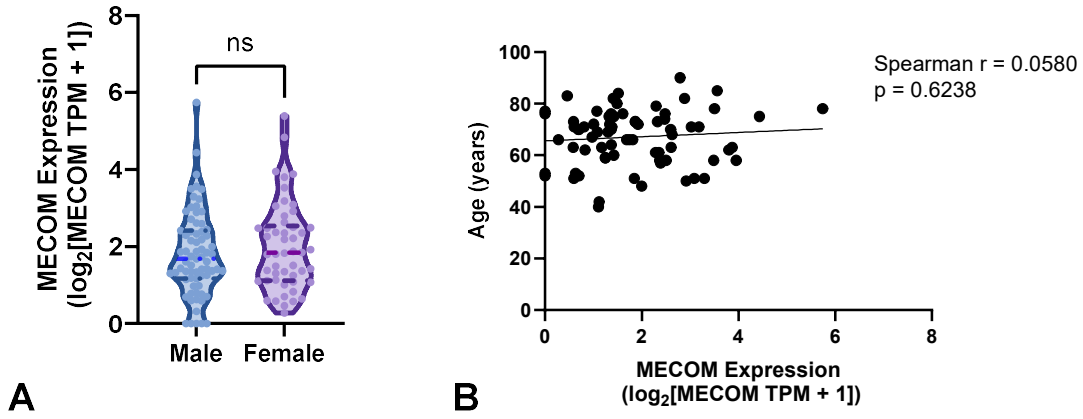


**FIGURE 37. *MECOM* EXPRESSION BY SEX AND AGE IN LIU COHORT. (A) *MECOM* expression ($log_2$[TPM+1]) in male (blue) and female (purple) patients. Points show individual samples with box/violin overlays; horizontal lines indicate medians; n per group shown above. Group difference assessed by two-sided Mann–Whitney; Hodges–Lehmann**

**median difference and 95% CI reported in text.**

**(B) correlation between age (years) and *MECOM* expression ($log_2$[tpm+1]); line shows non-parametric trend. Spearman r and p-value are displayed on the plot (n = 74).**

Similarly, *MECOM* expression did not differ significantly across melanoma subtypes (Kruskal–Wallis p = 0.70) (Figure 38). Median (interquartile range) $log_2$(MECOM TPM +1) values were Acral: 2.15 (0.810–5.29), Mucosal: 2.08 (0.759–2.08), Occult: 1.59 (0.550–4.44), and Skin: 2.53 (1.28–4.96). Post-hoc Dunn's pairwise tests were not pursued given the non-significant global test. The small number of rarer melanoma subtypes (and acral and mucosal melanoma in particular) likely influenced these results.

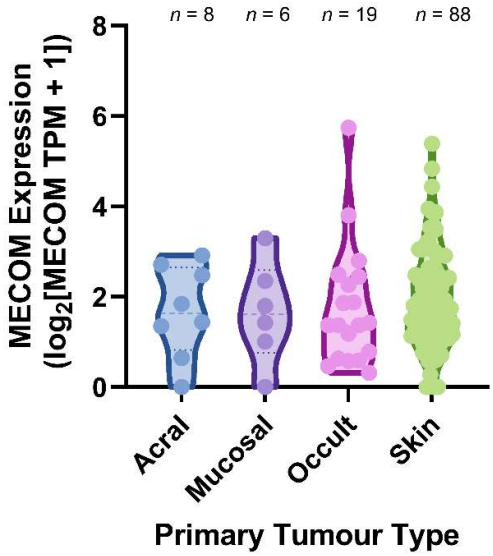


**FIGURE 38. *MECOM* EXPRESSION ACROSS MELANOMA SUBTYPES IN LIU COHORT.Violin plots with individual data points show *MECOM* expression (log2[*MECOM* TPM+1]) in acral (n = 8), mucosal (n = 6), occult/other (n = 19), and cutaneous/skin (n = 88) samples. Group comparison by Kruskal–Wallis yielded $H = 1.439$, df = 3, p = 0.6964, indicating no significant differences in *MECOM* expression across subtypes.**

### *5.2.2 Association of MECOM expression with survival in anti–PD-1–treated melanoma*

To assess whether MECOM expression is associated with clinical outcomes in advanced melanoma treated with anti-PD-1 therapy, patients were divided into HIGH MECOM and LOW MECOM groups based on the median RNA-seq expression. Kaplan-Meier curves were generated for progression-free survival (PFS) and overall survival (OS), and survival distributions were compared using the logrank (Mantel–Cox) test. Hazard ratios (HR) and 95% confidence intervals (CI) were calculated from the logrank analysis.

In the whole cohort (n = 121), HIGH MECOM patients had a median PFS of 30.3 months compared to 3.7 months for LOW MECOM, and median OS of 37.4 vs 16.8 months, but these differences were not statistically significant (PFS: HR = 0.679, 95% CI 0.412–1.12, p = 0.127; OS: HR = 0.646, 95% CI 0.392–1.06, p = 0.0845) (Figure 39; Table 13).

MECOM is implicated in transcriptional plasticity and phenotype switching, processes that underlie resistance to both MAPK-targeted therapy and immunotherapy. Prior MAPKi exposure induces an immune-evasive state and cross-resistance to PD-1 blockade (150), while prior CTLA-4 therapy alters immune contexture and changes predictors of PD-1 response (144). Therefore, subgroup analyses were performed to account for these biologically relevant modifiers. Excluding these patients allowed us to evaluate MECOM's association with clinical outcomes without this confounding effect.

When patients with prior MAPKi therapy were excluded, LOW MECOM was associated with significantly shorter PFS (NR vs 5.9 months; HR = 0.574, 95% CI 0.331–0.995, p = 0.0479) and a strong trend toward shorter OS (NR vs 17.1 months; HR = 0.577, 95% CI 0.333–1.00, p = 0.0514) (Figure 39; Table 13).

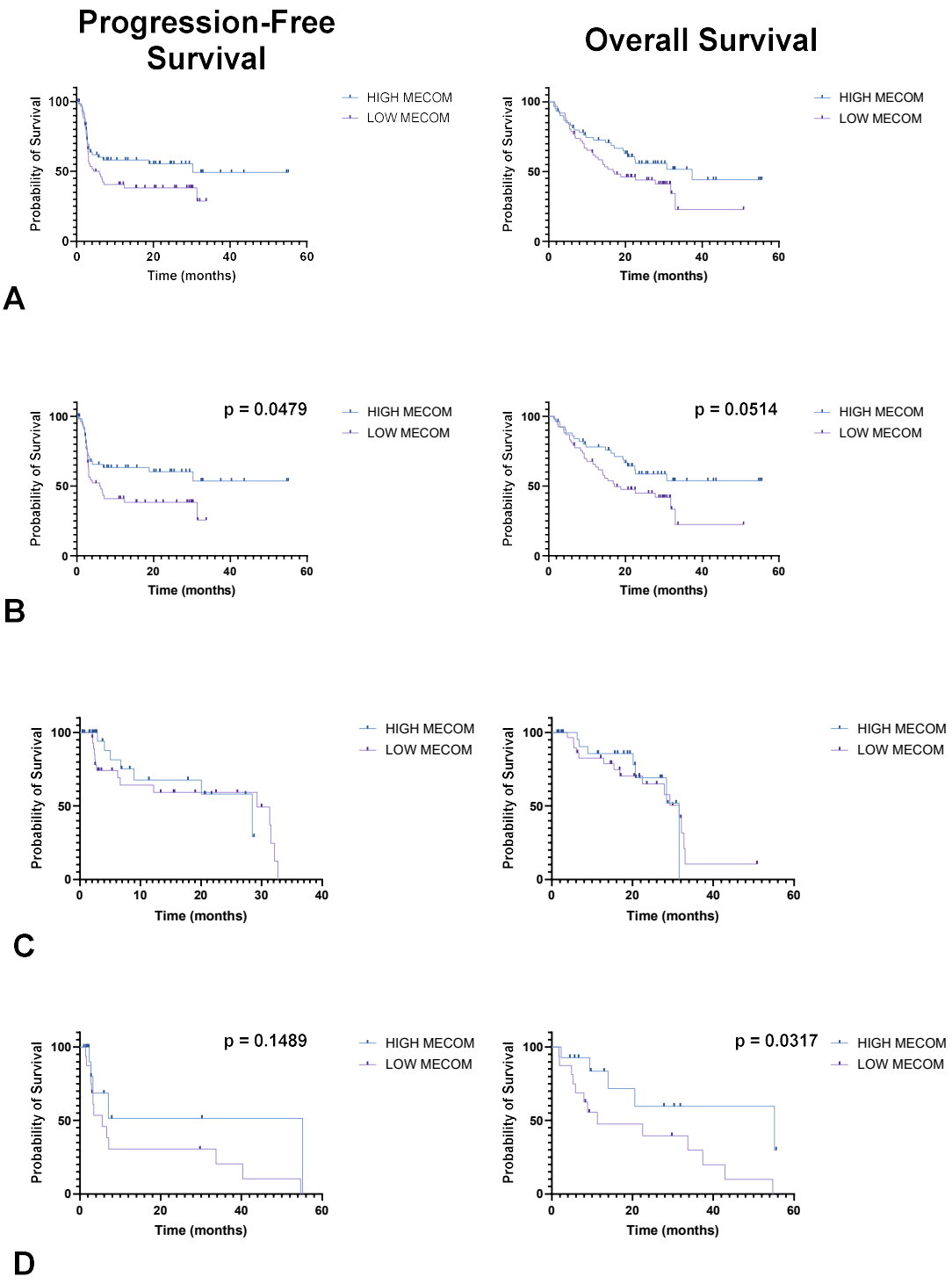


**FIGURE 39. KAPLAN–MEIER SURVIVAL CURVES FOR MECOM EXPRESSION GROUPS IN ANTI–PD-1–TREATED MELANOMA (LIU DATASET) (A–D) progression-free survival (left) and overall survival (right) comparing HIGH MECOM versus LOW MECOM (median split) in: (A) whole cohort (n = 121), (B) patients excluding prior MAPK inhibitor therapy (n = 104), (C) ipilimumab-naïve subgroup (n = 57), and (D) ipilimumab-experienced subgroup (n = 30) (Liu dataset). Tick marks indicate censored observations. Median survival times (months), hazard ratios (HR), 95% confidence intervals**

**(CI), and logrank p-values are summarized in TABLE 13. HIGH MECOM curves are shown in blue; LOW MECOM curves in purple.**

In subgroup analyses, ipilimumab-naïve (ipi-naïve) patients (n = 57) showed no significant association between *MECOM* expression and survival (PFS: HR = 0.877, p = 0.7536; OS: HR = 0.97, p = 0.9424). In contrast, among ipilimumab-experienced (ipi-experienced) patients (n = 30), LOW MECOM was associated with markedly shorter OS (55.2 vs 11.3 months; HR = 0.353, 95% CI 0.140–0.890, p = 0.0317) and a non-significant trend toward shorter PFS (55.2 vs 5.6 months; HR = 0.492, p = 0.1489).

Overall, *MECOM* expression was not significantly associated with survival in the full cohort. However, after excluding prior MAPKi therapy, LOW MECOM was linked to significantly shorter PFS and a trend toward shorter OS. Additionally, in ipi-experienced patients, LOW MECOM was associated with significantly worse OS. The lack of significance across the whole cohort suggests that *MECOM*'s impact may be context-specific, and related to prior treatment exposures which may modulate the tumour itself or the tumour microenvironment.

**TABLE 13. ASSOCIATION BETWEEN *MECOM* EXPRESSION (MEDIAN SPLIT: HIGH VS LOW) AND SURVIVAL OUTCOMES IN ADVANCED MELANOMA TREATED WITH ANTI–PD-1 THERAPY (LIU DATASET). Kaplan-Meier analyses were performed for progression-free survival (PFS) and overall survival (OS) using the logrank (Mantel–Cox) test. Hazard ratios (HR) and 95% confidence intervals (CI) are shown for HIGH MECOM relative to LOW MECOM. "NR" indicates median survival not reached because >50% of patients remained event-free at last follow-up. Subgroup analyses were conducted excluding prior MAPK inhibitor therapy and stratifying by prior CTLA-4 blockade (ipi-naïve vs ipi-experienced).**

| Group | Endpoint | *n* (HIGH /LOW MECOM) | Median (mo, HIGH vs LOW MECOM) | HR | 95% CI | Logrank *p* |
|---|---|---|---|---|---|---|
| Whole cohort | PFS | 60 / 61 | 30.3 vs 3.7 | 0.679 | 0.412 to 1.12 | 0.1271 |
| | OS | | 37.4 vs 16.8 | 0.646 | 0.392 to 1.06 | 0.0845 |
| Excluding MAPKI | PFS | 51 / 53 | NR vs 5.9 | 0.574 | 0.331 to 0.995 | **0.0479** |
| | OS | | NR vs 17.1 | 0.577 | 0.333 to 1.00 | 0.0514 |
| Ipi-naïve | PFS | 27 / 30 | 28.4 vs 29.3 | 0.877 | 0.365 to 2.11 | 0.7536 |
| | OS | | 31.5 vs 31.5 | 0.970 | 0.397 to 2.37 | 0.9424 |
| Ipi-experienced | PFS | 14 / 16 | 55.2 vs 5.6 | 0.492 | 0.194 to 1.25 | 0.1489 |
| | OS | | 55.2 vs 11.3 | 0.353 | 0.140 to 0.890 | **0.0317** |

### *5.2.3 MECOM Missense Mutation and Survival Outcomes*

To assess whether *MECOM* mutation status influences clinical outcomes, patients with available mutation and survival data (n = 124) were stratified by presence or absence of MECOM missense mutations. Thirty patient tumours (24.2%) harboured one or more *MECOM* missense mutations. Kaplan-Meier analysis showed no significant difference in PFS between *MECOM*-mutant and wild-type tumours (median PFS: 11.15 vs 3.89 months; HR = 0.649, 95% CI 0.405–1.04; logrank p =

0.1031; Figure 40). In contrast, OS was significantly longer in patients with *MECOM* missense mutations compared to wild-type (median OS: not reached vs 20.57 months; HR = 0.4153, 95% CI 0.236–0.731; logrank p = 0.0164; Figure 40). These findings suggest that *MECOM* missense mutations may be associated with improved OS in anti–PD-1–treated melanoma (although the effect on PFS was not statistically significant), and hence that *MECOM* mutation may define a biologically distinct subset with enhanced responsiveness to PD-1 blockade.

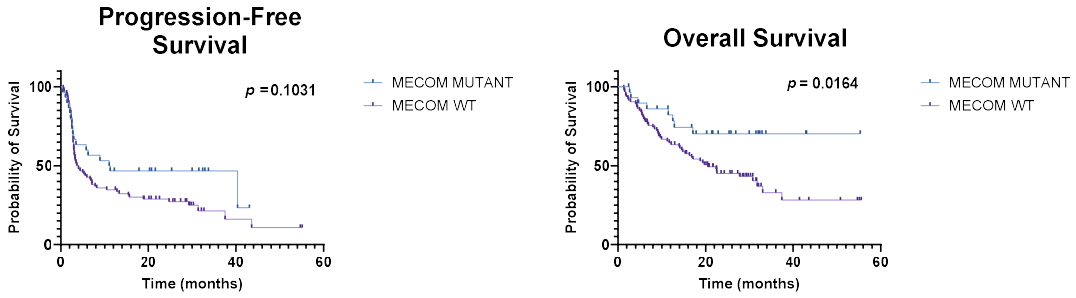


**FIGURE 40. KAPLAN–MEIER SURVIVAL CURVES FOR MECOM MUTATION STATUS IN ANTI–PD-1–TREATED MELANOMA (LIU DATASET). Progression-free survival (left) and overall survival (right) comparing patients with MECOM missense mutations (blue; n = 30) versus wild-type *MECOM* (purple; n = 94). Tick marks indicate censored observations. Median survival times (months), hazard ratios (HR), 95% confidence intervals (CI), and logrank p-values are detailed in the text. *MECOM*-mutant melanomas exhibited significantly longer OS (p = 0.0164) but no significant difference in PFS (p = 0.1031).**

### *5.2.4 No difference in response to anti-PD1 therapy in patients stratified by tumour MECOM expression*

We compared response rates between HIGH MECOM and LOW MECOM groups to anti-PD1 therapy using a 2×2 contingency table. Response included those patients who had a complete or partial response to therapy (CR/PR), versus non-responders who had progressive or stable disease (PD/SD), in accordance with the response evaluation criteria in solid tumours (RECIST 1.1) criteria (151). Among HIGH MECOM patients, 27/60 (45.0%) responded, compared to 20/61 (32.8%) in the LOW MECOM group (Table 14). The odds ratio for response in HIGH MECOM versus LOW MECOM was 1.68 (95% CI: 0.80–3.52). The association was not statistically significant (Chi-square test, p = 0.17; Fisher's exact test, p = 0.19). These counts are illustrated in Figure 41, which shows the number of responders and non-responders in each group.

**TABLE 14. ASSOCIATION BETWEEN MECOM EXPRESSION AND RESPONSE TO ANTI–PD-1 THERAPY IN LIU DATASET. Counts and response rates for HIGH and LOW MECOM groups. Odds ratio for response in HIGH versus LOW MECOM was 1.68 (95% ci: 0.80–3.52). Chi-square test p = 0.17; Fisher's exact test p = 0.19.**

| | Responder | Non-Responder | Response Rate |
|---|---|---|---|
| HIGH MECOM | 27 | 33 | 45% |
| LOW MECOM | 20 | 41 | 33% |

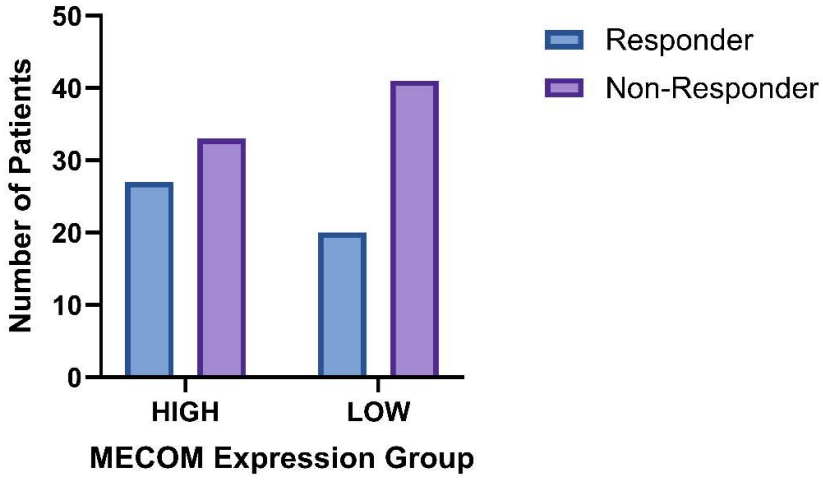


**FIGURE 41. BAR PLOT SHOWING ABSOLUTE COUNTS OF RESPONDERS (CR/PR) AND NON-RESPONDERS (SD/PD) IN PATIENTS WITH HIGH VERSUS LOW MECOM EXPRESSION IN LIU COHORT. Response counts were 27 responders and 33 non-responders in the HIGH MECOM group, and 20 responders and 41 non-responders in the LOW MECOM group. Odds ratio for response was 1.68 (95% CI: 0.80–3.52), p = 0.17 (Chi-square test). Fisher's exact test yielded p = 0.19. Pairwise testing was not performed given there were no significant differences between groups on global testing.**

### *5.2.5 MECOM EXPRESSION AND BASELINE METASTATIC PATTERNS*

We compared *MECOM* expression between patients with versus without metastases at six anatomical sites (brain, lung, bone, liver/visceral, lymph node, and any distant site [excluding lymph nodes, local invasion]) using two-sided Mann–Whitney tests (Figure 42). *MECOM* expression was significantly lower in patients with brain metastases (median *MECOM* expression (log2[TPM+1]): 1.12 vs 1.85, Mann–Whitney p = 0.0092), and this remained the lowest q-value after false discovery rate (FDR) correction across sites (q = 0.055). All other sites showed no significant differences (raw p ≥ 0.216; FDR-adjusted q ≥ 0.216).

Consistent with this, contingency analysis of HIGH versus LOW MECOM status and brain metastasis presence was significant by Chi-square (p = 0.0430), with an odds ratio of 0.27 (95% CI: 0.07–0.98), indicating that LOW MECOM status was more prevalent amongst patients with brain metastasis. All other site contingency analyses were non-significant (p ≥ 0.21). Sample sizes per group are indicated in Figure 42. These findings suggest that LOW MECOM tumours may be more likely to involve the brain at baseline, potentially reflecting distinct metastatic behaviour or immune contexture. However, given the small number of brain metastasis cases and the borderline significance following FDR correction, this observation should be considered exploratory.

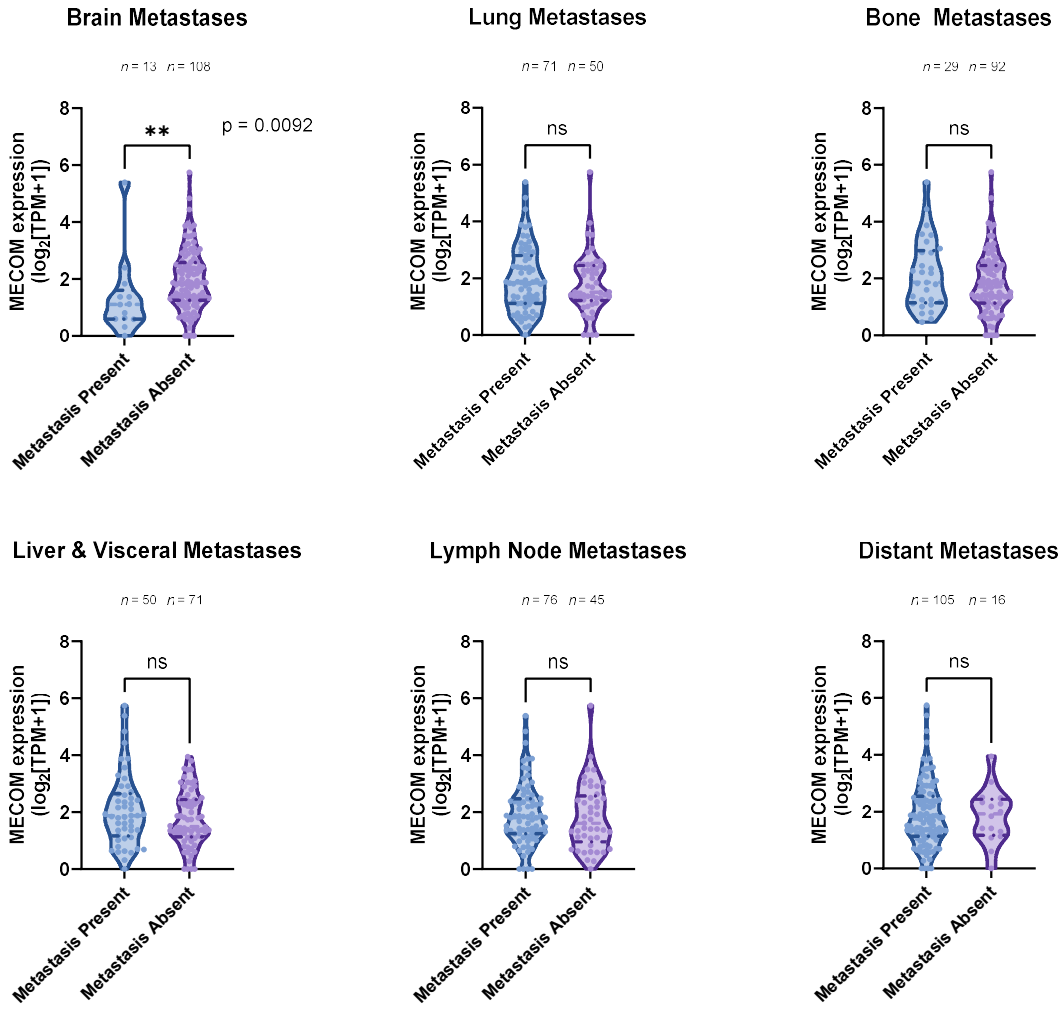


**FIGURE 42. *MECOM* EXPRESSION BY PRESENCE OR ABSENCE OF METASTASIS AT BASELINE IN LIU COHORT.Violin plots with individual data points show *MECOM* expression ($log_2$[TPM+1]) in patients with (metastasis present) versus without (metastasis absent) metastases at six anatomical sites: brain, lung, bone, liver/visceral, lymph**

**node, and any distant site. Horizontal lines indicate medians; sample sizes for each group are shown above the violins. Group differences were assessed using two-sided Mann–Whitney tests; FDR correction was applied across six comparisons. *MECOM* expression was significantly lower in patients with brain metastases (n = 13 vs 108; median 1.12 vs 1.85; p = 0.0092; FDR-adjusted q = 0.055), while all other sites were non-significant (q ≥ 0.216). Contingency analysis of HIGH versus LOW MECOM status and brain metastasis presence was significant by chi-square (p = 0.0430; OR = 0.27), whereas all other site contingency tests were non-significant.**

### *5.2.6 MECOM Expression Correlates with Interferon Signatures and PI3K–AKT–mTOR Pathway Activity*

To explore the immune context of *MECOM* expression, we correlated *MECOM* levels with ssGSEA-derived immune pathway scores in pre-treatment tumours from the same cohort of patients. *MECOM* expression showed weak positive correlations with antigen presentation signatures (MHC-I: r = 0.161, p = 0.0785; MHC-II: r = 0.152, p = 0.0753) and IL2–STAT5 signalling (r = 0.162, p = 0.0714), none of which reached statistical significance after multiple testing correction (Figure 43). A modest correlation was observed with the Complement pathway (r = 0.188, p = 0.0385; FDR-adjusted p = 0.077; Figure 43). In contrast, *MECOM* expression correlated significantly with interferon-related signatures: Interferon Gamma Response (r = 0.249, p = 0.0060; FDR-adjusted p = 0.036) and Interferon Alpha Response (r = 0.248, p = 0.0061; FDR-adjusted p = 0.0183; Figure 43). These findings suggest that tumours with higher *MECOM* expression may retain some interferon signalling capacity, although associations with antigen presentation and other immune pathways were weak and not significant after correction. Additionally, higher expression of *MECOM* may may be associated with an immune-inflamed phenotype, which could influence PD-1 responsiveness.

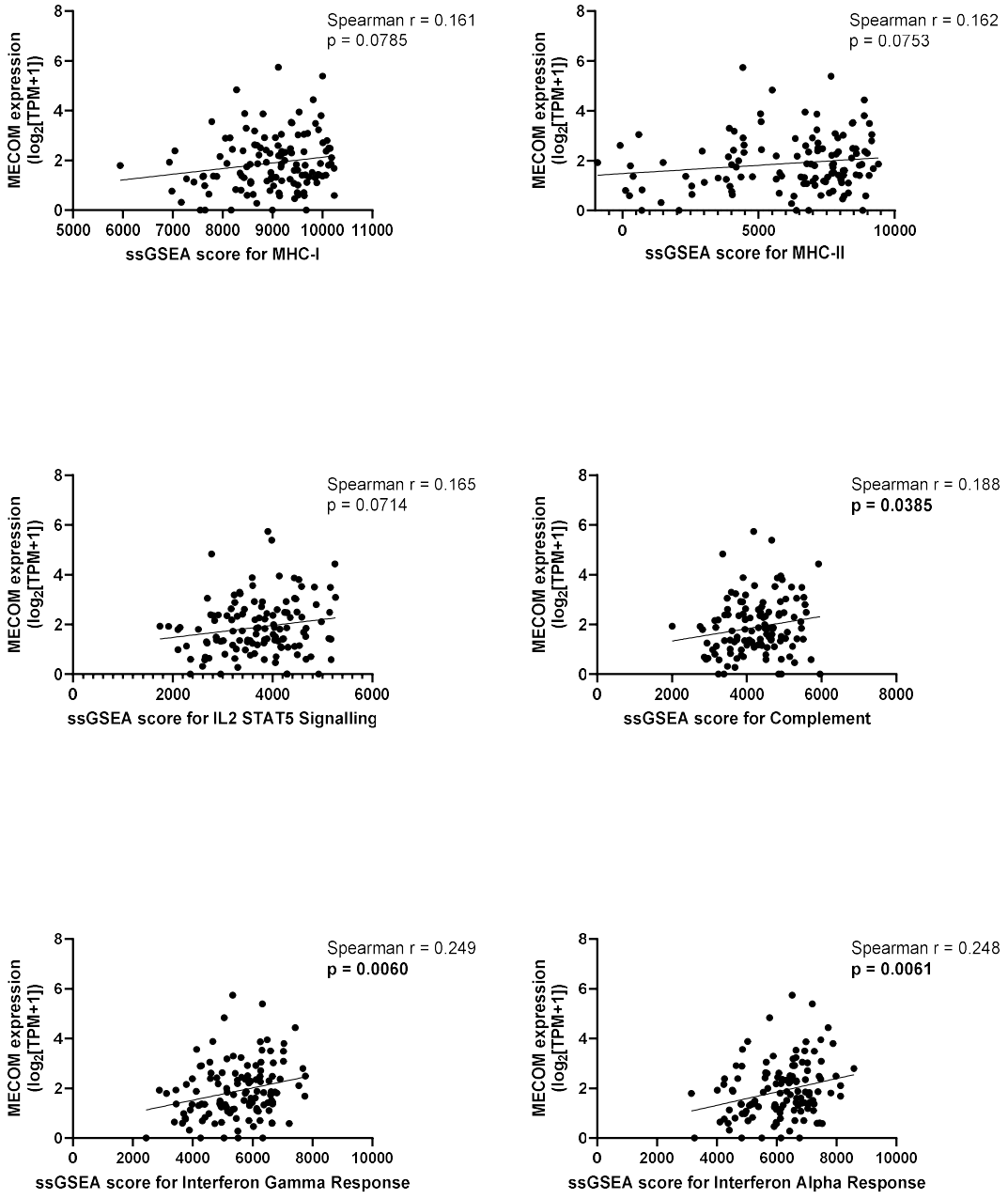


**FIGURE 43. CORRELATION BETWEEN MECOM EXPRESSION AND IMMUNE-RELATED SSGSEA SIGNATURES IN ANTI–PD-1–TREATED MELANOMA (LIU DATASET). Scatterplots show *MECOM* expression ($log_2$[TPM + 1]) versus ssGSEA scores for selected immune pathways: MHC-I, MHC-II, IL2–STAT5 signalling, complement, interferon gamma response, and interferon alpha response. Spearman correlation coefficients (r) and raw p-values are displayed on each plot (n = 121).**

To assess whether *MECOM* expression is linked to phenotype switching and oncogenic signalling, we correlated *MECOM* levels with ssGSEA scores for EMT, TGFβ, PI3K–AKT–mTOR, and KRAS pathways. *MECOM* showed a strong positive correlation with PI3K–AKT–mTOR signalling (Spearman r = 0.320, p = 0.0003; FDR-adjusted p = 0.0012) and a moderate correlation with KRAS signalling (r =

0.254, p = 0.0050; FDR-adjusted p = 0.0100; Figure 44). Associations with EMT (r = 0.103, p = 0.2596) and TGFβ signalling (r = 0.126, p = 0.1701) were weak and not statistically significant after correction (Figure 44). These findings suggest that higher *MECOM* expression in melanoma may preferentially activate PI3K–AKT–mTOR and KRAS pathways, consistent with a pro-survival and therapy-resistant phenotype, whereas EMT and TGFβ signatures were not strongly associated.

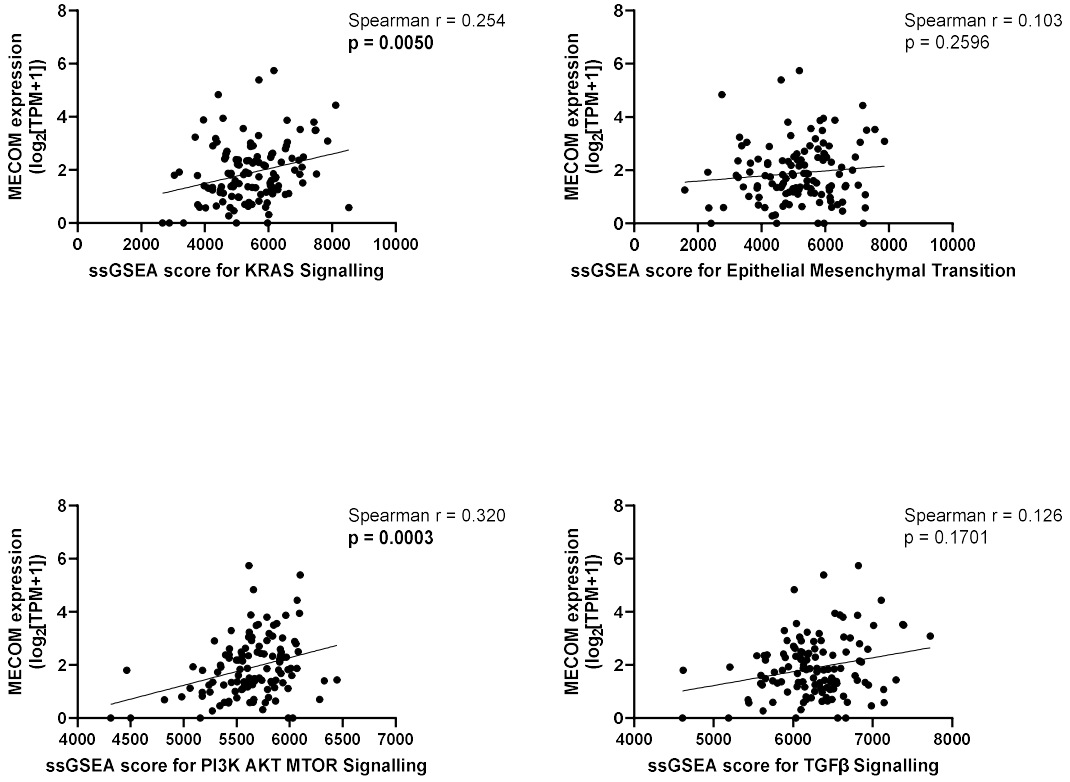


**FIGURE 44. CORRELATION BETWEEN MECOM EXPRESSION AND PHENOTYPE SWITCHING OR ONCOGENIC SIGNALING PATHWAYS IN LIU COHORT.Scatterplots show $log_2$[TPM+1] versus ssGSEA scores for KRAS signalling, epithelial–mesenchymal transition (EMT), PI3K–AKT–MTOR signalling, and TGFβ signalling. Spearman correlation coefficients (r) and raw p-values are displayed on each plot (n = 121).**

### *5.2.7 MECOM Expression Correlates with Immune Infiltration and Macrophage Polarization*

To evaluate the relationship between *MECOM* expression and tumour-immune interactions in anti-PD-1-treated melanoma, we correlated $\log_2$[TPM+1] with CIBERSORT LM22–derived immune fractions (Figure 45; scatterplots available in Supplementary Data Figure 50). *MECOM* showed strong positive correlations with the total immune infiltrate (Absolute score: r = 0.631, FDR p = 0.0004) and macrophages, particularly M2-like cells (r = 0.593, FDR p = 0.0004). Moderate positive associations were observed with CD8 T cells (r = 0.286, FDR p = 0.0040), activated CD4 memory T cells (r = 0.205, FDR p = 0.0053), and M1 macrophages (r = 0.275, FDR p = 0.0046). Correlations with activated dendritic cells (r = 0.174, FDR p = 0.076) and activated NK cells (r = 0.049, FDR p = 0.079) were borderline and did not meet the FDR threshold. Regulatory T cells did not correlate significantly with *MECOM* (r = −0.122, FDR p = 0.18). Overall, melanomas with higher *MECOM* expression appear highly immune-infiltrated with a prominent macrophage signal (M2 > M1) alongside measurable T-cell presence, suggesting a mixed, potentially suppressive, immune microenvironment.

Immune cell composition was inferred using CIBERSORT LM22 estimates provided as part of the Liu et al. dataset. No additional quality control filtering (e.g. exclusion based on CIBERSORT confidence metrics or p-values) was applied beyond ensuring completeness and correct mapping between RNA-seq samples and deconvolution outputs. As with all computational deconvolution approaches applied to bulk RNA-sequencing data, these estimates are subject to limitations including tumour purity effects, transcriptional overlap between immune subsets, and potential influence of tumour-intrinsic gene expression. Accordingly, these results should be interpreted as exploratory correlations reflecting relative immune contexture rather than precise quantification of immune cell abundance.

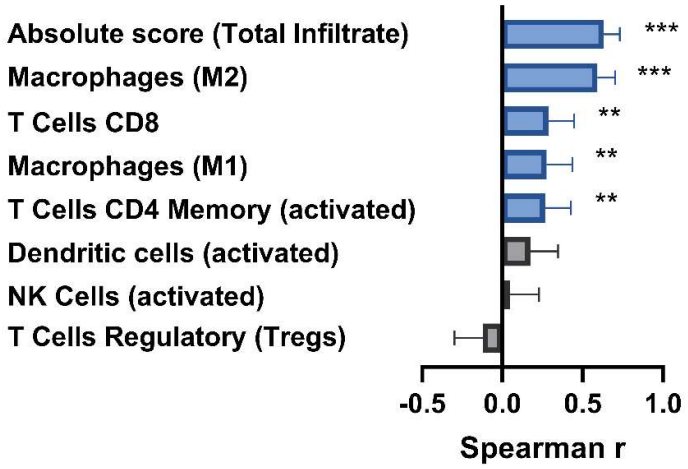


**FIGURE 45. CORRELATION OF *MECOM* EXPRESSION WITH LM22 IMMUNE CELL FRACTIONS IN ANTI-PD-1-TREATED MELANOMA (LIU DATASET).**

**Bars show Spearman correlation coefficients (r) between $\log_2$[TPM+1] and CIBERSORT LM22–derived immune subsets (n = 121). Blue bars indicate correlations significant after Benjamini-Hochberg FDR correction (FDR < 0.05);**

**grey bars indicate non-significant associations. Asterisks denote significance thresholds (** FDR < 0.01; *** FDR < 0.001). Absolute immune infiltrate score and macrophage subsets (M2 > M1) showed the strongest positive associations with *MECOM*, followed by CD8 and activated CD4 memory T cells. Correlations with NK cells, activated dendritic cells, and Tregs were weak or non-significant. Immune fractions were derived from bulk RNA-seq deconvolution and should be interpreted as relative estimates.**

## 5.3 Validation with The Cancer Genome Atlas Dataset

To assess whether findings from the Liu cohort could be replicated in an independent dataset, we analysed The Cancer Genome Atlas Skin Cutaneous Melanoma (TCGA-SKCM) cohort. TCGA provides comprehensive genomic and transcriptomic profiles with linked clinical data, but differs from the Liu dataset in key respects: most patients were treatment-naïve at sequencing, and detailed therapy histories or response endpoints (e.g., anti–PD-1 exposure, RECIST outcomes) are not available. Consequently, analyses were limited to demographic associations, survival outcomes, mutation status, and immune composition inferred from bulk RNA-sequencing data.

### *5.3.1 MECOM expression does not correlate with age or sex in TCGA melanoma cohort*

We first examined whether *MECOM* expression varied by demographic factors before assessing its association with clinical outcomes. Among 194 patients with advanced melanoma (Stage III/IV, for consistency with the Liu dataset) in TCGA, *MECOM* expression did not differ by sex (Mann–Whitney, ns; Hodges–Lehmann median difference in $\log_2$(RSEM + 1): Δ = 0.138, 95% CI -0.212 to 0.502; Figure 46A). *MECOM* expression also showed no significant correlation with age (Spearman r = 0.090, p = 0.216; Figure 46B). These findings are consistent with those observed in the Liu cohort, indicating that *MECOM* expression is not related to sex or age.

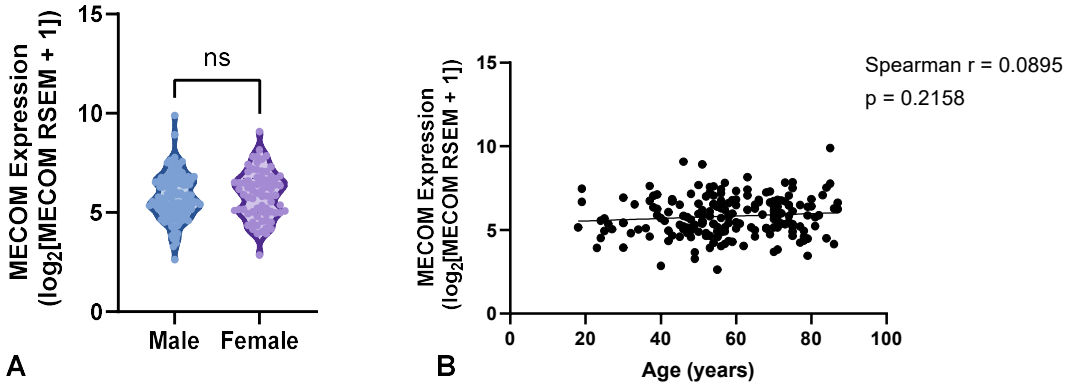


**FIGURE 46. *MECOM* EXPRESSION BY SEX AND AGE IN TCGA MELANOMA COHORT.**
**(A) Violin plots showing *MECOM* expression ($\log_2$[RSEM + 1]) in male versus female patients (Mann–Whitney test, ns; Hodges–Lehmann median difference = 0.138, 95% CI -0.212 to 0.502).**

**(B) Scatter plot of *MECOM* expression versus age (years) with Spearman correlation (r = 0.090, p = 0.216). *MECOM* expression does not vary significantly by sex or age.**

### *5.3.2 Association of MECOM expression with survival in TCGA melanoma cohort*

In the Liu dataset, *MECOM* expression was not significantly associated with survival in the overall cohort, although subgroup analyses suggested potential differences depending on prior therapy exposure. Such detailed treatment history was not available in TCGA; therefore, we limited our analysis to Kaplan–Meier curves for PFS and OS in the most similar full cohort of patients with advanced melanoma (n = 194).

Patients were stratified into HIGH and LOW MECOM groups by median RNA-seq expression ($\log_2$[RSEM + 1]). In the TCGA cohort, HIGH MECOM patients had a median PFS of 15.3 months compared to 23.9 months for LOW MECOM, and median OS of 49.0 versus 33.9 months. These differences were not statistically significant (PFS: HR = 1.37, 95% CI 0.973–1.92, p = 0.068; OS: HR = 0.88, 95% CI 0.628–1.23, p = 0.455) (Figure 47).

Overall, *MECOM* expression was not significantly associated with survival in this cohort, consistent with findings from the Liu dataset. However, interpretation should consider that TCGA patients were largely treatment-naïve at sequencing, and clinical modifiers such as prior MAPK or CTLA-4 therapy could not be accounted for.

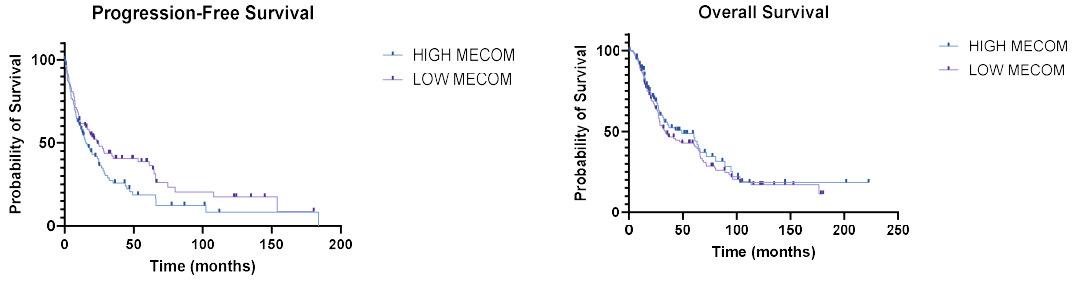


**FIGURE 47. KAPLAN–MEIER SURVIVAL CURVES FOR MECOM EXPRESSION GROUPS IN TCGA MELANOMA COHORT.**

**Progression-free survival (left) and overall survival (right) comparing HIGH MECOM versus LOW MECOM groups (median split; n = 194). Tick marks indicate censored observations. Median survival times (months), hazard ratios (HR), 95% confidence intervals (CI), and logrank p-values are reported in the text. HIGH MECOM curves are shown in blue; low MECOM curves in purple.**

### *5.3.3 MECOM missense mutation status and survival outcomes in TCGA melanoma cohort*

To evaluate whether *MECOM* mutation status influences clinical outcomes, patients with available

mutation and survival data (n = 194) were stratified by presence or absence of *MECOM* missense mutations. Forty-three melanoma samples (22.2%) harboured one or more *MECOM* missense mutations.

Kaplan–Meier analysis showed no significant difference in PFS between *MECOM*-mutant and wild-type tumours (median PFS: 18.2 vs 19.7 months; HR = 0.91, 95% CI 0.61–1.36; logrank p = 0.651; Figure 48). Similarly, OS did not differ significantly (median OS: 89.1 vs 60.2 months; HR = 0.78, 95% CI 0.48–1.25; logrank p = 0.330; Figure 48).

These findings fail to replicate those observed in the Liu cohort, where *MECOM* missense mutations were associated with significantly improved OS in anti-PD-1–treated melanoma. In TCGA, the absence of a survival advantage may reflect differences in treatment exposure, as most TCGA patients were sequenced prior to systemic therapy. Nevertheless, the trend towards improved PFS/OS in the TCGA *MECOM*-mutant group does align with the pattern observed in the Liu dataset, particularly < 5 years post diagnosis.

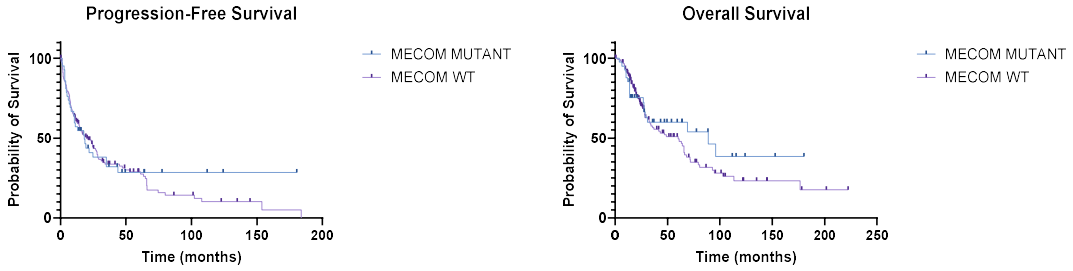


**FIGURE 48. KAPLAN–MEIER SURVIVAL CURVES FOR *MECOM* MUTATION STATUS IN TCGA MELANOMA COHORT. Progression-free survival (left) and overall survival (right) comparing *MECOM*-mutant melanomas (≥1 missense mutation n = 43) versus wild-type (n = 151). Tick marks indicate censored observations. Median survival times (months), hazard ratios (HR), 95% confidence intervals (CI), and logrank p-values are reported in the text. *MECOM*-mutant curves are shown in blue; wild-type curves in purple.**

### *5.3.4 Association of MECOM expression with immune cell composition in TCGA melanoma cohort*

To explore whether *MECOM* expression relates to immune contexture, we correlated $\log_2$(MECOM RSEM + 1) with CIBERSORT LM22–derived immune fractions from the PanImmune Atlas (n = 194) (152). Correlations were assessed using Spearman's rank method with Benjamini–Hochberg FDR correction.

*MECOM* expression showed weak negative correlations with activated dendritic cells (r = −0.184, raw p = 0.0126, FDR p = 0.088) and activated CD4 memory T cells (r = −0.138, raw p = 0.0618, FDR p = 0.216), and a weak negative association with activated NK cells (r = −0.115, raw p = 0.1201, FDR p = 0.280). All other subsets, including CD8 T cells, macrophages (M1 and M2), and regulatory T cells, showed near-zero correlations (r < 0.07) and were non-significant after FDR correction (Figure 49; scatterplots available in Supplementary Data, Figure 51).

Overall, *MECOM* expression in TCGA melanoma was not significantly associated with immune cell composition, contrasting with the Liu cohort where melanomas with higher *MECOM* expression were strongly immune-infiltrated with a macrophage-rich signature. This discrepancy may reflect differences in treatment status and tumour sampling between cohorts.

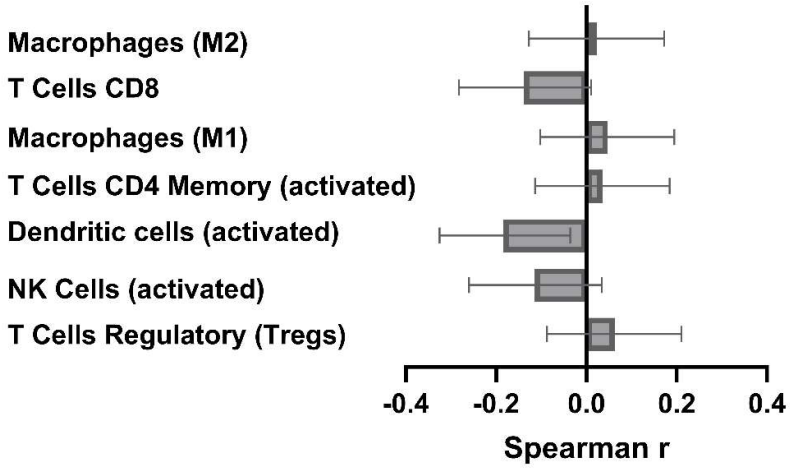


**FIGURE 49. CORRELATION OF *MECOM* EXPRESSION WITH IMMUNE CELL FRACTIONS IN TCGA MELANOMA COHORT. Bars show Spearman correlation coefficients (r) between *MECOM* $\log_2$(RSEM + 1) and CIBERSORT LM22–derived immune subsets (n = 194). Error bars represent 95% confidence intervals. None of the correlations met the FDR significance threshold (Benjamini–Hochberg, FDR < 0.05). The strongest raw association was a negative correlation with activated dendritic cells (r = −0.184, raw p = 0.0126, FDR p = 0.088).**

### *5.3.5 Summary and Limitations*

Unlike the Liu cohort, TCGA-SKCM lacks treatment-response data and detailed therapy history, limiting the ability to replicate associations with PD-1 outcomes or metastatic patterns. Additionally, immune estimates and pathway analyses reflect baseline tumour biology rather than post- or within-treatment changes. While *MECOM* expression and mutation status were not significantly associated with survival or immune contexture in TCGA, these findings highlight the importance of clinical context and cohort matching when interpreting biomarker associations. The absence of replication does not exclude a role for *MECOM* in immunotherapy response but underscores the need for prospective datasets with similar molecular and clinical annotations. A side-by-side comparison of findings from the Liu cohort and TCGA-SKCM is presented in Table 15, illustrating key differences in clinical context and available data that influenced replication outcomes.

**TABLE 15. COMPARISON OF MECOM ASSOCIATIONS IN ANTI–PD-1–TREATED MELANOMA (LIU COHORT) VERSUS TCGA-SKCM. Summary of key analyses including demographic associations, survival outcomes, mutation prevalence, immune correlations, and pathway signatures. TCGA lacks treatment-response data and metastatic site details, limiting replication of therapy-specific findings.**

| | Liu cohort (anti–PD-1 treated) | TCGA-SKCM (Stage III/IV) |
|---|---|---|
| **Cohort size** | 121 patients with RNA-seq and 124 patients with WES | 194 patients with RNA-seq and mutation data |
| **Expression vs demographics** | No correlation with sex (Δ = 0.125, 95% CI −0.239 to 0.553) or age (r = 0.058, p = 0.624) | No correlation with sex (Δ = 0.138, 95% CI −0.212 to 0.502) or age (r = 0.090, p = 0.216) |
| **Expression vs melanoma subtype** | No significant differences across subtypes (Kruskal–Wallis p = 0.70) | Not assessed |
| **Expression vs survival** | No significant association in full cohort (OS HR = 0.646, p = 0.085); subgroup analyses showed trends (ipi-experienced OS p = 0.0317) | No significant association (OS HR = 0.88, p = 0.455) |
| **Response to PD-1 therapy** | No significant difference (OR = 1.68, p = 0.17) | Not available |
| **Mutation prevalence** | 24.2% (≥1 *MECOM* missense mutation) | 22.2% (≥1 *MECOM* missense mutation) |
| **Mutation vs survival** | OS significantly longer in *MECOM*-mutant tumours (HR = 0.415, p = 0.016) | No significant difference (OS HR = 0.78, p = 0.330) |
| **Metastatic patterns** | MECOM LOW enriched in brain metastases | Not assessed (site-specific data unavailable) |
| **Immune correlations (CIBERSORT LM22)** | Strong positive correlation with total immune infiltrate (r = 0.631, FDR p = 0.0004); M2 macrophages (r = 0.593); CD8 T cells (r = 0.286) | No significant correlations after FDR correction; strongest raw association was negative with activated dendritic cells (r = −0.184, FDR p = 0.088) |
| **Pathway correlations (ssGSEA)** | Significant positive correlations with PI3K–AKT–mTOR (r = 0.320, FDR p = 0.0012) and KRAS (r = 0.254, FDR p = 0.010); interferon signatures also significant | Not assessed (scope limited by TCGA dataset) |

## 5.4 Conclusion

Analyses of the Liu cohort revealed that *MECOM* expression was not significantly associated with survival or response in the overall population but showed context-dependent trends suggesting improved survival in patients with higher *MECOM*-expressing melanomas and prior immune, but not targeted, therapy exposure. *MECOM* missense mutations were linked to improved overall survival, suggesting a biologically distinct subset. Melanomas with higher *MECOM* expression exhibited strong immune infiltration, dominated by macrophages, and correlated with interferon signalling and PI3K–AKT–mTOR pathway activation, consistent with a mixed immune-inflamed yet potentially suppressive phenotype.

In contrast, replication in TCGA was limited by the absence of treatment-response data and metastatic site information. *MECOM* expression and mutation status were not significantly associated with survival or immune contexture, and no pathway-level analyses were feasible. These discrepancies underscore the importance of clinical context when interpreting biomarker associations and highlight the need for prospective datasets integrating molecular and treatment-response data.

# CHAPTER 6: DISCUSSION

## 6.1 INTRODUCTION AND AIMS

Recent advances in immunotherapy and targeted treatments have transformed the management of advanced melanoma, substantially improving patient survival. Despite these significant improvements, therapeutic resistance remains a major clinical challenge, and treatment is often accompanied by intolerable side effects and high cost. Resistance is frequently linked to phenotype switching, a process involving coordinated changes in differentiation-associated transcriptional and functional traits. Melanoma cells can thus adopt a more dedifferentiated, 'stem-like' state that confers survival advantages to existing therapies. Preventing or reversing this transition represents a potential strategy to overcome resistance; however, the molecular triggers and regulatory networks driving phenotype plasticity remain poorly understood.

MECOM is a transcription factor with pleiotropic roles in embryogenesis, lineage specification, and cellular plasticity. It has been implicated as an oncogene in several malignancies, yet its functional significance in melanoma has not been mechanistically defined. While bioinformatic analyses suggest a potential oncogenic role (21), experimental evidence linking *MECOM* to melanoma phenotype switching is lacking. Given its established involvement in cell fate decisions, *MECOM* represents a compelling candidate for investigation in this context.

This study sought to address this knowledge gap by (i) developing experimental models of MECOM knockdown and overexpression in melanoma cell lines, (ii) characterizing the phenotypic consequences of MECOM modulation, and (iii) evaluating the clinical relevance of MECOM expression and mutation status using publicly available datasets. Through these complementary approaches, we aimed to clarify whether MECOM contributes to melanoma progression and therapeutic vulnerability via regulation of cellular phenotype. Throughout this chapter, the term "phenotype" refers to differentiation-associated functional and transcriptional traits rather than direct, marker-validated cell-state transitions, which were not assessed in this study.

## 6.2 KEY FINDINGS

This study provides the first experimental investigation into the role of MECOM in melanoma phenotype-associated traits and their potential clinical significance. Through a combination of cell-based models and bioinformatic analyses, the study demonstrates that MECOM exerts context-dependent effects on melanoma biology.

In Chapter 3, inducible MECOM knockdown models were developed in dedifferentiated melanoma cell lines with high endogenous MECOM expression to assess its functional role. Knockdown was technically achievable but inconsistent across constructs and cell lines. Despite these limitations, MECOM depletion reduced proliferation in a subset of dedifferentiated melanoma cell lines, suggesting a growth-supportive role for MECOM in these models. However, effects on migration,

anchorage-independent growth, and clonogenicity were minimal. Drug sensitivity profiling revealed that MECOM knockdown reduced vulnerability to Erastin in D38M cells, indicating partial modulation of ferroptosis sensitivity without evidence of a complete cell-state transition.

In Chapter 4, the impact of MECOM overexpression was examined in melanocytic melanoma cell lines with low baseline MECOM expression. Inducible systems proved unreliable and were confounded by cytotoxic induction conditions, prompting the development of a constitutive overexpression model. Constitutive MECOM overexpression in C001M cells significantly enhanced proliferation, migration, and clonogenic survival, and increased sensitivity to ferroptosis inducers. These effects were absent in C002M, highlighting cell-intrinsic variability and suggesting that MECOM's influence depends on additional molecular context.

In Chapter 5, clinically annotated datasets were analysed to determine the relevance of MECOM in advanced melanoma. Higher MECOM expression and *MECOM* missense mutations were associated with improved survival in anti-PD-1-treated patients, particularly in those without prior MAPK inhibitor therapy and in ipilimumab-experienced subgroups. *MECOM* expression correlated with reduced prevalence of brain metastases in the Liu cohort and was associated with an immune-active tumour microenvironment enriched for interferon signalling and PI3K–AKT–mTOR pathway activity. These associations were not replicated in TCGA, likely reflecting differences in treatment exposure and cohort composition.

Taken together, these data support a model in which MECOM acts as a context-dependent modifier of melanoma phenotypes, influencing proliferative behaviour, ferroptosis sensitivity, and immune associations in specific experimental models and clinical settings rather than operating as a uniform driver of phenotype switching. Within the clinical context, higher MECOM expression may promote a more immunogenic and favourable response pattern. These early insights highlight MECOM as a candidate biomarker and potential therapeutic target, warranting further mechanistic and translational investigation.

## 6.3 Role of *MECOM* in melanoma cell phenotype

Previous work in normal physiology has positioned MECOM as a critical regulator of cell fate decisions; its loss is embryonically lethal in mice and zebrafish due to widespread effects on brain and neuronal development, angiogenesis, craniofacial patterning, and cardiac morphogenesis (Hoyt, Goyama 2008). In addition to this apparent role in embryogenesis, MECOM expression is preserved in normal adult tissues, including the brain, genitourinary and gastrointestinal systems, and the skin (Human Protein Atlas proteinatlas.org; (153)). Insights from knockdown in hematopoietic stem cells have generated mixed data; in murine cells this led to an increase in proliferation rate, whereas in human cells no change was noted, suggesting species-specific or context-dependent roles. Overall, its function in normal tissues remains poorly characterised, leaving open questions about whether MECOM contributes to tissue homeostasis or cellular plasticity under physiological conditions.

In contrast, MECOM perturbation has been more extensively studied in malignancy, where its dysregulation is most striking. In AML cell lines, MECOM knockdown variably decreases proliferation, suggesting a cell line–specific attenuation of growth (154). Similarly, in other haematological malignancies, knockdown reduces proliferation through increased apoptosis (155, 156). In solid tumours, MECOM appears to exert comparable effects: in breast cancer cells, knockdown reduces growth via apoptosis (116), while in ovarian and pancreatic cancer cell lines, MECOM depletion consistently decreases proliferation (108-110, 118). Additionally, in both haematological malignancies and solid tumours MECOM depletion has also been shown to decrease clonogenicity and migration (73, 110, 113, 117, 118). These findings collectively position MECOM as an oncogenic driver that promotes survival and proliferation across diverse cancer types.

Within this context, our results partially align with these observations but reveal important nuances. Although we observed evidence of reduced growth following MECOM knockdown in melanoma cell lines, the effect was inconsistent across cell lines and shRNA constructs. Importantly, this change was contrary to the expected finding with a transition to a more differentiated phenotype. Further, we did not detect an effect on clonogenicity or migration, traits that are critical for long-term tumour survival and metastatic potential. In our models, however, MECOM knockdown did not significantly alter clonogenicity or migration, suggesting that these phenotypes may be less dependent on MECOM in melanoma or require additional cooperating factors.

Several factors may account for these discrepancies. First, knockdown efficiency was variable, and partial depletion may have been insufficient to elicit a robust phenotype switch. Second, the impact of MECOM may be highly context dependent, reflecting intrinsic differences in transcriptional programs or epigenetic states between melanoma subtypes. Third, the duration of knockdown appears critical: when cells were pre-induced for seven days prior to proliferation assays, modest reductions in growth were observed, whereas 48-hour induction produced no detectable effect. This suggests that MECOM's influence on melanoma cell phenotype may require sustained transcriptional reprogramming rather than acute modulation of cell cycle regulators. Other research has suggested that phenotype switching in response to a BRAF inhibitor can take more than three weeks of continuous treatment (19). Fourth, the literature has consistently provided evidence of differential or even contradictory effects of MECOM and EVI1 isoforms, such that knockdown strategies targeting shared regions may confound their individual contributions. Finally, our assays did not specifically disentangle proliferation from apoptosis, and therefore any increase in apoptosis may have been masked or poorly detected.

To further clarify MECOM's functional role, we next examined the consequences of forced MECOM expression in melanocytic melanoma cell lines. High levels of MECOM expression are linked to multiple cancer types and poor prognosis within that context, and generally, the literature supports overexpression of MECOM as producing the counter-state to that induced through knockdown. In other words, if knockdown reduces proliferation, clonogenicity, and migration, overexpression would be expected to enhance these traits. This has been observed in ovarian cancer (26), nasopharyngeal carcinoma (127), and head and neck squamous cell carcinoma (126), where overexpression of

MECOM or EVI1 increases cell proliferation, colony formation and/or migration. These phenotypes are consistent with MECOM's proposed role in promoting aggressive behaviour and metastatic potential.

Somewhat contradictorily, both MECOM and EVI1 overexpression in the myelomonocytic cell line U937T (157) and ovarian epithelial cells lead to decreased proliferation, and also an absence of clonal expansion in the latter (26). Further, EVI1 overexpression specifically, has been noted to induce fatal MDS in mice (103), and other haematological malignancies such as acute B-lymphoblastic leukemia in myeloid progenitors (104), yet delay proliferation and reduce colony formation in erythroid progenitors (158, 159) and the myeloid UT-7/GM cell line (160). These findings highlight that MECOM's functional impact is highly context-dependent, varying not only between physiological and malignant states but also across cell types and differentiation stages.

In our study, constitutive MECOM overexpression in melanocytic melanoma cell lines produced a more aggressive phenotype in C001M cells. Proliferation was significantly increased from Day 3 onward, with differences persisting through Day 7, and clonogenic survival was enhanced nearly threefold compared to controls. Overexpression also accelerated wound closure, indicating a potential role in promoting migratory capacity. These findings align with expectations based on prior literature and support MECOM's capacity to promote aggressive cellular traits in in certain cancer contexts. However, the absence of similar effects in C002M underscores cell-intrinsic variability and suggests that MECOM's oncogenic influence may depend on additional molecular context, such as cooperating transcription factors or chromatin accessibility. It may also suggest a 'permissive' role of MECOM in promoting these oncogenic traits; C001M does not typically demonstrate endogenous MECOM expression while C002M does, at a low level (per RNA-seq [Chapter 3, Section 3.2] and Western Blot [Chapter 4, Section 4.4]). Given the substantive evidence that MECOM acts in concert with epigenetic co-activators or repressors, its ability to alter phenotype may therefore be predicated on the absence or presence of these other proteins.

## 6.4 Differentiation state and inducers of ferroptosis

Ferroptosis is a non-apoptotic, iron-dependent cell death process. It is triggered by the accumulation of lipid reactive oxygen species (ROS) in phospholipids, ultimately causing membrane rupture and cell death (161). Its execution is antagonised by cystine import through system $Xc^-$ (SLC7A11/SLC3A2) and by lipid peroxidase activities (notably GPX4 and MGST1) that detoxify phospholipid hydroperoxides (161, 162). Melanoma cells occupy four progressive differentiation states (undifferentiated, neural crest-like, transitory, melanocytic). Dedifferentiated states can emerge under selective pressure from MAPK inhibitors and immunotherapy (163-165). Across cell lines and patient-derived models, dedifferentiation increases sensitivity to ferroptosis induction (e.g., Erastin targeting system $Xc^-$ and RSL-3 inhibiting GPX4), whereas melanocytic cells are comparatively resistant (19). Mechanistically, dedifferentiated lines exhibit lower basal glutathione, stronger GSH

depletion after Erastin, and both iron chelation (DFO) and lipid antioxidants (Trolox) rescue Erastin-induced death, establishing that cell death is both iron and ROS dependent (19).

Our findings recapitulated this pattern in the parental cell lines, confirming that differentiation state strongly influences vulnerability to lipid peroxidation-driven cell death. We hypothesised that *MECOM* expression may promote a dedifferentiated phenotype, and therefore its overexpression in melanocytic cells would increase ferroptosis sensitivity, while its knockdown in dedifferentiated cells would reduce sensitivity. Our data partially supported these predictions: MECOM overexpression in C001M increased sensitivity to Erastin and RSL-3, while MECOM knockdown in D38M reduced sensitivity to Erastin. The magnitude of these MECOM-driven shifts was modest and not observable across all cell lines or drug conditions compared to the parental state differences, suggesting that MECOM is unlikely to be driving the broad transcriptional/metabolic reprogramming underlying phenotype switching alone.

MITF (microphthalmia-associated transcription factor) has been identified as a master regulator of melanocyte and immune cell lineage (166), and is upregulated in melanocytic melanomas compared with dedifferentiated subtypes (19). Using combined Chip-seq and RNA-seq data, MECOM has been demonstrated to transcriptionally repress the expression of MITF in haematopoietic progenitors, thus preventing their differentiation (167). Importantly, this function appears to be modulated by its C-terminal domain, which is common to both the MECOM and EVI1 isoforms. High MITF melanoma cells exhibit enhanced resistance to oxidative stress because MITF transcriptionally upregulates APE-1, a critical redox sensor and DNA repair enzyme, enabling efficient detoxification and survival under ROS stress (168). MITF also drives expression of PGC1α, a regulator of mitochondrial biogenesis and ROS-detoxifying enzymes, which increases mitochondrial capacity and antioxidant defense (169). Together, these buffer melanocytic cells against oxidative damage, contributing to their relative resistance to ROS-inducing drugs compared to dedifferentiated states. Importantly, sensitivity to lipid peroxidation-driven ferroptosis varies more sharply across differentiation states than sensitivity to generic ROS stress, highlighting a mechanistic link between phenotype and lipid redox homeostasis (19). Thus, *MECOM*-associated dedifferentiation could attenuate MITF/PGC1α activity, weakening antioxidant defences and indirectly increasing ferroptosis susceptibility.

While MECOM has a potential role in melanoma as a repressor of MITF expression, Tyrosine-protein kinase receptor (TYRO3) has been identified as an upstream promoter of MITF expression through nuclear translocation of its upstream mediator Sox10 (170). This suggests it may contribute to promotion of the melanocytic phenotype, and is notable given the strong inverse relationship between expression of MECOM and SOX10. High TYRO3 expression correlates with poor response to anti–PD-1/PD-L1 therapy and worse prognosis in melanoma. Mechanistically, TYRO3 suppresses ferroptosis via AKT/NRF2 activation, upregulating antioxidant programs such as SLC7A11 and GPX4 (171). TYRO3 also modifies the tumour microenvironment by reducing M1-like macrophages (pro-inflammatory, antitumour) and increasing M2-like macrophages (anti-inflammatory, protumour), largely through VEGF-mediated signalling, promoting an anti-inflammatory tumour microenvironment.

Together, this ferroptosis resistance mechanism not only promotes tumour survival under oxidative stress but also contributes to immune checkpoint therapy resistance, highlighting TYRO3 as a potential therapeutic target in melanoma and providing a further link between differentiation states, the resultant tumour microenvironment, and treatment resistance.

Our MECOM perturbation results showed only modest shifts in ferroptosis sensitivity compared to the pronounced differences between parental phenotypes. Several factors may explain this discrepancy. First, MECOM may act as a permissive factor rather than a dominant driver of phenotype switching, requiring cooperation with other transcriptional or epigenetic regulators such as chromatin remodellers. Direct confirmation of phenotype changes through RNA-seq profiling would strengthen interpretation of these findings. Second, ferroptosis sensitivity is influenced by multiple metabolic axes (iron handling, glutathione synthesis, lipid composition), which may not be fully reprogrammed by MECOM alone. Third, cell line-specific context and compensatory pathways (e.g., NRF2 activation or TYRO3 signalling) could buffer against MECOM-induced changes. Finally, experimental conditions (drug dose, exposure time) may limit detection of subtle shifts in ferroptosis sensitivity.

These results do strengthen the rationale for upfront combination therapies incorporating ferroptosis-inducing drugs, as proposed by Tsoi et al. Such approaches could prevent the emergence of dedifferentiated, therapy-resistant states and exploit vulnerabilities associated with oxidative stress adaptation. However, our data indicate that MECOM modulation alone is unlikely to replicate the ferroptosis sensitivity shifts observed during full phenotype switching, emphasizing the need for multi-target strategies that address both transcriptional plasticity and metabolic dependencies.

## 6.5 Clinical Implications of MECOM Expression in Melanoma

In this study, we observed that MECOM expression was associated with differences in clinical outcomes in advanced melanoma treated with anti–PD-1 therapy, but in a context-dependent manner. Across the whole cohort, higher MECOM expression was associated with a trend toward longer progression-free and overall survival (PFS; OS), although this did not reach statistical significance. Notably, when patients with prior MAPK inhibitor exposure were excluded, low MECOM expression correlated with significantly shorter PFS and a trend toward shorter OS. Similarly, in the ipilimumab-experienced subgroup, low MECOM expression was associated with markedly shorter OS and trend towards shorter PFS; the power of this analysis was somewhat limited by low patient numbers (n = 30). Critically, these associations between MECOM expression and survival did not replicate in the TCGA melanoma cohort, where prior treatment exposures were unknown, precluding subgroup analysis, and where patients were not uniformly treated with anti–PD-1 therapy. This highlights the importance of treatment context and immune modulation in interpreting MECOM's prognostic relevance.

This contrasts with the prevailing literature in other malignancies, where MECOM overexpression predicts poor prognosis and therapy resistance, as seen in AML (172) and several solid tumours

including glioblastoma multiforme (124) and breast (116), nasopharyngeal (127), endometrial (132) and cholangiocarcinoma (122). However, exceptions exist: in lung adenocarcinoma, MECOM downregulation was linked to worse outcomes and immune infiltration (120), echoing our observation that low MECOM may be detrimental in melanoma. Isoform-specific effects may also contribute to conflicting reports. Most studies utilising RNA-seq data do not distinguish between MECOM and EVI1 isoforms, despite evidence that high EVI1 predicts poor survival while MECOM amplification may correlate with improved outcomes. Without isoform-level resolution, interpretation remains challenging.

Furthermore, our significant associations emerged primarily in subgroups previously exposed to ipilimumab or MAPK inhibitors, which are known to alter the tumour microenvironment (144, 150). MAPK inhibitors in particular are known to promote an immune-evasive state and cross-resistance to PD-1 blockade (150) suggesting that MECOM's impact may be amplified or unmasked under conditions of immune pressure.

These findings suggest that MECOM's role in melanoma may diverge from its established oncogenic function in hematologic and epithelial cancers through engagement with the immune system. Indeed, our analysis of the Liu dataset suggests that higher MECOM expression is related to a complex and mixed inflammatory tumour microenvironment. Single sample Gene Set Enrichment Analysis indicated only weak enrichment of antigen presentation and T-cell proliferation pathways, while interferon-related signatures were clearly more prominent. This suggests that tumours with higher MECOM expression retain interferon signalling competence and an inflamed transcriptional program, even if classical antigen presentation pathways are not strongly upregulated.

Immune deconvolution using CIBERSORT further supports a highly infiltrated tumour microenvironment (TME) characterized by abundant macrophages (particularly M2-like cells), alongside a significant CD8 and activated CD4 memory T-cell presence. This pattern reflects an "inflamed but myeloid-suppressed" phenotype: interferon-driven inflammation and T-cell infiltration coexist with a dominant immunosuppressive macrophage compartment. This TME could enable partial responsiveness to PD-1 blockade while limiting the magnitude of benefit unless the myeloid niche is also targeted. This profile parallels features linked to PD-1 sensitivity in recent studies: IFN-γ–inflamed, T-cell–rich tumours with variable antigen presentation often respond to checkpoint blockade, particularly when MHC-I/II expression is restored on therapy (173, 174). Our observation that higher MECOM associates with this inflamed state and improved survival suggests MECOM may mark a TME primed for PD-1 benefit, yet possibly constrained by myeloid suppression - a concept echoed by evidence that tumour-associated macrophage-driven resistance can be mitigated through macrophage-targeted strategies (174, 175).

More precisely, our findings demonstrated significantly improved OS and a trend towards improved PFS in patients with high MECOM-expressing tumours who had previously been treated by ipilimumab, and who went on to received anti-PD-1 therapy. Ipilimumab is thought to modulate the tumour microenvironment by promoting the activity of T-cells in tumour and lymphoid tissue. It

appears to enhance effector T-cell function and/or deplete the immune-suppressive regulatory T cells (176). High MECOM expression in the Liu cohort was also associated with continued expression of MHCI and II, increased total immune infiltrate, CD8 positive T cells, and activated CD4 memory T cells. These results indicate, in the Liu cohort, a confluence of factors – a permissive TME facilitated by high MECOM and prior ipilimumab therapy may "prime" the system for a more robust response to anti-PD-1 therapy. The exact role of MECOM in this dynamic remains unclear, however a recent study of publicly available RNA-seq and CHiP-seq data in ovarian cancer also found a correlation between high EVI1 (but not MECOM) expression and an increased proportion of $CD4^+$ T and $CD8^+$T cells, and improved survival (177). To disentangle MECOM mutation effects from global TMB, overall MECOM expression, and immune context, prospective studies should co-profile MECOM genotype/expression and tumour immune signatures.

Overall survival in the Liu cohort was significantly correlated with the presence of MECOM missense mutations. MECOM is uniquely highly mutated in melanoma – approximately one quarter of patients within both the Liu and TCGA datasets had at least one *MECOM* missense mutation. *MECOM* mutations in other cohorts have been characterised as carrying UVB-signatures, suggesting that there may be a direct link between *MECOM* mutations and melanoma pathobiology (21). Importantly, previous research has shown that overall tumour mutational burden (TMB) correlates with superior clinical response and improved survival in anti–PD-1-treated advanced melanoma (144, 178-180). Accumulated genetic mutations are hypothesised to generate neoantigens, which when presented by major histocompatibility complex (MHC) molecules of tumour cells to host T cells trigger an anti-tumour immune response. Tumour cells often possess the ability to evade this immune response, but this can be restored through therapies such as immune checkpoint blockade (anti-PD1 therapy) (181). Out of the malignancies in the literature which have assessed the relationship between tumour *MECOM* abundance and survival, lung adenocarcinoma was one of the few exceptions which suggested a positive relationship (120). This is notable as lung adenocarcinoma shares a core characteristic of melanoma: high TMB which correlates strongly with response to anti-PD1 therapy (182).

It is plausible that tumours harbouring MECOM mutations also exhibit higher TMB *in general*, and that any observed benefit from anti–PD-1 therapy may reflect this broader genomic context rather than the specific MECOM alteration. Alternatively, MECOM mutations could directly modify its functional properties through altering protein–protein interactions or DNA-binding specificity. Despite extensive cataloguing of MECOM mutations in the context of melanoma (for example, TCGA dataset) a high-resolution structure of MECOM has not been determined to map the significance of these mutations onto. AlphaFold predictions suggest MECOM is largely intrinsically disordered (aside from well-characterized zinc finger domains), with low confidence in global structural accuracy (pTM score 0.23; (183)). Many of the documented, high-frequency *MECOM* mutations associated with melanoma fall explicitly within these disordered regions, rather than within annotated domains (see Figure 4). Intrinsically disordered proteins, as predicted for MECOM, exhibit high contextual functional complexity, interacting with diverse partners through multiple binding scenarios (184). Mutations

within such regions may introduce additional complexity, potentially driving significant downstream effects. This provides a rationale for the highly context-dependent impacts of its perturbation reflected within the literature and in our own findings.

Finally, our data suggest an inverse relationship between MECOM expression and the presence of brain metastases. The brain is a common site of metastatic spread in melanoma; while approximately 7% of patients present with a brain metastasis, up to 60% will die with a brain metastasis (185). By contrast, in a case report of 35 dedifferentiated melanoma, only one patient had brain metastases (186). This apparent discrepancy may reflect heterogeneity within dedifferentiated states. Recent transcriptomic studies indicate that NGFR marks a neural crest-like melanoma phenotype, which is distinct from the most undifferentiated $EGFR^{+}/NGFR^{-}$ state (19). Importantly, $NGFR^{+}$ programs have been implicated in brain metastatic progression and therapy resistance (187), suggesting that neural crest-like melanomas, rather than fully dedifferentiated $NGFR^{-}$ melanomas, may preferentially metastasise to the brain. Consistent with this, our observation that melanomas with low MECOM expression were more likely to be associated with brain metastases aligns with the enrichment of NGFR in invasive, stem-like states and supports a model in which MECOM loss accompanies phenotype switching toward a neural crest-like program conducive to intracranial spread.

Across independent datasets, early brain metastases in melanoma show a significant enrichment for hotspot KRAS mutations (8% in a discovery cohort vs ~2% in TCGA), which are clonal, mutually exclusive with BRAF and NRAS, and associated with markedly poorer survival (HR ≈ 10) (188). In our cohort, however, higher MECOM expression correlated with KRAS and PI3K–AKT–mTOR signatures, rather than with EMT or TGFβ, suggesting that MECOM may preferentially engage pro-survival signalling even in the absence of RAS mutations. This pattern is consistent with evidence that MECOM can directly regulate KRAS transcription and potentiate downstream MAPK signalling in solid tumours (94, 109). Hence, the activation of KRAS-dependent programs (mutation-driven or MECOM-mediated) in melanoma may facilitate early haematogenous dissemination and brain metastatic deposition, whereas subsequent intracranial progression preferentially selects for NGFR-associated invasive/stem-like states that are less dependent on MECOM. MECOM/KRAS signalling and NGFR-driven plasticity may represent sequential or partially overlapping routes to brain metastasis, or early risk versus late maintenance, rather than mutually exclusive paths.

## 6.6 Limitations and Future Directions

This study provides preliminary insights into MECOM's role in melanoma biology, but several limitations constrain interpretation and highlight important avenues for future research. First, the use of knockdown rather than knockout approaches introduces uncertainty. Knockdown efficiency was variable and often incomplete, which may have been insufficient to drive durable transcriptional reprogramming or reveal dependencies that require near-total loss of function. Nonetheless, knockdown remains the most appropriate method for isoform-specific interrogation, as shRNA constructs can be designed to selectively repress *MECOM* or *EVI1* isoforms. Future work should

therefore combine optimized knockdown strategies for isoform-level resolution with CRISPR/Cas9 knockout models to clarify the functional impact of complete MECOM loss, ideally complemented by rescue experiments.

Second, the small number of melanoma cell lines examined, and their intrinsic heterogeneity, limit the generalisability of our findings. Responses to MECOM perturbation varied significantly between lines, reflecting the pre-existing transcriptional and epigenetic diversity seen in melanoma. Expanding analyses to a broader panel of cell lines spanning the full differentiation spectrum, including patient-derived and brain metastasis models, will be essential to determine whether the observed findings represent universal or context-dependent effect.

Third, clinical associations were evaluated primarily in a single anti–PD-1 dataset, with limited subgroup sizes and incomplete treatment metadata in the comparator cohort (TCGA). The absence of independent immunotherapy datasets precludes robust validation and raises the possibility that observed associations may be cohort-specific. Replication in additional treatment-defined cohorts with matched clinical and RNA-seq data is needed to confirm MECOM's prognostic relevance and differentiate effects from broader immune and mutational contexts.

Additionally, it is important to note that clinical immune analyses presented here are associative and derived from bulk RNA-sequencing data. Immune infiltration and cell-type proportions were inferred using computational deconvolution approaches, which rely on assumptions regarding tumour purity, reference expression signatures, and linear mixture models. As such, these estimates may be influenced by stromal content, tumour heterogeneity, and transcriptional co-linearity. While standard quality control and multiple-testing correction were applied, immune deconvolution results should be interpreted as hypothesis-generating rather than definitive measures of immune composition.

Mechanistic interpretation is also constrained by the lack of integrated 'omics' data. Time limitations, inconsistent functional results, and difficulty detecting the FLAG-epitope intended for immunoprecipitation pulldown prevented the inclusion of ChIP-seq, RNA-seq, and proteomic analyses that would have confirmed direct MECOM binding to target loci, clarified transcriptional profiles and phenotype switches, and identified protein interaction partners. Similarly, metabolomic and lipidomic profiling would have strengthened conclusions regarding ferroptosis sensitivity. Future studies should incorporate multi-omics approaches, including ChIP-seq or CUT&RUN to map MECOM binding sites genome-wide. Using MECOM's identified consensus binding motif (51, 56), bioinformatic analysis could identify enrichment within promoter regions of key genes such as MITF, KRAS, and ferroptosis regulators. This would provide compelling evidence of direct transcriptional control and is readily achievable by a bioinformatic pipeline.

Additional future directions include leveraging larger cohorts to explore the prognostic significance of recurrent MECOM mutations. Kaplan–Meier analyses comparing variants could reveal whether specific mutations confer differential immunogenicity or therapeutic sensitivity. These findings could then be functionally validated by introducing selected mutations into syngeneic mouse melanoma

models using CRISPR and assessing responses to immune checkpoint inhibitors. Such experiments would clarify whether MECOM mutations act as passive markers of high tumour mutational burden or exert direct effects on immune recognition and therapy response. The relationship between high and low MECOM-expressing melanomas and patterns of brain metastases could similarly be investigated using MECOM knockout vs overexpressing melanoma in a mouse model of brain metastases (189).

Finally, experimental design factors may have limited detection of subtle phenotypic shifts. Ferroptosis assays were conducted under fixed dosing and short exposure windows, which may not capture nuanced changes in lipid ROS handling or antioxidant buffering. Incorporating standardized dose–time matrices, lipid ROS quantification, and rescue experiments with iron chelators or antioxidants would strengthen conclusions (19). Isoform-level resolution and direct measurement of phenotype switching through RNA-seq profiling should also be prioritised to confirm whether MECOM modulation drives the transcriptional profile changes predicted by our functional assays.

In summary, addressing these limitations through CRISPR-based and isoform-specific depletion strategies, multi-omics datasets, and replication in clinically annotated cohorts will be essential to define MECOM's mechanistic role in melanoma. These efforts will clarify whether MECOM functions as a permissive modifier of cellular plasticity, a driver of KRAS/PI3K signalling, or a modulator of an inflamed but myeloid-suppressed tumour microenvironment that facilitates response to PD-1–based therapies.

## 6.7 Conclusion

This study provides the first experimental and clinical exploration of MECOM in melanoma, revealing its complex and context dependent role in tumour biology and therapeutic response. Functional assays demonstrated that MECOM overexpression in melanocytic melanoma cells promotes proliferation, migration, and clonogenic survival, while knockdown in dedifferentiated cells produced inconsistent effects, suggesting that MECOM acts as a permissive factor for aggressive traits rather than a dominant driver of phenotype switching in the absence of direct state-marker validation. Ferroptosis sensitivity was modestly influenced by MECOM modulation, reinforcing the concept that broader transcriptional and metabolic programs govern vulnerability to oxidative stress.

Clinical analyses highlighted a divergence from MECOM's established oncogenic role in other cancers. In anti–PD-1-treated melanoma, higher MECOM expression and MECOM missense mutations were associated with improved survival, particularly in ipilimumab-experienced patients, and correlated with an inflamed tumour microenvironment enriched for interferon signalling. Conversely, low MECOM tumours were more frequently linked to brain metastases, aligning with NGFR-driven invasive states described in recent transcriptomic studies. Pathway correlations further suggest that MECOM expression is associated with PI3K–AKT–mTOR and KRAS signalling, implicating it in oncogenic programs that may influence early dissemination and immune responsiveness.

Taken together, these findings position MECOM as a complex regulatory factor in melanoma, impacting proliferative behaviour and immune context rather than acting as a sole determinant of dedifferentiation. While preliminary, this work underscores MECOM's potential as a biomarker of immunotherapy response and a candidate for therapeutic targeting. Future studies integrating genome-wide binding analyses, multi-omics profiling, and validation in larger, treatment-defined cohorts will be critical to clarify MECOM's mechanistic role and to determine whether its modulation can be leveraged to overcome resistance and improve outcomes in advanced melanoma.

# CHAPTER 7: REFERENCES


1. Australian Institute of Health and Welfare. Skin cancer in Australia. Canberra: AIHW; 2016.
2. Australian Institute of Health and Welfare. Cancer data in Australia. Canberra: AIHW; 2023.
3. Arnold M, Singh D, Laversanne M, Vignat J, Vaccarella S, Meheus F, et al. Global Burden of Cutaneous Melanoma in 2020 and Projections to 2040. JAMA Dermatology. 2022;158(5):495-503.
4. Wolchok JD, Chiarion-Sileni V, Gonzalez R, Rutkowski P, Grob JJ, Cowey CL, et al. Overall Survival with Combined Nivolumab and Ipilimumab in Advanced Melanoma. N Engl J Med. 2017;377(14):1345-56.
5. Blank CU, Lucas MW, Scolyer RA, van de Wiel BA, Menzies AM, Lopez-Yurda M, et al. Neoadjuvant Nivolumab and Ipilimumab in Resectable Stage III Melanoma. N Engl J Med. 2024;391(18):1696-708.
6. Zheng DX, Bozym DJ, Tarantino G, Sullivan RJ, Liu D, Jenkins RW. Overcoming Resistance Mechanisms to Melanoma Immunotherapy. Am J Clin Dermatol. 2025;26(1):77-96.
7. Casagrande S, Sopetto GB, Bertalot G, Bortolotti R, Racanelli V, Caffo O, et al. Immune-Related Adverse Events Due to Cancer Immunotherapy: Immune Mechanisms and Clinical Manifestations. Cancers (Basel). 2024;16(7).
8. Elliott TM, Whiteman DC, Olsen CM, Gordon LG. Estimated Healthcare Costs of Melanoma in Australia Over 3 Years Post-Diagnosis. Appl Health Econ Health Policy. 2017;15(6):805-16.
9. Alexandrov LB, Nik-Zainal S, Wedge DC, Aparicio SAJR, Behjati S, Biankin AV, et al. Signatures of mutational processes in human cancer. Nature. 2013;500(7463):415-21.
10. Brash DE. UV signature mutations. Photochem Photobiol. 2015;91(1):15-26.
11. Davies H, Bignell GR, Cox C, Stephens P, Edkins S, Clegg S, et al. Mutations of the BRAF gene in human cancer. Nature. 2002;417(6892):949-54.
12. Lee J-H, Choi J-W, Kim Y-S. Frequencies of BRAF and NRAS mutations are different in histological types and sites of origin of cutaneous melanoma: a meta-analysis. British Journal of Dermatology. 2011;164(4):776-84.
13. Pollock PM, Harper UL, Hansen KS, Yudt LM, Stark M, Robbins CM, et al. High frequency of BRAF mutations in nevi. Nat Genet. 2003;33(1):19-20.
14. Kalaora S, Nagler A, Wargo JA, Samuels Y. Mechanisms of immune activation and regulation: lessons from melanoma. Nature Reviews Cancer. 2022;22(4):195-207.
15. Larkin J, Chiarion-Sileni V, Gonzalez R, Grob JJ, Cowey CL, Lao CD, et al. Combined Nivolumab and Ipilimumab or Monotherapy in Untreated Melanoma. New England Journal of Medicine. 2015;373(1):23-34.
16. Lim SY, Shklovskaya E, Lee JH, Pedersen B, Stewart A, Ming Z, et al. The molecular and functional landscape of resistance to immune checkpoint blockade in melanoma. Nature Communications. 2023;14(1):1516.
17. Long GV, Stroyakovskiy D, Gogas H, Levchenko E, de Braud F, Larkin J, et al. Dabrafenib and trametinib versus dabrafenib and placebo for Val600 BRAF-mutant melanoma: a multicentre, double-blind, phase 3 randomised controlled trial. Lancet. 2015;386(9992):444-51.
18. Swanton C, André F, Mardis E. Deciphering root causes of intrinsic BRAF inhibitor resistance in melanoma: ushering in a new genomics case reports feature for Annals of Oncology. Annals of Oncology. 2014;25(5):917-8.
19. Tsoi J, Robert L, Paraiso K, Galvan C, Sheu KM, Lay J, et al. Multi-stage Differentiation Defines Melanoma Subtypes with Differential Vulnerability to Drug-Induced Iron-Dependent Oxidative Stress. Cancer Cell. 2018;33(5):890-904.e5.
20. Sarkar D, Leung EY, Baguley BC, Finlay GJ, Askarian-Amiri ME. Epigenetic regulation in human melanoma: past and future. Epigenetics. 2015;10(2):103-21.
21. Lee JJ, Sholl LM, Lindeman NI, Granter SR, Laga AC, Shivdasani P, et al. Targeted next-generation sequencing reveals high frequency of mutations in epigenetic regulators across treatment-naïve patient melanomas. Clinical Epigenetics. 2015;7(1):59.
22. Pinheiro I, Margueron R, Shukeir N, Eisold M, Fritzsch C, Richter Florian M, et al. Prdm3 and Prdm16 are H3K9me1 Methyltransferases Required for Mammalian Heterochromatin Integrity. Cell. 2012;150(5):948-60.
23. Hohenauer T, Moore AW. The Prdm family: expanding roles in stem cells and development. Development. 2012;139(13):2267-82.
24. Di Tullio F, Schwarz M, Zorgati H, Mzoughi S, Guccione E. The duality of PRDM proteins: epigenetic and structural perspectives. The FEBS Journal. 2022;289(5):1256-75.

25. Ivanochko D, Halabelian L, Henderson E, Savitsky P, Jain H, Marcon E, et al. Direct interaction between the PRDM3 and PRDM16 tumor suppressors and the NuRD chromatin remodeling complex. Nucleic Acids Research. 2018;47(3):1225-38.
26. Nanjundan M, Nakayama Y, Cheng KW, Lahad J, Liu J, Lu K, et al. Amplification of MDS1/EVI1 and EVI1, Located in the 3q26.2 Amplicon, Is Associated with Favorable Patient Prognosis in Ovarian Cancer. Cancer Research. 2007;67(7):3074-84.
27. Goyama S, Nitta E, Yoshino T, Kako S, Watanabe-Okochi N, Shimabe M, et al. EVI-1 interacts with histone methyltransferases SUV39H1 and G9a for transcriptional repression and bone marrow immortalization. Leukemia. 2010;24(1):81-8.
28. Montavon T, Shukeir N, Erikson G, Engist B, Onishi-Seebacher M, Ryan D, et al. Complete loss of H3K9 methylation dissolves mouse heterochromatin organization. Nature Communications. 2021;12(1):4359.
29. Mzoughi S, Tan YX, Low D, Guccione E. The role of PRDMs in cancer: one family, two sides. Current Opinion in Genetics & Development. 2016;36:83-91.
30. Pasqualucci L, Compagno M, Houldsworth J, Monti S, Grunn A, Nandula SV, et al. Inactivation of the PRDM1/BLIMP1 gene in diffuse large B cell lymphoma. Journal of Experimental Medicine. 2006;203(2):311-7.
31. Tam W, Gomez M, Chadburn A, Lee JW, Chan WC, Knowles DM. Mutational analysis of PRDM1 indicates a tumor-suppressor role in diffuse large B-cell lymphomas. Blood. 2006;107(10):4090-100.
32. Mandelbaum J, Bhagat G, Tang H, Mo T, Brahmachary M, Shen Q, et al. BLIMP1 Is a Tumor Suppressor Gene Frequently Disrupted in Activated B Cell-like Diffuse Large B Cell Lymphoma. Cancer Cell. 2010;18(6):568-79.
33. Calado DP, Zhang B, Srinivasan L, Sasaki Y, Seagal J, Unitt C, et al. Constitutive Canonical NF-κB Activation Cooperates with Disruption of BLIMP1 in the Pathogenesis of Activated B Cell-like Diffuse Large Cell Lymphoma. Cancer Cell. 2010;18(6):580-9.
34. Küçük C, Iqbal J, Hu X, Gaulard P, De Leval L, Srivastava G, et al. PRDM1 is a tumor suppressor gene in natural killer cell malignancies. Proceedings of the National Academy of Sciences. 2011;108(50):20119-24.
35. Vrzalikova K, Leonard S, Fan Y, Bell A, Vockerodt M, Flodr P, et al. Hypomethylation and Over-Expression of the Beta Isoform of BLIMP1 is Induced by Epstein-Barr Virus Infection of B Cells; Potential Implications for the Pathogenesis of EBV-Associated Lymphomas. Pathogens. 2012;1(2):83-101.
36. Zhang Y-W, Xie H-Q, Chen Y, Jiao B, Shen Z-X, Chen S-J, et al. Loss of promoter methylation contributes to the expression of functionally impaired PRDM1β isoform in diffuse large B-cell lymphoma. International Journal of Hematology. 2010;92(3):439-44.
37. György I, Fejér Gr, Ghosh N, Seto E, Wright KL. Identification of a Functionally Impaired Positive Regulatory Domain I Binding Factor 1 Transcription Repressor in Myeloma Cell Lines1. The Journal of Immunology. 2003;170(6):3125-33.
38. He L, Yu JX, Liu L, Buyse IM, Wang M-s, Yang Q-c, et al. RIZ1, but not the Alternative RIZ2 Product of the Same Gene, Is Underexpressed in Breast Cancer, and Forced RIZ1 Expression Causes G2-M Cell Cycle Arrest and/or Apoptosis1. Cancer Research. 1998;58(19):4238-44.
39. Steele-Perkins G, Fang W, Yang X-H, Van Gele M, Carling T, Gu J, et al. Tumor formation and inactivation of RIZ1, an Rb-binding member of a nuclear protein–methyltransferase superfamily. Genes & Development. 2001;15(17):2250-62.
40. Pastural E, Takahashi N, Dong WF, Bainbridge M, Hull A, Pearson D, et al. RIZ1 repression is associated with insulin-like growth factor-1 signaling activation in chronic myeloid leukemia cell lines. Oncogene. 2007;26(11):1586-94.
41. Shadat NMA, Koide N, Khuda IIE, Dagvadorj J, Tumurkhuu G, Naiki Y, et al. Retinoblastoma Protein-Interacting Zinc Finger 1 (RIZ1) Regulates the Proliferation of Monocytic Leukemia Cells via Activation of p53. Cancer Investigation. 2010;28(8):806-12.
42. Yang T, Ren C, Jiang A, Yu Z, Li G, Wang G, et al. RIZ1 is regulated by estrogen and suppresses tumor progression in endometrial cancer. Biochemical and Biophysical Research Communications. 2017;489(2):96-102.
43. Chadwick RB, Jiang G-L, Bennington GA, Yuan B, Johnson CK, Stevens MW, et al. Candidate tumor suppressor RIZ is frequently involved in colorectal carcinogenesis. Proceedings of the National Academy of Sciences. 2000;97(6):2662-7.
44. Zhao Z, Hu Y, Shen X, Lao Y, Zhang L, Qiu X, et al. HBx represses RIZ1 expression by DNA methyltransferase 1 involvement in decreased miR-152 in hepatocellular carcinoma. Oncol Rep. 2017;37(5):2811-8.

45. Sorrentino A, Rienzo M, Ciccodicola A, Casamassimi A, Abbondanza C. Human PRDM2: Structure, function and pathophysiology. Biochimica et Biophysica Acta (BBA) - Gene Regulatory Mechanisms. 2018;1861(7):657-71.
46. Davis CA, Haberland M, Arnold MA, Sutherland LB, McDonald OG, Richardson JA, et al. PRISM/PRDM6, a Transcriptional Repressor That Promotes the Proliferative Gene Program in Smooth Muscle Cells. Molecular and Cellular Biology. 2006;26(7):2626-36.
47. Wu Y, Ferguson JE, Wang H, Kelley R, Ren R, McDonough H, et al. PRDM6 is enriched in vascular precursors during development and inhibits endothelial cell proliferation, survival, and differentiation. Journal of Molecular and Cellular Cardiology. 2008;44(1):47-58.
48. Kundu A, Nam H, Shelar S, Chandrashekar DS, Brinkley G, Karki S, et al. PRDM16 suppresses HIF-targeted gene expression in kidney cancer. Journal of Experimental Medicine. 2020;217(6).
49. Shi Q, Song G, Song L, Wang Y, Ma J, Zhang L, et al. Unravelling the function of prdm16 in human tumours: A comparative analysis of haematologic and solid tumours. Biomedicine & Pharmacotherapy. 2024;178:117281.
50. Nishikata I, Sasaki H, Iga M, Tateno Y, Imayoshi S, Asou N, et al. A novel EVI1 gene family, MEL1, lacking a PR domain (MEL1S) is expressed mainly in t(1;3)(p36;q21)-positive AML and blocks G-CSF–induced myeloid differentiation. Blood. 2003;102(9):3323-32.
51. Funabiki T, Kreider BL, Ihle JN. The carboxyl domain of zinc fingers of the Evi-1 myeloid transforming gene binds a consensus sequence of GAAGATGAG. Oncogene. 1994;9(6):1575-81.
52. Bluteau O, Sebert M, Leblanc T, Peffault de Latour R, Quentin S, Lainey E, et al. A landscape of germ line mutations in a cohort of inherited bone marrow failure patients. Blood. 2018;131(7):717-32.
53. Germeshausen M, Ancliff P, Estrada J, Metzler M, Ponstingl E, Rütschle H, et al. MECOM-associated syndrome: a heterogeneous inherited bone marrow failure syndrome with amegakaryocytic thrombocytopenia. Blood Adv. 2018;2(6):586-96.
54. Niihori T, Ouchi-Uchiyama M, Sasahara Y, Kaneko T, Hashii Y, Irie M, et al. Mutations in MECOM, Encoding Oncoprotein EVI1, Cause Radioulnar Synostosis with Amegakaryocytic Thrombocytopenia. Am J Hum Genet. 2015;97(6):848-54.
55. Ripperger T, Hofmann W, Koch JC, Shirneshan K, Haase D, Wulf G, et al. MDS1 and EVI1 complex locus (MECOM): a novel candidate gene for hereditary hematological malignancies. Haematologica. 2018;103(2):e55-e8.
56. Delwel R, Funabiki T, Kreider BL, Morishita K, Ihle JN. Four of the seven zinc fingers of the Evi-1 myeloid-transforming gene are required for sequence-specific binding to GA(C/T)AAGA(T/C)AAGATAA. Mol Cell Biol. 1993;13(7):4291-300.
57. Cattaneo F, Nucifora G. EVI1 recruits the histone methyltransferase SUV39H1 for transcription repression. Journal of Cellular Biochemistry. 2008;105(2):344-52.
58. Spensberger D, Delwel R. A novel interaction between the proto-oncogene Evi1 and histone methyltransferases, SUV39H1 and G9a. FEBS Letters. 2008;582(18):2761-7.
59. Basta J, Rauchman M. The nucleosome remodeling and deacetylase complex in development and disease. Transl Res. 2015;165(1):36-47.
60. Torrado M, Low JKK, Silva APG, Schmidberger JW, Sana M, Sharifi Tabar M, et al. Refinement of the subunit interaction network within the nucleosome remodelling and deacetylase (NuRD) complex. Febs j. 2017;284(24):4216-32.
61. Bard-Chapeau EA, Gunaratne J, Kumar P, Chua BQ, Muller J, Bard FA, et al. EVI1 oncoprotein interacts with a large and complex network of proteins and integrates signals through protein phosphorylation. Proc Natl Acad Sci U S A. 2013;110(31):E2885-94.
62. Lugthart S, Figueroa ME, Bindels E, Skrabanek L, Valk PJM, Li Y, et al. Aberrant DNA hypermethylation signature in acute myeloid leukemia directed by EVI1. Blood. 2011;117(1):234-41.
63. Senyuk V, Premanand K, Xu P, Qian Z, Nucifora G. The Oncoprotein EVI1 and the DNA Methyltransferase Dnmt3 Co-Operate in Binding and De Novo Methylation of Target DNA. PLOS ONE. 2011;6(6):e20793.
64. Dickstein J, Senyuk V, Premanand K, Laricchia-Robbio L, Xu P, Cattaneo F, et al. Methylation and silencing of miRNA-124 by EVI1 and self-renewal exhaustion of hematopoietic stem cells in murine myelodysplastic syndrome. Proceedings of the National Academy of Sciences. 2010;107(21):9783-8.
65. Zou D, Chen Y, Han Y, Lv C, Tu G. Overexpression of microRNA-124 promotes the neuronal differentiation of bone marrow-derived mesenchymal stem cells. Neural Regeneration Research. 2014;9(12):1241-8.

66. Wang Y, Huang C, Chintagari NR, Xi D, Weng T, Liu L. miR-124 regulates fetal pulmonary epithelial cell maturation. American Journal of Physiology-Lung Cellular and Molecular Physiology. 2015;309(4):L400-L13.
67. Paredes R, Kelly JR, Geary B, Almarzouq B, Schneider M, Pearson S, et al. EVI1 phosphorylation at S436 regulates interactions with CtBP1 and DNMT3A and promotes self-renewal. Cell Death Dis [Internet]. 2020 2020/10//; 11(10):[878 p.]. Available from: http://europepmc.org/abstract/MED/33082307

https://www.nature.com/articles/s41419-020-03099-0.pdf

https://doi.org/10.1038/s41419-020-03099-0

https://europepmc.org/articles/PMC7576810

https://europepmc.org/articles/PMC7576810?pdf=render.
68. Laricchia-Robbio L, Fazzina R, Li D, Rinaldi CR, Sinha KK, Chakraborty S, et al. Point Mutations in Two EVI1 Zn Fingers Abolish EVI1-GATA1 Interaction and Allow Erythroid Differentiation of Murine Bone Marrow Cells. Molecular and Cellular Biology. 2006;26(20):7658-66.
69. Senyuk V, Sinha KK, Li D, Rinaldi CR, Yanamandra S, Nucifora G. Repression of RUNX1 Activity by EVI1: A New Role of EVI1 in Leukemogenesis. Cancer Research. 2007;67(12):5658-66.
70. Laricchia-Robbio L, Premanand K, Rinaldi CR, Nucifora G. EVI1 Impairs Myelopoiesis by Deregulation of PU.1 Function. Cancer Research. 2009;69(4):1633-42.
71. Izutsu K, Kurokawa M, Imai Y, Maki K, Mitani K, Hirai H. The corepressor CtBP interacts with Evi-1 to repress transforming growth factor β signaling. Blood. 2001;97(9):2815-22.
72. Palmer S, Brouillet J-P, Kilbey A, Fulton R, Walker M, Crossley M, et al. Evi-1 Transforming and Repressor Activities Are Mediated by CtBP Co-repressor Proteins*. Journal of Biological Chemistry. 2001;276(28):25834-40.
73. Pastoors D, Havermans M, Mulet-Lazaro R, Brian D, Noort W, Grasel J, et al. Oncogene EVI1 drives acute myeloid leukemia via a targetable interaction with CTBP2. Science Advances. 2024;10(20):eadk9076.
74. Nitta E, Izutsu K, Yamaguchi Y, Imai Y, Ogawa S, Chiba S, et al. Oligomerization of Evi-1 regulated by the PR domain contributes to recruitment of corepressor CtBP. Oncogene. 2005;24(40):6165-73.
75. Senyuk V, Chakraborty S, Mikhail FM, Zhao R, Chi Y, Nucifora G. The leukemia-associated transcription repressor AML1/MDS1/EVI1 requires CtBP to induce abnormal growth and differentiation of murine hematopoietic cells. Oncogene. 2002;21(20):3232-40.
76. Ding B, Yuan F, Damle PK, Litovchick L, Drapkin R, Grossman SR. CtBP determines ovarian cancer cell fate through repression of death receptors. Cell Death & Disease. 2020;11(4):286.
77. Li J, Wang Y, Wang L, Hao D, Li P, Su M, et al. Metabolic modulation of CtBP dimeric status impacts the repression of DNA damage repair genes and the platinum sensitivity of ovarian cancer. International Journal of Biological Sciences. 2023;19(7):2081-96.
78. Paliwal S, Ho N, Parker D, Grossman SR. CtBP2 Promotes Human Cancer Cell Migration by Transcriptional Activation of Tiam1. Genes & Cancer. 2012;3(7-8):481-90.
79. Kurokawa M, Mitani K, Irie K, Matsuyama T, Takahashi T, Chiba S, et al. The oncoprotein Evi-1 represses TGF-β signalling by inhibiting Smad3. Nature. 1998;394(6688):92-6.
80. Ramesh S, Wildey GM, Howe PH. Transforming growth factor β (TGFβ)-induced apoptosis: The rise and fall of Bim. Cell Cycle. 2009;8(1):11-7.
81. Inman GJ. Switching TGFβ from a tumor suppressor to a tumor promoter. Current Opinion in Genetics & Development. 2011;21(1):93-9.
82. Yeh H-W, Lee S-S, Chang C-Y, Lang Y-D, Jou Y-S. A New Switch for TGFβ in Cancer. Cancer Research. 2019;79(15):3797-805.
83. Bordereaux D, Fichelson S, Tambourin P, Gisselbrecht S. Alternative splicing of the Evi-1 zinc finger gene generates mRNAs which differ by the number of zinc finger motifs. Oncogene. 1990;5(6):925-7.
84. Sayadi A, Jeyakani J, Seet SH, Wei CL, Bourque G, Bard FA, et al. Functional features of EVI1 and EVI1Δ324 isoforms of MECOM gene in genome-wide transcription regulation and oncogenicity. Oncogene. 2016;35(18):2311-21.
85. Kilbey A, Bartholomew C. Evi-1 ZF1 DNA binding activity and a second distinct transcriptional repressor region are both required for optimal transformation of Rat1 fibroblasts. Oncogene. 1998;16(17):2287-91.

86. Maicas M, Vázquez I, Alis R, Marcotegui N, Urquiza L, Cortés-Lavaud X, et al. The MDS and EVI1 complex locus (MECOM) isoforms regulate their own transcription and have different roles in the transformation of hematopoietic stem and progenitor cells. Biochimica et Biophysica Acta (BBA) - Gene Regulatory Mechanisms. 2017;1860(6):721-9.
87. Gröschel S, Sanders Mathijs A, Hoogenboezem R, de Wit E, Bouwman Britta AM, Erpelinck C, et al. A Single Oncogenic Enhancer Rearrangement Causes Concomitant EVI1 and GATA2 Deregulation in Leukemia. Cell. 2014;157(2):369-81.
88. Perkins AS, Mercer JA, Jenkins NA, Copeland NG. Patterns of Evi-1 expression in embryonic and adult tissues suggest that Evi-1 plays an important regulatory role in mouse development*. Development. 1991;111(2):479-87.
89. Morishita K, Parganas E, Parham DM, Matsugi T, Ihle JN. The Evi-1 zinc finger myeloid transforming gene is normally expressed in the kidney and in developing oocytes. Oncogene. 1990;5(9):1419-23.
90. Hoyt PR, Bartholomew C, Davis AJ, Yutzey K, Gamer LW, Potter SS, et al. The Evil proto-oncogene is required at midgestation for neural, heart, and paraxial mesenchyme development. Mechanisms of Development. 1997;65(1):55-70.
91. Goyama S, Yamamoto G, Shimabe M, Sato T, Ichikawa M, Ogawa S, et al. Evi-1 Is a Critical Regulator for Hematopoietic Stem Cells and Transformed Leukemic Cells. Cell Stem Cell. 2008;3(2):207-20.
92. Shull LC, Sen R, Menzel J, Goyama S, Kurokawa M, Artinger KB. The conserved and divergent roles of Prdm3 and Prdm16 in zebrafish and mouse craniofacial development. Dev Biol. 2020;461(2):132-44.
93. Lv J, Meng S, Gu Q, Zheng R, Gao X, Kim J-d, et al. Epigenetic landscape reveals MECOM as an endothelial lineage regulator. Nature Communications. 2023;14(1):2390.
94. Birdwell C, Fiskus W, Kadia TM, DiNardo CD, Mill CP, Bhalla KN. EVI1 dysregulation: impact on biology and therapy of myeloid malignancies. Blood Cancer J. 2021;11(3):64.
95. Polprasert C, Chanswangphuwana C, Owattanapanich W, Kungwankiattichai S, Rattarittamrong E, Rattanathammethee T, et al. Clinical Characteristics and Outcomes of Myeloid Neoplasms with Mecom Rearrangement: Results from a Nationwide Multicenter Study. Blood. 2023;142(Supplement 1):4213-.
96. Arber DA, Orazi A, Hasserjian RP, Borowitz MJ, Calvo KR, Kvasnicka H-M, et al. International Consensus Classification of Myeloid Neoplasms and Acute Leukemias: integrating morphologic, clinical, and genomic data. Blood. 2022;140(11):1200-28.
97. Yamazaki H, Suzuki M, Otsuki A, Shimizu R, Bresnick Emery H, Engel James D, et al. A Remote GATA2 Hematopoietic Enhancer Drives Leukemogenesis in inv(3)(q21;q26) by Activating EVI1 Expression. Cancer Cell. 2014;25(4):415-27.
98. Lugthart S, Gröschel S, Beverloo HB, Kayser S, Valk PJ, van Zelderen-Bhola SL, et al. Clinical, molecular, and prognostic significance of WHO type inv (3)(q21q26. 2)/t (3; 3)(q21; q26. 2) and various other 3q abnormalities in acute myeloid leukemia. Journal of clinical oncology. 2010;28(24):3890-8.
99. Cui W, Sun J, Cotta CV, Medeiros LJ, Lin P. Myelodysplastic syndrome with inv (3)(q21q26. 2) or t (3; 3)(q21; q26. 2) has a high risk for progression to acute myeloid leukemia. American journal of clinical pathology. 2011;136(2):282-8.
100. Hinai AA, Valk PJM. Review: Aberrant EVI1 expression in acute myeloid leukaemia. British Journal of Haematology. 2016;172(6):870-8.
101. Sitailo S, Sood R, Barton K, Nucifora G. Forced expression of the leukemia-associated gene EVI1 in ES cells: a model for myeloid leukemia with 3q26 rearrangements. Leukemia. 1999;13(11):1639-45.
102. Kustikova OS, Schwarzer A, Stahlhut M, Brugman MH, Neumann T, Yang M, et al. Activation of Evi1 inhibits cell cycle progression and differentiation of hematopoietic progenitor cells. Leukemia. 2013;27(5):1127-38.
103. Buonamici S, Li D, Chi Y, Zhao R, Wang X, Brace L, et al. EVI1 induces myelodysplastic syndrome in mice. The Journal of Clinical Investigation. 2004;114(5):713-9.
104. Cuenco GM, Ren R. Both AML1 and EVI1 oncogenic components are required for the cooperation of AML1/MDS1/EVI1 with BCR/ABL in the induction of acute myelogenous leukemia in mice. Oncogene. 2004;23(2):569-79.
105. Brooks DJ, Woodward S, Thompson FH, Dos Santos B, Russell M, Yang JM, et al. Expression of the zinc finger gene EVI-1 in ovarian and other cancers. British Journal of Cancer. 1996;74(10):1518-25.

106. Engler DA, Gupta S, Growdon WB, Drapkin RI, Nitta M, Sergent PA, et al. Genome wide DNA copy number analysis of serous type ovarian carcinomas identifies genetic markers predictive of clinical outcome. PLoS One. 2012;7(2):e30996.
107. Di Palma T, Zannini M. PAX8 as a Potential Target for Ovarian Cancer: What We Know so Far. Onco Targets Ther. 2022;15:1273-80.
108. Bleu M, Mermet-Meillon F, Apfel V, Barys L, Holzer L, Bachmann Salvy M, et al. PAX8 and MECOM are interaction partners driving ovarian cancer. Nat Commun. 2021;12(1):2442.
109. Singh I, Karna A, Prajapati A, Solanki U, Mukherjee A, Uppal S, et al. Epigenetic targeting of MECOM/KRAS axis by JIB-04 impairs tumorigenesis and cisplatin resistance in MECOM-amplified ovarian cancer. Cell Death Discovery. 2025;11(1):326.
110. Chen Y, Jiang Q, Xue Y, Chen W, Hua M. CRISPR-Cas9-mediated deletion enhancer of MECOM play a tumor suppressor role in ovarian cancer. Funct Integr Genomics. 2024;24(4):125.
111. Deng X, Cao Y, Liu Y, Li F, Sambandam K, Rajaraman S, et al. Overexpression of Evi-1 oncoprotein represses TGF-β signaling in colorectal cancer. Molecular Carcinogenesis. 2013;52(4):255-64.
112. Nayak KB, Kuila N, Mohapatra AD, Panda AK, Chakraborty S. EVI1 targets ΔNp63 and upregulates the cyclin dependent kinase inhibitor p21 independent of p53 to delay cell cycle progression and cell proliferation in colon cancer cells. The International Journal of Biochemistry & Cell Biology. 2013;45(8):1568-76.
113. Nayak KB, Sajitha IS, Kumar TRS, Chakraborty S. Ecotropic viral integration site 1 promotes metastasis independent of epithelial mesenchymal transition in colon cancer cells. Cell Death & Disease. 2018;9(2):18.
114. Chen Y, Ying Y, Wang M, Ma C, Jia M, Shi L, et al. A distal super-enhancer activates oncogenic ETS2 via recruiting MECOM in inflammatory bowel disease and colorectal cancer. Cell Death & Disease. 2023;14(1):8.
115. Lu Y, Quan J, Liu F, Huang B. Systematic pan-cancer analysis of the prognostic value of MECOM in human cancer. Discover Oncology. 2024;15(1):694.
116. Wang H, Schaefer T, Konantz M, Braun M, Varga Z, Paczulla AM, et al. Prominent Oncogenic Roles of EVI1 in Breast Carcinoma. Cancer Research. 2017;77(8):2148-60.
117. Wu L, Wang T, He D, Li X, Jiang Y. miR-1 inhibits the proliferation of breast cancer stem cells by targeting EVI-1. Onco Targets Ther. 2018;11:8773-81.
118. Tanaka M, Suzuki HI, Shibahara J, Kunita A, Isagawa T, Yoshimi A, et al. EVI1 oncogene promotes KRAS pathway through suppression of microRNA-96 in pancreatic carcinogenesis. Oncogene. 2014;33(19):2454-63.
119. Backx E, Wauters E, Baldan J, Van Bulck M, Michiels E, Heremans Y, et al. MECOM permits pancreatic acinar cell dedifferentiation avoiding cell death under stress conditions. Cell Death & Differentiation. 2021;28(9):2601-15.
120. Li M, Ren H, Zhang Y, Liu N, Fan M, Wang K, et al. MECOM/PRDM3 and PRDM16 Serve as Prognostic-Related Biomarkers and Are Correlated With Immune Cell Infiltration in Lung Adenocarcinoma. Front Oncol. 2022;12:772686.
121. Ma Y, Kang B, Li S, Xie G, Bi J, Li F, et al. CRISPR-mediated MECOM depletion retards tumor growth by reducing cancer stem cell properties in lung squamous cell carcinoma. Mol Ther. 2022;30(11):3341-57.
122. Tanaka M, Shibahara J, Ishikawa S, Ushiku T, Morikawa T, Shinozaki-Ushiku A, et al. EVI1 expression is associated with aggressive behavior in intrahepatic cholangiocarcinoma. Virchows Archiv. 2019;474(1):39-46.
123. Yasui K, Konishi C, Gen Y, Endo M, Dohi O, Tomie A, et al. EVI1, a target gene for amplification at 3q26, antagonizes transforming growth factor-β-mediated growth inhibition in hepatocellular carcinoma. Cancer Sci. 2015;106(7):929-37.
124. Hou A, Zhao L, Zhao F, Wang W, Niu J, Li B, et al. Expression of MECOM is associated with unfavorable prognosis in glioblastoma multiforme. Onco Targets Ther. 2016;9:315-20.
125. Queisser A, Hagedorn S, Wang H, Schaefer T, Konantz M, Alavi S, et al. Ecotropic viral integration site 1, a novel oncogene in prostate cancer. Oncogene. 2017;36(11):1573-84.
126. Grandits AM, Bromberger S, Heller G, Reinoehl BA, Tomasich E, Schossleitner K, et al. EVI1 Promotes the Proliferation and Invasive Properties of Human Head and Neck Squamous Cell Carcinoma Cells. Int J Mol Sci. 2022;23(3).
127. Lu Y, Liang Y, Zheng X, Deng X, Huang W, Zhang G. EVI1 promotes epithelial-to-mesenchymal transition, cancer stem cell features and chemo-/radioresistance in nasopharyngeal carcinoma. J Exp Clin Cancer Res. 2019;38(1):82.

128. Somaiah N, Beird HC, Barbo A, Song J, Mills Shaw KR, Wang WL, et al. Targeted next generation sequencing of well-differentiated/dedifferentiated liposarcoma reveals novel gene amplifications and mutations. Oncotarget. 2018;9(28):19891-9.
129. Koos B, Bender S, Witt H, Mertsch S, Felsberg J, Beschorner R, et al. The Transcription Factor Evi-1 Is Overexpressed, Promotes Proliferation, and Is Prognostically Unfavorable in Infratentorial Ependymomas. Clinical Cancer Research. 2011;17(11):3631-7.
130. Hao D, He S, Harada K, Pizzi MP, Lu Y, Guan P, et al. Integrated genomic profiling and modelling for risk stratification in patients with advanced oesophagogastric adenocarcinoma. Gut. 2021;70(11):2055-65.
131. Xie P, Yin Q, Wang S, Song D. Prognostic Protein Biomarker Screening for Thyroid Carcinoma Based on Cancer Proteomics Profiles. Biomedicines. 2024;12(9).
132. Harrington SP, Romani J, Jatoi A, Weroha SJ, Mariani A, Cliby WA, et al. MECOM amplified endometrial cancer, a novel subset of copy number high tumors associated with poor prognosis. Gynecologic Oncology Reports. 2025;62:101993.
133. Capparelli C, Purwin TJ, Glasheen M, Caksa S, Tiago M, Wilski N, et al. Targeting SOX10-deficient cells to reduce the dormant-invasive phenotype state in melanoma. Nature Communications. 2022;13(1):1381.
134. Newsom-Stewart CM, Bhatt DP, Major MB, Kaufman CK. Mapping of the hSOX10 protein interactome in human melanoma. bioRxiv. 2025:2025.09.03.672723.
135. Conway JR, Dietlein F, Taylor-Weiner A, AlDubayan S, Vokes N, Keenan T, et al. Integrated molecular drivers coordinate biological and clinical states in melanoma. Nature Genetics. 2020;52(12):1373-83.
136. Diazzi S, Tartare-Deckert S, Deckert M. The mechanical phenotypic plasticity of melanoma cell: an emerging driver of therapy cross-resistance. Oncogenesis. 2023;12(1):7.
137. Wouters J, Kalender-Atak Z, Minnoye L, Spanier KI, De Waegeneer M, Bravo González-Blas C, et al. Robust gene expression programs underlie recurrent cell states and phenotype switching in melanoma. Nature Cell Biology. 2020;22(8):986-98.
138. Pavey S, Johansson P, Packer L, Taylor J, Stark M, Pollock PM, et al. Microarray expression profiling in melanoma reveals a BRAF mutation signature. Oncogene. 2004;23(23):4060-7.
139. Dutton-Regester K, Aoude LG, Nancarrow DJ, Stark MS, O'Connor L, Lanagan C, et al. Identification of TFG (TRK-fused gene) as a putative metastatic melanoma tumor suppressor gene. Genes, Chromosomes and Cancer. 2012;51(5):452-61.
140. Erbacher P, Roche AC, Monsigny M, Midoux P. Putative Role of Chloroquine in Gene Transfer into a Human Hepatoma Cell Line by DNA/Lactosylated Polylysine Complexes. Experimental Cell Research. 1996;225(1):186-94.
141. Clark PR, Stopeck AT, Brailey JL, Wang Q, McArthur J, Finer MH, et al. Polycations and cationic lipids enhance adenovirus transduction and transgene expression in tumor cells. Cancer Gene Therapy. 1999;6(5):437-46.
142. Yu Y, Lowy MM, Elble RC. Tet-On lentiviral transductants lose inducibility when silenced for extended intervals in mammary epithelial cells. Metab Eng Commun. 2016;3:64-7.
143. Geissmann Q. OpenCFU, a new free and open-source software to count cell colonies and other circular objects. PLoS One. 2013;8(2):e54072.
144. Liu D, Schilling B, Liu D, Sucker A, Livingstone E, Jerby-Arnon L, et al. Integrative molecular and clinical modeling of clinical outcomes to PD1 blockade in patients with metastatic melanoma. Nature Medicine. 2019;25(12):1916-27.
145. Gossen M, Bujard H. Anhydrotetracycline, a novel effector for tetracycline controlled gene expression systems in eukaryotic cells. Nucleic Acids Res. 1993;21(18):4411-2.
146. Kent MR, Jay AN, Kendall GC. New dual inducible cellular model to investigate temporal control of oncogenic cooperating genes. Sci Rep. 2024;14(1):20773.
147. Topczewska JM, Postovit L-M, Margaryan NV, Sam A, Hess AR, Wheaton WW, et al. Embryonic and tumorigenic pathways converge via Nodal signaling: role in melanoma aggressiveness. Nature Medicine. 2006;12(8):925-32.
148. Keshet GI, Goldstein I, Itzhaki O, Cesarkas K, Shenhav L, Yakirevitch A, et al. MDR1 expression identifies human melanoma stem cells. Biochemical and Biophysical Research Communications. 2008;368(4):930-6.
149. Chen B, Khodadoust MS, Liu CL, Newman AM, Alizadeh AA. Profiling Tumor Infiltrating Immune Cells with CIBERSORT. Methods Mol Biol. 2018;1711:243-59.
150. Haas L, Elewaut A, Gerard CL, Umkehrer C, Leiendecker L, Pedersen M, et al. Acquired resistance to anti-MAPK targeted therapy confers an immune-evasive tumor microenvironment and cross-resistance to immunotherapy in melanoma. Nat Cancer. 2021;2(7):693-708.

151. Eisenhauer EA, Therasse P, Bogaerts J, Schwartz LH, Sargent D, Ford R, et al. New response evaluation criteria in solid tumours: revised RECIST guideline (version 1.1). Eur J Cancer. 2009;45(2):228-47.
152. Thorsson V, Gibbs DL, Brown SD, Wolf D, Bortone DS, Ou Yang T-H, et al. The Immune Landscape of Cancer. Immunity. 2018;48(4):812-30.e14.
153. Uhlén M, Fagerberg L, Hallström BM, Lindskog C, Oksvold P, Mardinoglu A, et al. Tissue-based map of the human proteome. Science. 2015;347(6220):1260419.
154. Schmoellerl J, Barbosa IAM, Minnich M, Andersch F, Smeenk L, Havermans M, et al. EVI1 drives leukemogenesis through aberrant ERG activation. Blood. 2023;141(5):453-66.
155. Konantz M, André MC, Ebinger M, Grauer M, Wang H, Grzywna S, et al. EVI-1 modulates leukemogenic potential and apoptosis sensitivity in human acute lymphoblastic leukemia. Leukemia. 2013;27(1):56-65.
156. Perkins AS, del Campo JJ, Xiao Y-Y, Zhang Y, Lin SJ, Dudley J, et al. EVI1 Blocks Apoptosis in DA-1 Myeloid Leukemia Cells Via Enhanced Transcription of the Prosurvival Gene Bcl2a1 (A1). Blood. 2008;112(11):3805.
157. Konrad TA, Karger A, Hackl H, Schwarzinger I, Herbacek I, Wieser R. Inducible expression of EVI1 in human myeloid cells causes phenotypes consistent with its role in myelodysplastic syndromes. Journal of Leukocyte Biology. 2009;86(4):813-22.
158. Kreider BL, Orkin SH, Ihle JN. Loss of erythropoietin responsiveness in erythroid progenitors due to expression of the Evi-1 myeloid-transforming gene. Proc Natl Acad Sci U S A. 1993;90(14):6454-8.
159. Louz D, van den Broek M, Verbakel S, Vankan Y, van Lom K, Joosten M, et al. Erythroid defects and increased retrovirally-induced tumor formation in Evi1 transgenic mice. Leukemia. 2000;14(11):1876-84.
160. Shimizu S, Nagasawa T, Katoh O, Komatsu N, Yokota J, Morishita K. EVI1 is expressed in megakaryocyte cell lineage and enforced expression of EVI1 in UT-7/GM cells induces megakaryocyte differentiation. Biochem Biophys Res Commun. 2002;292(3):609-16.
161. Dixon Scott J, Lemberg Kathryn M, Lamprecht Michael R, Skouta R, Zaitsev Eleina M, Gleason Caroline E, et al. Ferroptosis: An Iron-Dependent Form of Nonapoptotic Cell Death. Cell. 2012;149(5):1060-72.
162. Yang Wan S, SriRamaratnam R, Welsch Matthew E, Shimada K, Skouta R, Viswanathan Vasanthi S, et al. Regulation of Ferroptotic Cancer Cell Death by GPX4. Cell. 2014;156(1):317-31.
163. Müller J, Krijgsman O, Tsoi J, Robert L, Hugo W, Song C, et al. Low MITF/AXL ratio predicts early resistance to multiple targeted drugs in melanoma. Nature Communications. 2014;5(1):5712.
164. Tirosh I, Izar B, Prakadan SM, Wadsworth MH, Treacy D, Trombetta JJ, et al. Dissecting the multicellular ecosystem of metastatic melanoma by single-cell RNA-seq. Science. 2016;352(6282):189-96.
165. Kim YJ, Sheu KM, Tsoi J, Abril-Rodriguez G, Medina E, Grasso CS, et al. Melanoma dedifferentiation induced by IFN-γ epigenetic remodeling in response to anti-PD-1 therapy. J Clin Invest. 2021;131(12).
166. Kawakami A, Fisher DE. The master role of microphthalmia-associated transcription factor in melanocyte and melanoma biology. Laboratory Investigation. 2017;97(6):649-56.
167. Iida K, Nakanishi M, Nakahara J, Asada S, Isobe T, Yabushita T, et al. MECOM promotes leukemia progression and inhibits mast cell differentiation through functional competition with GATA2. bioRxiv. 2024:2024.05.20.594903.
168. Liu F, Fu Y, Meyskens FL, Jr. MiTF regulates cellular response to reactive oxygen species through transcriptional regulation of APE-1/Ref-1. J Invest Dermatol. 2009;129(2):422-31.
169. Vazquez F, Lim J-H, Chim H, Bhalla K, Girnun G, Pierce K, et al. PGC1α Expression Defines a Subset of Human Melanoma Tumors with Increased Mitochondrial Capacity and Resistance to Oxidative Stress. Cancer Cell. 2013;23(3):287-301.
170. Zhu S, Wurdak H, Wang Y, Galkin A, Tao H, Li J, et al. A genomic screen identifies TYRO3 as a MITF regulator in melanoma. Proc Natl Acad Sci U S A. 2009;106(40):17025-30.
171. Jiang Z, Lim S-O, Yan M, Hsu JL, Yao J, Wei Y, et al. TYRO3 induces anti–PD-1/PD-L1 therapy resistance by limiting innate immunity and tumoral ferroptosis. The Journal of Clinical Investigation. 2021;131(8).
172. Barjesteh van Waalwijk van Doorn-Khosrovani S, Erpelinck C, van Putten WL, Valk PJ, van der Poel-van de Luytgaarde S, Hack R, et al. High EVI1 expression predicts poor survival in acute myeloid leukemia: a study of 319 de novo AML patients. Blood. 2003;101(3):837-45.
173. Shklovskaya E, Lee JH, Lim SY, Stewart A, Pedersen B, Ferguson P, et al. Tumor MHC Expression Guides First-Line Immunotherapy Selection in Melanoma. Cancers (Basel). 2020;12(11).

174. Johnson DB, Estrada MV, Salgado R, Sanchez V, Doxie DB, Opalenik SR, et al. Melanoma-specific MHC-II expression represents a tumour-autonomous phenotype and predicts response to anti-PD-1/PD-L1 therapy. Nat Commun. 2016;7:10582.
175. Zhang H, Liu L, Liu J, Dang P, Hu S, Yuan W, et al. Roles of tumor-associated macrophages in anti-PD-1/PD-L1 immunotherapy for solid cancers. Molecular Cancer. 2023;22(1):58.
176. Korman AJ, Garrett-Thomson SC, Lonberg N. The foundations of immune checkpoint blockade and the ipilimumab approval decennial. Nature Reviews Drug Discovery. 2022;21(7):509-28.
177. Lan N, Bai S, Chen M, Wang X, Feng Z, Gao Y, et al. MECOM Locus classical transcript isoforms affect tumor immune microenvironment and different targets in ovarian cancer. J Ovarian Res. 2024;17(1):207.
178. Forschner A, Battke F, Hadaschik D, Schulze M, Weißgraeber S, Han CT, et al. Tumor mutation burden and circulating tumor DNA in combined CTLA-4 and PD-1 antibody therapy in metastatic melanoma - results of a prospective biomarker study. J Immunother Cancer. 2019;7(1):180.
179. Riaz N, Havel JJ, Makarov V, Desrichard A, Urba WJ, Sims JS, et al. Tumor and Microenvironment Evolution during Immunotherapy with Nivolumab. Cell. 2017;171(4):934-49.e16.
180. Hugo W, Zaretsky JM, Sun L, Song C, Moreno BH, Hu-Lieskovan S, et al. Genomic and Transcriptomic Features of Response to Anti-PD-1 Therapy in Metastatic Melanoma. Cell. 2016;165(1):35-44.
181. Xie N, Shen G, Gao W, Huang Z, Huang C, Fu L. Neoantigens: promising targets for cancer therapy. Signal Transduction and Targeted Therapy. 2023;8(1):9.
182. Ricciuti B, Wang X, Alessi JV, Rizvi H, Mahadevan NR, Li YY, et al. Association of High Tumor Mutation Burden in Non–Small Cell Lung Cancers With Increased Immune Infiltration and Improved Clinical Outcomes of PD-L1 Blockade Across PD-L1 Expression Levels. JAMA Oncology. 2022;8(8):1160-8.
183. Abramson J, Adler J, Dunger J, Evans R, Green T, Pritzel A, et al. Accurate structure prediction of biomolecular interactions with AlphaFold 3. Nature. 2024;630(8016):493-500.
184. Uversky VN. Intrinsically Disordered Proteins and Their “Mysterious” (Meta)Physics. Frontiers in Physics. 2019;Volume 7 - 2019.
185. Ajithkumar T, Parkinson C, Fife K, Corrie P, Jefferies S. Evolving treatment options for melanoma brain metastases. The Lancet Oncology. 2015;16(13):e486-e97.
186. Agaimy A, Stoehr R, Hornung A, Popp J, Erdmann M, Heinzerling L, et al. Dedifferentiated and undifferentiated melanomas: report of 35 new cases with literature review and proposal of diagnostic criteria. The American Journal of Surgical Pathology. 2021;45(2):240-54.
187. Radke J, Schumann E, Onken J, Koll R, Acker G, Bodnar B, et al. Decoding molecular programs in melanoma brain metastases. Nature Communications. 2022;13(1):7304.
188. Rabbie R, Ferguson P, Wong K, Couturier D-L, Moran U, Turner C, et al. The mutational landscape of melanoma brain metastases presenting as the first visceral site of recurrence. British Journal of Cancer. 2021;124(1):156-60.
189. Almazan J, Turapov T, Holmen SL. Protocol for developing a melanoma brain metastasis mouse model for preclinical drug testing and brain tumor progression monitoring. STAR Protoc. 2025;6(3):104081.

# SUPPLEMENTARY DATA

**TABLE 16. RAW COUNTS FOR SOFT AGAR ASSAY PRIOR TO NORMALIZATION IN D23M. Counts of soft agar colonies formed by D23M melanoma cells transduced with scramble or *MECOM*-targeting shRNAs (#1, #2, #3) under untreated (No IPTG) and IPTG-treated (+IPTG) conditions. Images were captured at ×4 magnification after 3 weeks of incubation; colonies were counted manually.**

| | | Scramble shRNA | | | shRNA#1 | | | shRNA#2 | | | shRNA#3 | | |
|---|---|---|---|---|---|---|---|---|---|---|---|---|---|
| Biological Replicate 1 | No IPTG | 108 | 81 | 105 | 63 | 94 | 84 | 51 | 63 | 52 | 106 | 115 | 106 |
| | IPTG | 93 | 70 | 102 | 86 | 78 | 88 | 57 | 43 | 43 | 70 | 71 | 66 |
| Biological Replicate 2 | No IPTG | 42 | 44 | 40 | 32 | 42 | 38 | 58 | 59 | 42 | 31 | 41 | 39 |
| | IPTG | 37 | 35 | 35 | 16 | 44 | 29 | 55 | 54 | 38 | 26 | 18 | 30 |

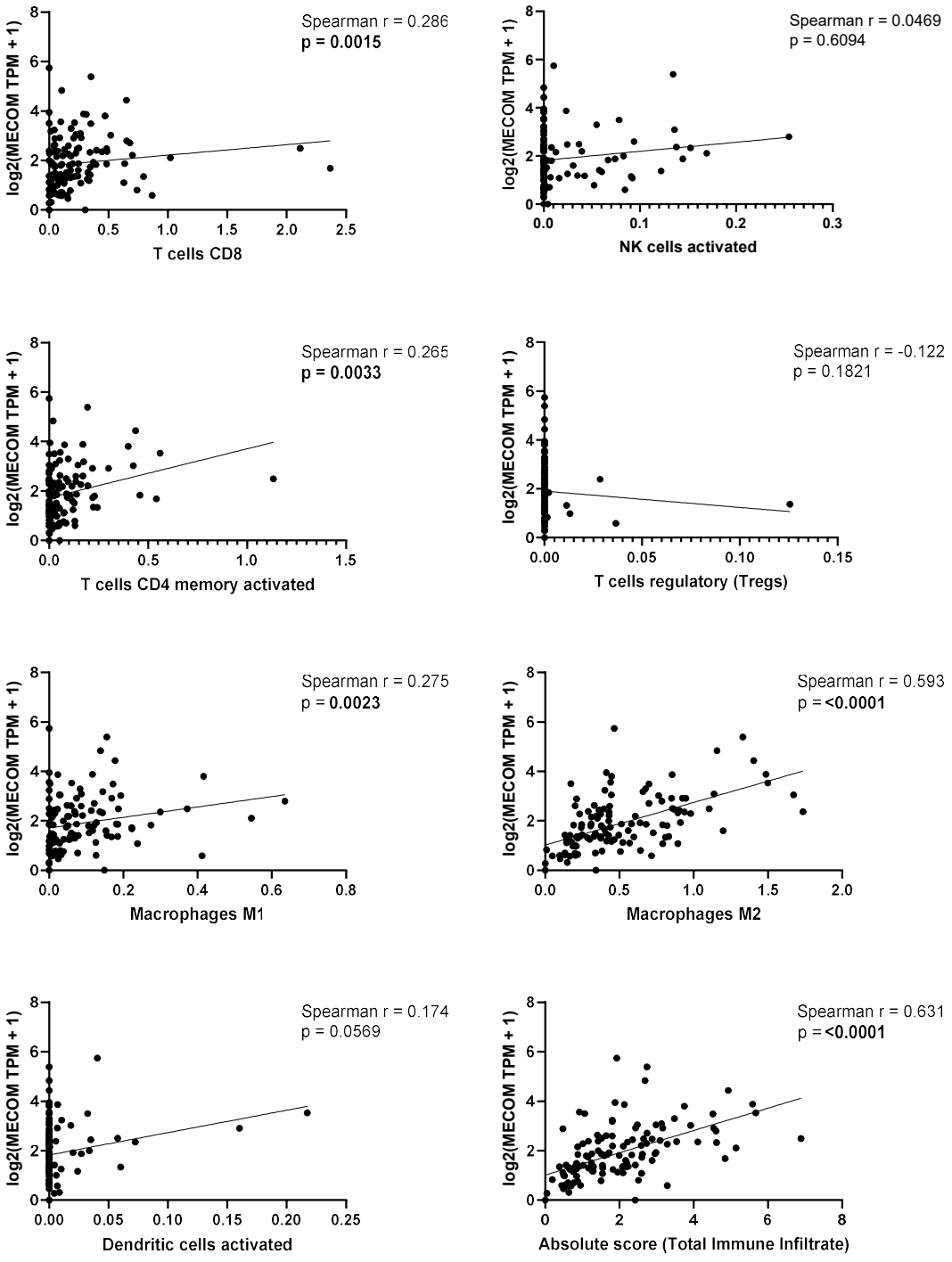


**FIGURE 50. CORRELATION BETWEEN MECOM EXPRESSION AND IMMUNE CELL FRACTIONS IN ANTI–PD-1-TREATED MELANOMA. Scatterplots show spearman correlations between $log_2$(TPM + 1) MECOM expression and CIBERSORT LM22–derived estimates of immune subsets, including CD8 t cells, activated CD4 memory T cells, regulatory T cells (Tregs), activated NK cells, activated dendritic cells, macrophages (m1 and m2), and total immune infiltrate (absolute score). MECOM expression demonstrated strong positive associations with overall immune infiltration (r = 0.631, FDR p = 0.0004) and M2 macrophages (r = 0.593, fdr p = 0.0004), with moderate correlations for CD8 T cells, activated CD4 memory T cells, and M1 macrophages. Correlations with activated dendritic cells and NK cells were borderline, and regulatory T cells showed no significant association.**

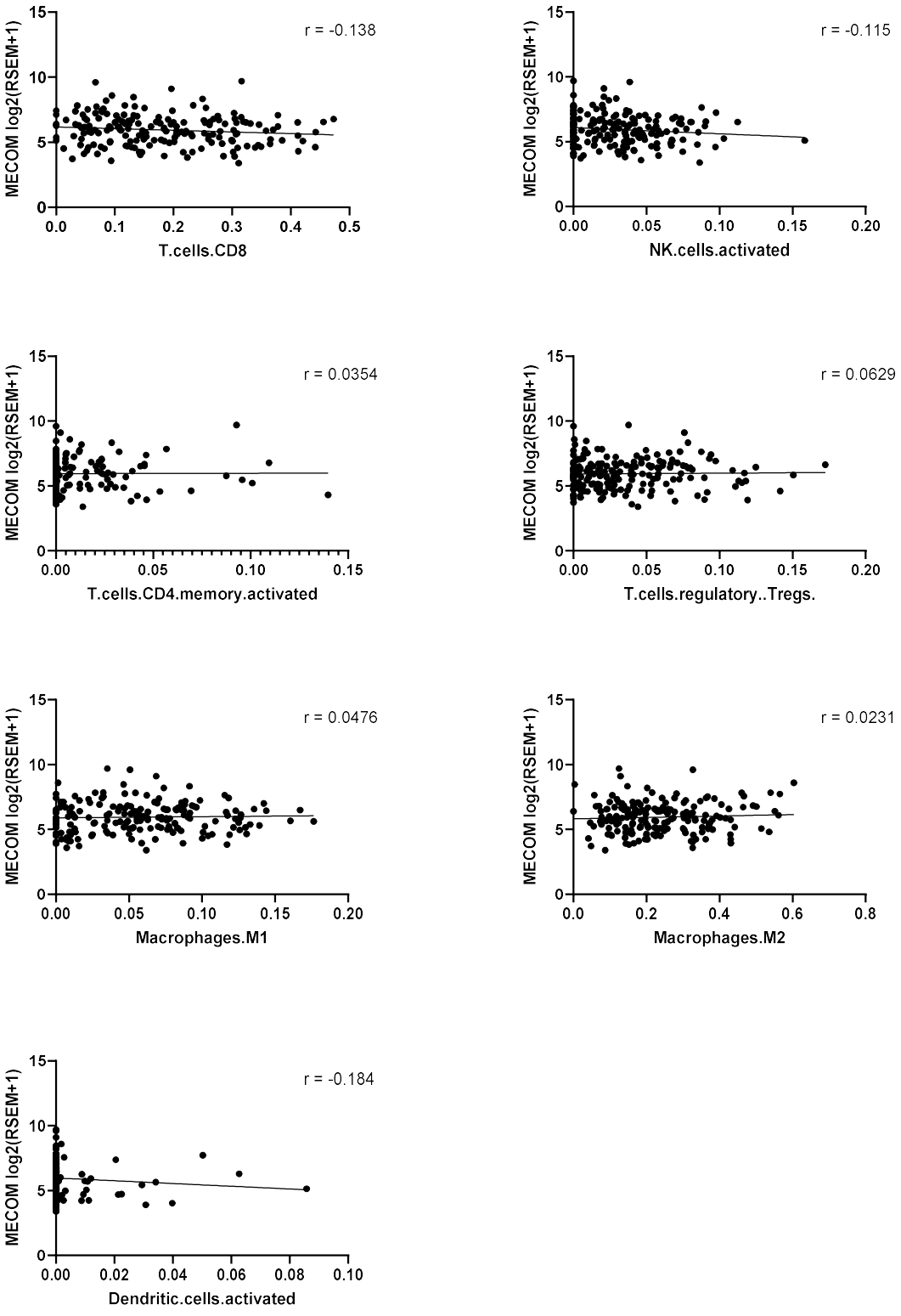


**FIGURE 51. CORRELATION BETWEEN MECOM EXPRESSION AND IMMUNE CELL FRACTIONS IN TCGA MELANOMA (PANIMMUNE ATLAS).Scatterplots show spearman correlations between $log_2$(MECOM RSEM + 1) expression and CIBERSORT LM22–derived estimates of immune subsets, including cd8 t cells, activated CD4 memory T cells, regulatory**

**T cells (Tregs), activated NK cells, activated dendritic cells, and macrophages (m1 and m2). MECOM expression demonstrated weak negative correlations with activated dendritic cells (r = −0.184, FDR p = 0.088) and activated CD4 memory T cells (r = −0.138, FDR p = 0.216), and a borderline negative association with activated NK cells (r = −0.115, FDR p = 0.280). All other subsets showed near-zero correlations and were non-significant after FDR correction. Overall, MECOM expression was not significantly associated with immune composition in TCGA melanoma, contrasting with the strong immune infiltration observed in the anti–PD-1-treated Liu cohort.**